AN ABSTRACT OF THE THESIS OF

James McManus for the degree of Doctor of Philosophy in Oceanography presented on February 17, 1992.

TITLE: On the Chemical and Physical Limnology of Crater Lake, Oregon

Redacted for Privacy

Abstract Approved: _____

Robert W. Collier

Active inputs of hydrothermally-enriched fluids at the bottom of Crater Lake, Oregon create small vertical and horizontal heterogeneities in the deep-lake temperature and salt distribution. To characterize the physical properties of Crater Lake, and to constrain the modes and time scales of mixing of heat and salt, I have developed an experimental approach to derive an in situ specific conductance and temperature dependant expression for salinity in Crater Lake.

The heat and salt budgets of the deep lake, which are dominated by subsurface hydrothermal activity, are constrained by a time series of CTD data and by data from a thermistor chain mooring. The net (conductive and convective) heat flow due to hydrothermal activity is ~1 W m^{-2} and the corresponding salt flux is ~5 μg $m^{-2} \cdot sec^{-1}$. The annual vertical exchange of surface water with water from the lake's hypolimnion occurs during early winter and to some extent during late spring. This exchange mixes the hydrothermal heat and salt from the deep lake to the surface.

The eastern portion of the South Basin of Crater Lake is the dominant region of hydrothermal input. Detailed mapping of the near-bottom temperature and salinity distribution in this basin has allowed the development of constraints which identify the possible modes of entry for the enriched fluids into the deep lake.

Small temporal and spatial variations in the distribution of dissolved oxygen in the deep lake yield information on the mixing time-scales, carbon flux, and the relative importance of hydrothermal activity on the oxygen budget. An increase in deep lake oxygen during the winter of 1988-89 indicates that 30-45% of deep lake water was replaced with well-oxygenated surface water. The consumption rate of dissolved oxygen in the deep basin of Crater Lake is ~4.4 mmol O_2 m^{-2} day^{-1}. This consumption of oxygen is primarily due to the oxidation of organic matter and, to a lesser extent, the

oxidation of reduced inorganic species which are introduced to the system via the subsurface hydrothermal springs.

ON THE CHEMICAL AND PHYSICAL LIMNOLOGY OF CRATER LAKE, OREGON

by

James McManus

A THESIS

submitted to

Oregon State University

in partial fulfillment of the
requirements for the degree of

Doctor of Philosophy

Completed February 17, 1992
Commencement June 1992

APPROVED:

Redacted for Privacy

Robert W. Collier, Asst. Professor of Oceanography, in charge of major

Redacted for Privacy

Douglas R. Caldwell, Dean of College of Oceanography

Redacted for Privacy

Dean of Graduate School

Date Thesis is Presented February 17, 1992

Typed by James McManus for James McManus

ACKNOWLEDGEMENTS

I would like to thank Bob Collier for his guidance, support, and friendship over the past four years. Jack Dymond has also offered a great deal of advice and support during my time at OSU. Comments made by both Bob and Jack have improved the thesis. Gary Larson has been extremely helpful in getting me on the lake at difficult times. I wish to thank the other members of my committee Chih-An Huh, Pete Nelson, Ted Strub, and Ian Tinsley. Ted Strub has been particularly helpful with the physical limnology sections of the thesis.

The oceanography faculty have been very generous with their time and I feel fortunate to have been a student at OSU. I wish to extend my gratitude particularly to Dave Hebert, Rob Holman, Lou Gordon, Laurie Padman, and Fred Prahl.

Chris Moser, Bobbie Conard, and Brad Beeson from OSU were all very helpful in the field. Mark Buktenica and the rest of the Crater Lake "Lake Team" (Scott, John, Deb, Mike, and Will) have provided many hours (day and night) of assistance in the field. Geoff Wheat gave up his summer to help us at Crater Lake in 1989. Everyone's dedication and sense of humor have been an inspiration.

Like most graduate students, the friendships that I have forged over the past four and a half years have helped me maintain some level of sanity. Pat and Bob have been special friends to both Carol and I. John Sharp has been a good friend, officemate, and housemate. My dear friend and officemate, Chi Meredith, has made my life a little richer. The Bucktenicas have made the summers at Crater Lake enjoyable for both Carol and I. Without fellow sufferers and dear friends Roald and Hernan the graduate student experience would not have been complete. Our conversations were fun and educational and the beer was always good. Ahmed Rushdi was a good friend and offered some critical graduate student survival tips before he finished. Gary and Susan Klinkhammer have been great friends during the last year and I look forward to working with Gary in the near future.

I appreciate the support and love that I've received from my family. Most of all I would like to thank my dearest friend Carol, her love, devotion, and support have made my life richer and a little easier.

TABLE OF CONTENTS

LIST OF FIGURES

LIST OF TABLES

APPENDIX TABLES

ON THE CHEMICAL AND PHYSICAL LIMNOLOGY OF CRATER LAKE, OREGON

I. INTRODUCTION

This thesis is a compilation of manuscripts which attempt to refine current knowledge on the physical and chemical properties of the water column in Crater Lake, Oregon. The work in this thesis serves as a compliment to a four year study, the goal of which was to identify the nature and magnitude of hydrothermal activity in Crater Lake (Collier et al. 1991). Both this thesis and the hydrothermal program were part of a larger, broader program aimed at determining whether the lake's clarity was decreasing (Larson 1990).

Prior to the work of this thesis, little had been done to constrain the physics of the water column in Crater Lake. Neal et al. (1971; 1972) and Simpson (1970a) were among the first to demonstrate that the thermal gradient in the deep lake (>350 m) was at least two orders of magnitude greater than the adiabatic gradient. Williams and Von Herzen (1983) provided the first treatment of the water column physics; however, they lacked the appropriate salinity data necessary to constrain possible convective processes in the lake. The work of Williams and Von Herzen (1983) demonstrated that in order to accurately define the physics of the water column, more precise determinations of the lake's salt distribution would have to be obtained. All prior solute measurements demonstrated that the lake was well-mixed with respect to total dissolved solids (see Drake et al. 1990, and references therein). The first task, therefore, of my work was to accurately define the distribution of temperature and salinity in the water column of Crater Lake, OR. Only after establishing the distribution of these properties was it possible to examine the mechanisms and time scales of mixing in the water column of Crater Lake. Understanding the mechanisms and time scales of mixing are critical to constraining the geochemical cycles active in the lake.

Chapter II of this thesis has been accepted for publication by Limnology and Oceanography. This chapter describes the method used to precisely determine the salinity distribution in the water column of Crater Lake. The utility of carefully determining the salinity of a fresh water body is clearly demonstrated for Crater Lake, a lake with active inputs of heat and salt. The physical and chemical properties of the water column indicate that the South Basin of the lake is the dominant region of hydrothermal fluid inputs.

The physical limnology of Crater Lake is discussed in chapters III and IV. These two chapters will be submitted to the Journal of Geophysical Research as companion papers. In both chapters the importance of hydrothermal activity on the physics of the lake is discussed and I demonstrate that hydrothermal activity contributes to the rapid horizontal mixing of deep lake water between the South Basin and the rest of the deep lake.

In Chapter III, I examine some of the mixing processes in Crater Lake. Within this section I first present the deep lake budgets for heat and salt. These budgets derive from direct observations of the accumulation of heat and salt in the water column over time. Through the use of thermistor chain data as well as a time-series of CTD data, I examine the breakdown of the summer thermocline which is followed by deep lake ventilation. In addition, the thermistor chain data and dissolved oxygen data provide constraints on the timing and extent of deep lake ventilation. I also discuss the small-scale physics of the deep lake and evaluate the significance of double diffusive convection in the deep lake. Finally, I assess the significance of hydrothermal activity on the physics of the deep water column.

A detailed survey of the physical and chemical properties of the South Basin of Crater Lake, reveal the location of dominant hydrothermal inputs to this basin (Chapter IV). The data from this chapter of the thesis show that the distribution of heat and salt varies with the bathymetry in the eastern portion of this basin. From observations of the changes in the heat to salt ratio along the sediment-water interface in the South Basin, I explore the possible modes of entry of the hydrothermal fluids.

The affects of mixing, carbon flux, and hydrothermal activity on the oxygen budget are assessed in Chapter V. Based on changes in the oxygen budget, I suggest that the characteristic time-scale of deep water renewal is 2.5-3.5 years. This estimate is in agreement with the work of Simpson (1970a, b) and is consistent with the recent work of Weiss et al. (unpublished data). The oxygen budget is dominated by the flux of particulate organic carbon (~98%). This particulate organic carbon is largely recycled within the deep water column (Dymond and Collier 1990). Based on the oxygen budget, the estimated flux of this organic carbon is ~3.4 mmol m^{-2} d^{-1}. Reduced inorganic species introduced to the deep lake via hydrothermal activity do not significantly contribute to the deep lake oxygen budget; however, these reduced species, mainly iron and manganese, do consume sufficient oxygen in the near-bottom waters of the South Basin such that they influence the hydrography of this region of the lake.

The appendix to the thesis contains major element data which does not appear in the body of the report. Much of this data has been incorporated into a report on the hydrothermal nature of Crater Lake (Collier et al. 1991). The data simply supports the body of this work, particularly Chapter II; however, as study continues at Crater Lake, need may arise for the data collected in support of this thesis. Many of the samples have been preserved (Collier et al. 1991) and stored at OSU.

II. ON THE PHYSICAL PROPERTIES OF CRATER LAKE, OREGON: A METHOD FOR THE DETERMINATION OF A CONDUCTIVITIY AND TEMPERTURE DEPENDENT EXPRESSION FOR SALINITY

ABSTRACT

Active inputs of thermally and chemically enriched fluids at the bottom of Crater Lake, OR create small vertical and horizontal heterogeneities in the deep-lake temperature and salt distribution. Using an internally recording CTD and a precise definition for salinity as a function of in situ conductivity and temperature, I assess the significant effects of these inputs on the density structure and mixing processes in Crater Lake. To characterize the physical properties of Crater Lake I have developed an experimental approach to derive a specific conductance and temperature dependant expression for salinity in freshwater.

INTRODUCTION

The use of an internally recording conductivity, temperature, and pressure sensor (CTD) with a narrow-range conductivity cell, enables the acquisition of high precision in situ water column measurements for limnological applications. These sensitive, high precision measurements enable accurate characterization of the physical properties of lakes. Such precision is particularly important where small thermal and chemical anomalies may affect the overall physics of a lake. This work outlines a method for the careful calibration of the conductivity sensor, modified for low conductivity fluids, for a CTD (SEACAT® model SBE19, Sea-Bird Electronics, Inc.) and an approach for converting in situ conductivity and temperature into salinity or total dissolved solids. I apply the expression obtained for salinity in combination with the equation of state for waters in the limnological range (Chen and Millero 1986) and determine the density and salinity structure for Crater Lake, Oregon, a well-mixed, ultra-oligotrophic lake which has active inputs of thermally and chemically enriched fluids.

In order to evaluate the distribution of total dissolved solids (TDS) in a given system, it is usually necessary to convert in situ conductivity measurements to conductivity at a standard reference temperature or to a temperature independent term. Snoeyink and Jenkins (1980) have defined an approximate relationship between TDS and conductivity at 25°C. Sorensen and Glass (1987) present an equation which converts in situ specific conductance measurements to specific conductance at 25°C. Although the combined equations yield an approximate expression for TDS, we will show that this approach lacks the accuracy necessary for our applications.

An alternative to normalizing specific conductance to 25°C would be to experimentally determine the relationship between temperature, in situ conductivity, and salinity (or TCS relationship) in a given limnological system. We have determined the TCS relationship for Crater Lake water in a temperature-controlled environment using water collected directly from the lake. The accuracy of the resulting conductivity and temperature dependent salinity measurement is limited by the analytical accuracy of the total salt determination for the lake water, while the precision of the relationship is limited by the precision of the CTD's conductivity measurement.

Two basic assumptions to the approach of relating specific conductance to TDS or salinity are; that the proportions of the major ions in the natural system are relatively constant, and that the "salinity" expression represents all the dissolved solids in the fluid. Since mixtures of different electrolytes will exhibit slightly different

electrochemical responses, the major ions for an individual system must remain in constant proportion in time and space. Likewise, the importance of representing all the dissolved solids in a system has particular application to the current work where silicic acid is an important dissolved solid in the salinity measurement.

To evaluate "total dissolved solids" (TDS) or "salinity" as a function of conductivity for a freshwater system the major components of TDS must be ionic and affect the conductivity of the water. Silicic acid, which is a common dissolved component in many fresh water systems, is a major contributor to the dissolved solids load and the density of Crater Lake water. The first dissociation constant of silicic acid is ~9.5, so silicic acid is completely protonated in lakes that are approximately neutral to acidic (Turner et al. 1981). Therefore silicic acid does not provide a strong conductometric response in solution. Thus, in using in situ CTD data to determine the salinity and the density of a fluid, silicic acid must either be measured directly or its concentration must be related to variations in the ionic material (conductance).

The assumption that the proportions of the individual ions in the natural system are relatively constant is usually met in lakes with long water and salt residence times relative to their characteristic mixing rate, or in aquatic systems which have a single or dominant source for all the salts in the system. In addition, the approach and applications described in the text will be most useful for long term studies of a single system, as is the case for the present work. The value of a precise expression for salinity is that it allows one to accurately characterize the vertical density structure, using an equation of state for lake water, and thus, the stability of a water column.

An equation of state for freshwater was presented in Chen and Millero (1977a, b, 1986). The equation of state describes the density of a fluid as a function of pressure, temperature, and salinity. Other physical and chemical properties of the fluid which are dependent on pressure, specific volume (ρ^{-1}), and temperature ("PVT" properties), such as the temperature of maximum density (T_{md}) and the specific heat capacity, are derived from this equation of state (Chen and Millero 1977a).

The vertical stability (E) of a fluid parcel is generally assessed by considering the exchange of two adjacent water parcels. In practice, if the density of the water column (calculated at some reference pressure) increases with increasing depth then the water column is stable. Mathematically this is defined by the relationship:

$$E = -(\rho^{-1})(\partial\rho\ \partial z^{-1}) \qquad (II.1)$$

where ρ is the density the fluid would have at its in situ temperature, a reference pressure, and its salinity, and z is the depth. For the case where we compare the density of a fluid with respect to the surface, we use the potential temperature, 1 atmosphere pressure, and the in situ salinity, i.e. $\rho = \rho(\theta,0,S)$.

Chen and Millero (1977a) point out that the density of a fluid, is partly dependent upon the total salt content, and that systems near the T_{md} can not necessarily be treated as "pure" water. When the in situ temperature is nearly at the T_{md}, the question of stability becomes particularly sensitive to the salinity of the medium because the T_{md} is lowered by small increases in total dissolved solids. Additionally, it has been shown that the pressure effects on the temperature of maximum density in limnological systems will affect the vertical stability of a displaced water parcel (Farmer and Carmack 1981; Carmack and Farmer 1982). It is apparent that when considering the vertical stability of a fluid parcel, both the affects of salinity and pressure on the density must be included.

A common approach of characterizing fluid stability, which includes the gravitational constant (g), is the Brunt-Väisälä (buoyancy) frequency (Chen and Millero 1977a, b, 1986); where the frequency N (radians/second) is defined by the expression:

$$N^2 = gE \qquad \text{(II.2)}$$

where E is the stability. When N^2 is positive, a fluid parcel is stable and when N^2 is negative, the parcel is unstable. Qualitatively, the buoyancy frequency is the oscillation frequency of a parcel of water after a small vertical displacement from its equilibrium level. Chen and Millero (1977a, b, 1986) provide an equation for the buoyancy frequency which is calculated from a combination of the polynomials presented in their work:

$$N^2 = (-g^2\, V^{-2})[(\partial V\, \partial S^{-1})_p(dS\, dP^{-1})+(\partial V\, \partial T^{-1})_p] \times [(dT\, dP^{-1})-(\partial T\, \partial P^{-1})_{adia}] > 0 \qquad \text{(II.3)}$$

where V is the specific volume (ρ^{-1}), T the temperature, S the salinity, P the pressure, and $(\partial T\, \partial P^{-1})_{adia}$ is the adiabatic temperature gradient. Because the salinity term appears in all of the expressions for the PVT properties of limnological interest, changes in the vertical salt distribution will affect the stability of a water column. The importance of salinity in determining the physical and chemical properties of a lake system is clearly

demonstrated in Crater Lake which has a hyperadiabatic thermal gradient (Neal et al. 1971, 1972) which we will show is stabilized by a salinity gradient.

Crater Lake rests inside the collapsed caldera of Mount Mazama in the Cascade Range of southern Oregon. At 590 m, it is the deepest lake in the United States. The lake is predominantly precipitation fed. Approximately 80% of the precipitation falls directly on the lake surface with the remainder entering the lake system as runoff from the caldera slopes (Redmond 1990). Roughly half of the annual precipitation is lost due to evaporation with the remainder being lost due to seepage (Redmond 1990). The fetch of the lake is relatively short (approximately 10 km), and the lake surface has some shielding from winds because of the steep caldera walls which extend to nearly 300 m above the lake surface. An extensive review of the geology, hydrology, ecology, and chemistry of Crater Lake can be found in Drake et al. (1990).

Evidence for the active input of hydrothermally enriched fluids into the bottom of Crater Lake has been reported (Williams and Von Herzen 1983; Dymond et al. 1989; Collier et al. 1990a). Some investigators (Williams and Von Herzen 1983) have postulated that because the temperature gradient below 350 m is greater than the adiabatic gradient, the hypolimnion of the lake is unstable and undergoing convection. However, because high precision data demonstrating increases in salinity with temperature were unavailable, their hypothesis was based solely on the thermal structure of the water column. We will show that the variations in the vertical and horizontal density structure of the water column in Crater Lake is influenced both by saline and by thermal effects. As first pointed out by Collier et al. (1990a) the hyperadiabatic temperature gradient in Crater Lake is stabilized by a salinity gradient. In limnological systems, like Crater Lake, where small variations in temperature and salinity may play an important role in the overall physics of the lake, high precision temperature and salinity measurements are essential for understanding lake mixing processes.

METHODS

Cations were analyzed using a Perkin-Elmer 5000 flame atomic absorption spectrophotometer (AAS). Each sample was analyzed at least twice with multiple readings for each analysis and a standard was referenced between the two sample analyses. Chloride and sulfate analyses were performed using ion chromatography (IC). Bicarbonate concentrations are the difference between the sum of the major cations and major anions on an equivalent ion basis. These results were consistent with the alkalinity and pH data obtained for the water column in Crater Lake as determined by closed-system pH measurements and Gran titrations of alkalinity. Silicic acid was determined by a colorimetric molybdenum blue method using an Alpkem rapid flow analyzer.

Direct density measurements of water samples were made using a high precision flow digital densimeter (model 02D, Sodev Inc.) with a programmable circulating thermostat. The accuracy of the measurement is ±2 ppm.

Calibration of the conductivity sensor

For this discussion I first consider the conductance theory relevant to the experiments. Then I outline the method employed for the calibration of the conductivity sensor. The fluid used for the conductivity cell calibration was a KCl solution ranging in concentration from 0 (distilled water) to 2.3 mM.

Specific conductance (κ), in siemens meter^{-1}, is inversely proportional to the electrical resistance (R), of 1 cm of fluid, such that: $\kappa = (1/R) \times (L/A)$; where A is the area and L is the length of the cell. The specific conductance of a strong electrolyte solution is the product of the equivalent conductance (Λ) and the concentration of the salt (C), in equiv cm^{-3}:

$$\kappa = \Lambda C \qquad \text{(II.4)}$$

where the equivalent conductance (Λ) is the conductance of 1 gr equivalent of the solute measured between two electrodes 1 cm apart for an aqueous electrolyte solution. Λ, which is itself a function of the concentration of the solute, is calculated from the Onsager equation (Conway 1952):

$$\Lambda = \Lambda_\infty - (F + V\Lambda_\infty)\, C^{1/2} \qquad \text{(II.5)}$$

where expressions for the relaxation effect (F) and the effect of the viscosity of the fluid (V) as a function of temperature for a specific salt (KCl) were generated from data presented by Conway (1952). A third-order relationship was derived from tabulated data presented by Robinson and Stokes (1955) for the equivalent conductance of KCl at infinite dilution (Λ_∞). Output from the CTD conductivity sensor is expressed as frequency and the calibrations which we calculate for the instrument are expressed in siemens m^{-1} ($S\ m^{-1}$) which we convert to the more conventional $\mu S\ cm^{-1}$.

The conductivity sensor was calibrated by placing the CTD into a plastic lined insulated bath which contained approximately 300 liters of distilled water. A submersible pump was attached to the conductivity sensor to maintain a constant flow of the fluid through the conductivity cell, and a plastic sheet was used to cover the bath to minimize evaporation. The bath temperature was slowly increased from 2°C to 20°C while the CTD recorded data at 1 min intervals. We repeated this process with two separate additions of approximately 23 gr of KCl such that our calibration included the full range of specific conductance and temperature observed in Crater Lake. Discrete water samples were taken from the large bath throughout the run for high-precision conductometric analysis in the laboratory. The KCl bath solutions are herein referred to as the "standardizing fluid."

The specific conductances of subsamples of the standardizing fluid, taken from the bath during the calibration run, were determined against a separate set of high precision KCl standards using a Radiometer CDM83 conductivity bridge. A second order equation was derived for the relationship between observed specific conductance (κ) and concentration of KCl . Small differences between the observed specific conductance, derived from the CTD and the calculated specific conductances, based on Eq. II.4 and II.5, were well below the resolution of the CTD and for our application the Onsager model, Eq. II.5, provided sufficient accuracy for the calibration of the CTD conductivity sensor.

In Table II.1, I present representative sample values used for calibrating the conductivity sensor. The three groups of $\kappa_{(25°C)}$ in Table II.1 represent the distilled water bath, the first addition of KCl, and the second addition of KCl. The KCl concentrations represent approximations based on the KCl standards as described above. Despite cleaning the CTD, the insulated bath, etc., some contaminant salts existed in the bath such that the distilled water bath gave conductivity readings. The CTD calculates conductivity from frequency and temperature using a relationship provided by Sea-Bird Electronics, Inc. There are no systematic errors in the CTD's interpretation of conductivity (κ_{CTD}) when compared to the theoretical specific conductance (κ_t) in Table II.1. The error in the conductivity measurements is defined as the difference between the theoretical specific conductance (κ_t) in Table II.1, and the specific conductance measured by the CTD (κ_{CTD}) in Table II.1. The standard deviation of the errors is ± 0.4 $\mu S\ cm^{-1}$. This is a measure of the absolute accuracy of the conductivity measurement. During the same calibration experiment, the CTD temperature sensor was also calibrated using a Mueller bridge standard triple point cell according to the IPTS 68 temperature scale. On the basis of this calibration, the temperature sensor was accurate to within 0.001°C of the factory calibration.

Table II.1. Sample values for κ and KCl concentration (mM). T (°C) represents the temperature of the bath at the time a sample was taken. $\kappa_{(25°C)}$ is the specific conductance ($\mu S\ cm^{-1}$) for the standardizing fluid samples, measured at 25°C in the laboratory using a conductivity bridge. [KCl] is determined by the relationship relating the specific conductance to [KCl] for the laboratory standards. κ_t is the theoretical specific conductance for the samples at the temperatures that they were collected during the calibration and is calculated from Eq. II.4 and II.5.

T (°C)	$\kappa_{(25°C)}$	[KCl] mM	κ_t	$\kappa_{(CTD)}$
5.608	26.1	0.177	16.7	16.5
10.538	26.1	0.177	19.1	19.2
19.414	26.1	0.177	23.4	24.3
15.652	185.0	1.263	152.1	151.6
2.784	186.0	1.270	109.5	109.1
2.940	334.0	2.305	198.2	199.5
21.123	334.0	2.305	310.1	310.0

The absolute accuracy of the conductivity measurement (±0.4 μS cm^{-1}), is only slightly greater than the resolution of the instrument (±0.2-0.3 μS cm^{-1}). Experience indicates that conductivity and temperature recalibration may be necessary prior to each field season for optimum precision and accuracy when comparing data from year to year. In conjunction with the conductometric calibration of the cell, it is also necessary to calibrate the response of the conductivity cell to the total salt content of the specific medium of interest, in this case Crater Lake water.

Converting in situ specific conductance into salinity

Having established a calibration method for the conductivity cell, I now describe a method which allows development of an equation which converts in situ specific conductance to the salinity of a natural water body (i.e. Crater Lake). In order to accomplish this task ~150 liters of Crater Lake water was placed into an insulated bath and the temperature of the bath was varied between 2 and 20°C. Temperature and conductivity were measured at 1 min intervals throughout the experiment and water samples were collected at each 5°C increase in temperature. I subsequently added ~150 liters of distilled water to dilute the Crater Lake water and repeated the experiment. To ensure consistency between the lake water samples used in the calibration and our water column samples, I cross-calibrated the "calibration water" samples with water column samples of known composition. The ratio of the concentration of each solute measured in the diluted calibration water to the concentration of that solute in the undiluted calibration water permits a semi-quantitative evaluation of the absolute accuracy of the data set (Table II.2). The average ratio for each solute is 0.599, with a coefficient of variation of 1.8%. Additionally, the data agrees with the USGS data set within the reported standard deviations of both data sets (Nathenson 1990).

Before detailing our development of an equation representing the salinity of a water body, I will briefly review another approach to the problem of relating conductivity to the dissolved solids in a solution and I will demonstrate why this approach is inadequate for the applications of this work.

In order to use published equations relating salinity (or TDS) to in situ conductance, in situ conductivity must be converted to conductivity at a fixed reference temperature. Sorenson and Glass (1987) present an empirical relationship which relates the conductivity measurement of mixed electrolyte (environmental) samples at any temperature to conductivity at 25°C:

Table II.2. Results from the analysis of the undiluted lake water and the diluted lake water used in the CTD calibration. Since HCO_3^- is calculated as the difference between the cations and the anions, an ion balance is not meaningful. The ratio of the concentration of each solute in the diluted lake water to that in the undiluted lake water will yield a measure of our analytical quality control. The coefficient of variation (CV) for the various solute ratios is 1.8%.

	Undiluted Lake Water			Diluted Lake Water			
Solute	Concentration		CV	Concentration		CV	Solute Ratio
	(mM)	(mg liter^{-1})	(%)	(mM)	(mg liter^{-1})	(%)	DLW/ULW
Na^+	0.4475	10.29	0.170	0.2723	6.259	0.888	0.608
K^+	0.04253	1.663	0.113	0.0259	1.011	0.190	0.608
Mg^{++}	0.1081	2.628	0.116	0.0649	1.577	0.416	0.600
Ca^{++}	0.1664	6.670	0.707	0.0986	3.951	0.573	0.592
Cl^-	0.2577	9.137	0.995	0.1528	5.417	0.628	0.593
SO_4^{--}	0.0996	9.572	0.495	0.0580	5.572	0.563	0.582
HCO_3^-	0.5821	35.52	N/A	0.3562	21.74	N/A	0.612
Σions	1.7039	75.5		1.0287	45.5		
H_4SiO_4	0.2964	28.50	0.233	0.1775	17.06	0.292	0.559
TDS (salinity)	2.0003	104.0		1.2062	62.6		

$$C_{25} = C_t(\eta_t/\eta_{25})^K \qquad (II.6)$$

where C_t ($\mu S\ cm^{-1}$) is the in situ conductivity, C_{25} ($\mu S\ cm^{-1}$) is the conductivity at 25°C, η is the viscosity and the exponent K was empirically derived as a function of the total hydrogen ion content. Approximations in Snoeyink and Jenkins (1980) relate the specific conductance ($\mu S\ cm^{-1}$) to TDS:

$$TDS = 0.64 \times C_{25} \qquad (II.7)$$

where TDS (mg $liter^{-1}$) is now a direct function of the concentration of the electrolytes or salts.

Summation of the individual electrolytes (Σ electrolytes) for the calibration lake water (Table II.2) yields a total ion concentration of 75.5 mg $liter^{-1}$ and for the diluted calibration lake water 45.5 mg $liter^{-1}$. Because Eq. II.7 only relates specific conductance to the dissolved ionic species, silicic acid is excluded from the total electrolytes reported in Table II.2. Equation II.7 overestimates the Σ electrolytes by 1 mg $liter^{-1}$ for the total ion concentration = 75.5 mg $liter^{-1}$ and underestimates the Σ electrolytes by nearly 1.5 mg $liter^{-1}$ for the total ion concentration = 45.5 mg $liter^{-1}$ (Fig. II.1). This offset in Eq. II.7 suggests that there are systematic errors in the relationship which vary as a function of ion concentration. These errors are larger than the individual ion measurement errors that result from our analytical uncertainties. Such errors are too large to define the salt distribution of Crater Lake and demonstrate a need for an equation which converts in situ conductivity and temperature into salinity for Crater Lake water.

In order to avoid errors in estimating salinity from conductivity (Fig. II.1) I experimentally determined the TCS relationship for Crater Lake water. The salinity calibration covered ranges in temperature between 0 and 25°C and ranges in specific conductance between 40 and 120 $\mu S\ cm^{-1}$. The applicable range for Eq. II.8 in Crater Lake is approximately 60 to 120 mg $liter^{-1}$, which is sufficient for the purposes of this work. The primary reason for choosing natural lake water over artificial media was the very high concentration of silicic acid in Crater Lake which is difficult to reproduce in artificial media. For systems without high concentrations of silicic acid an artificial mixture of the appropriate salts would likely suffice.

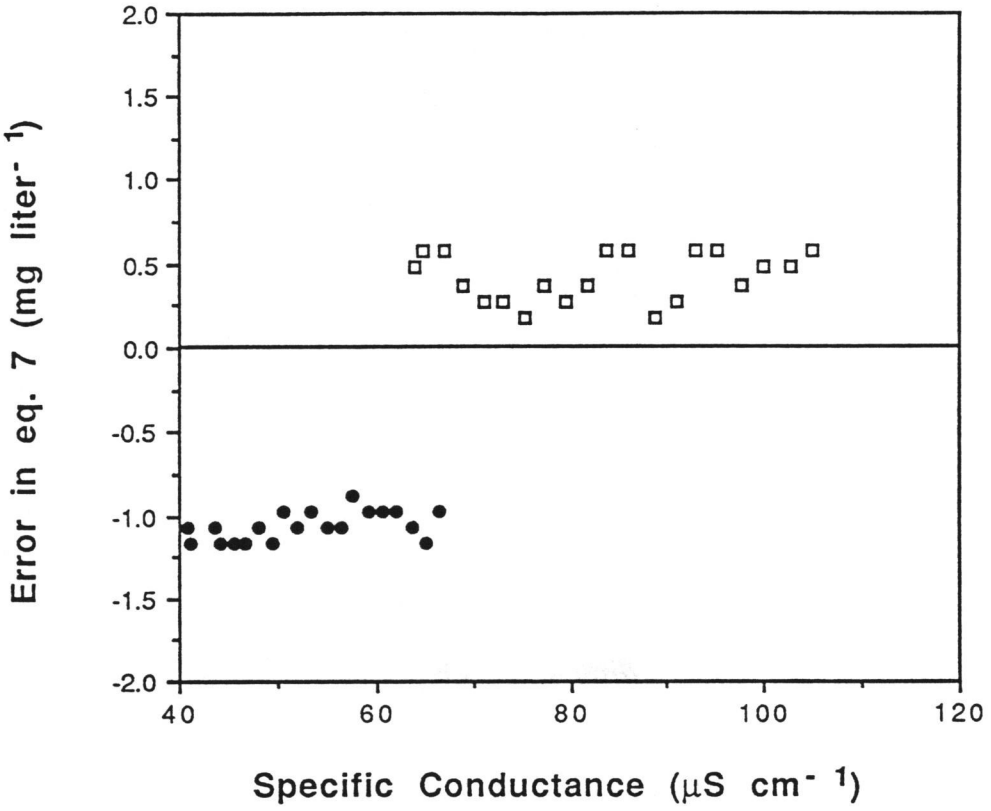

Fig. II.1. Error in Eq. 7 vs. specific conductance. The error represents the difference between the measured concentration of ions (Table II.2) and that predicted using Eq. II.7 for subsamples of the lake water calibrations. The sample specific conductances for TDS = 45.5 mg liter^{-1} (•) and TDS = 75.5 mg liter^{-1} (□) are taken from the CTD during the calibration and vary with water temperature.

Silicic acid accounts for a significant portion of the salinity in Crater Lake - more than 25% by weight (Table II.2). Because the salinity must represent all of the dissolved solids in solution for accurate calculation of the physical and chemical properties of lake water the concentration of silicic acid must be included as part of the measurement of salinity. Although silicic acid is not an electrolyte, the ratio of silicic acid to the major ions in the water column of Crater Lake is constant as is suggested by Fig. II.2a-c. Because of this proportionality, silicic acid will vary directly with specific conductance. Therefore, the salinity, which now includes silicic acid, is 104.0 mg liter^{-1} and 62.6 mg liter^{-1} for the lake water and diluted lake water respectively (Table II.2).

Taking the conductivity and temperature data from the CTD in conjunction with the salinity data and using a least-squares regression, we obtain an expression for salinity as a function of conductivity and temperature which is similar in form to the expression used for seawater (Cox et al. 1967):

$$S = a_0 + a_1 C_t^{0.5} + a_2 C_t + a_3 C_t^{1.5} + a_4 C_t^2 + b_1 C_t T^{0.5} + b_2 C_t T + b_3 C_t T^{1.5} + b_4 C_t T^2 + b_5 C_t T^{2.5} + b_6 C_t T^3 \qquad \text{(II.8)}$$

where a_i and b_i are constants which need to be determined for each individual system, S is the salinity in milligrams liter^{-1}, C_t is the in situ conductivity, and T the temperature. Figure II.3 demonstrates the precision of the equation as a function of conductivity by illustrating differences between the laboratory-determined salinity of a sample and the salinity of the sample predicted by Eq. II.8. There appears to be no systematic errors in the salinity expression with respect to conductivity (cf. Fig. II.3 to II.1) or temperature for either the low salinity water (filled diamonds) or the high salinity water (open boxes). The salinity calculated according to Eq. II.8 has a standard deviation of ±0.1 mg liter^{-1} for the bath samples; however, the resolution of the CTD conductivity measurement limits the precision of the salinity measurements to approximately ±0.2 mg liter^{-1}.

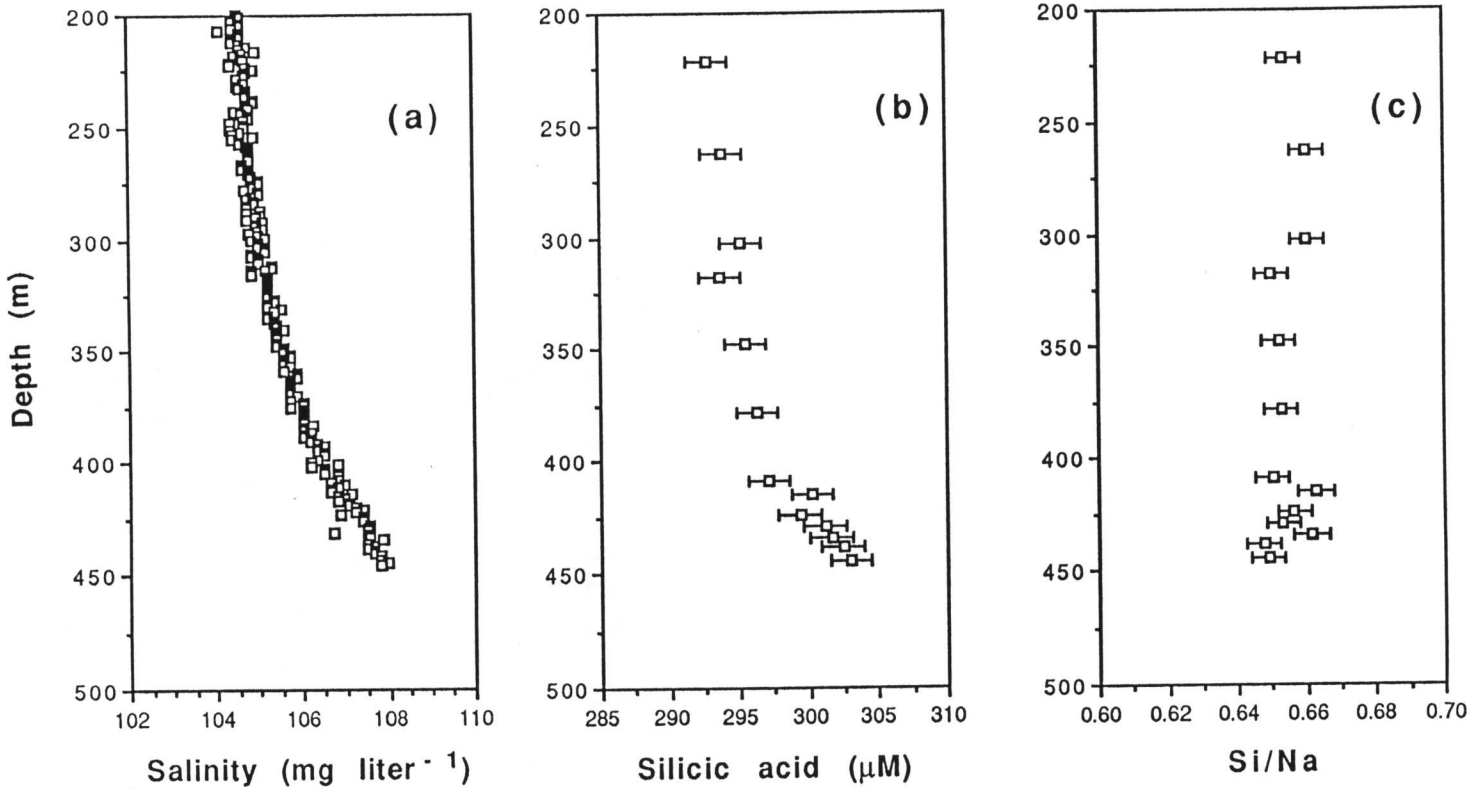

Fig. II.2. CTD and chemistry data from August 1988; (a) Salinity (including silicic acid) as calculated from Eq. II.8, where a_0 = -50.5103, a_1 = 1836.3964, a_2 = -1.3524 x 10^4, a_3 = 1.5624 x 10^5, a_4 = -3.00448 x 10^5, b_1 = 11634.88, b_2 = -1.1218 x 10^4, b_3 = 4959.9155, b_4 = -1234.5981, b_5 = 161.3464, b_6 = -8.57375, (b) silicic acid (μM), and (c) the ratio of silicic acid to sodium. The figure demonstrates the covariance of the dissolved constituents with depth in the deep lake and illustrates the constant ratio between silicic acid and the strong electrolytes (using sodium as an example).

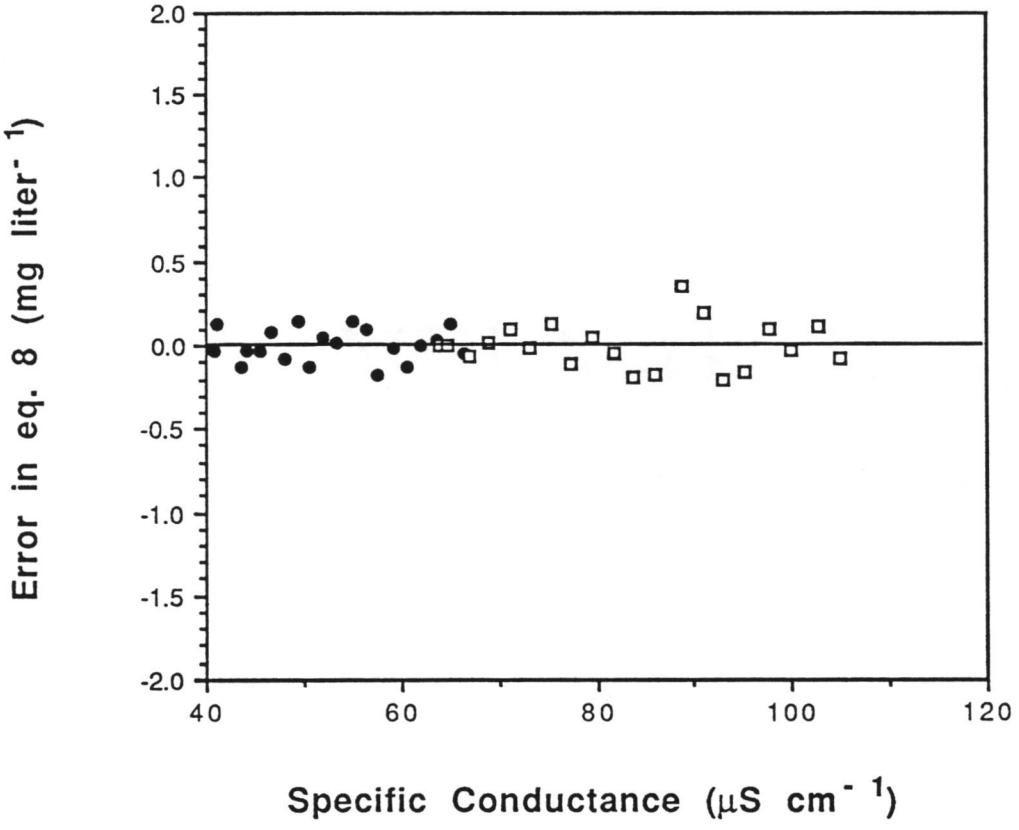

Fig. II.3. The error in Eq. II.8 vs. specific conductance. The error represents the difference between the salinity predicted from Eq. II.8 and the salinity of the calibration water Table II.2. The variation in specific conductance in the two lake water data sets is due to the variation of temperature during the experiment.

THE INFLUENCE OF SILICIC ACID ON THE DENSITY OF CRATER LAKE WATER

In Crater Lake the change of salinity with depth parallels the change in silicic acid content (Fig. II.2a, b). The covariation of salinity and silicic acid is also demonstrated by the uniform Si/Na values with depth (Fig. II.2c). Therefore, although specific conductance is not a direct measure of silicic acid concentration, the concentration of silicic acid is directly proportional to conductance and dissolved ions in Crater Lake. The dominant source of the strong electrolytes and the silicic acid to Crater Lake is subsurface hydrothermal activity (Collier et al. 1990).

In order to evaluate the influence of silicic acid on the density of Crater Lake water, the relative density ($\Delta\rho$) of Crater Lake water was measured directly. Here the relative density of lake water is defined as the density of the fluid at 1-atm pressure and 25°C, minus the density of pure water at that temperature and pressure. I also used Eq. II.8, with constants that include the silicic acid content of Crater Lake as part of the total salinity, to calculate salinity from the CTD data collected at the same time as the water column samples. I then applied the equation of state from Chen and Millero (1986) to this hydrographic data for a temperature of 25°C to match the laboratory density measurements. For comparison purposes, I applied an expression with the same form as Eq. 8, but which does not include the silicic acid content of the lake water, and the equation of state was again applied to the hydrographic data (Fig. II.4). Within the accuracy of the equation of state ($\pm$2 ppm) and within the accuracy of the density measurement ($\pm$2 ppm), the agreement between the predicted $\Delta\rho$, derived from the hydrographic data which included the silicic acid content of the lake water, and the measured $\Delta\rho$, from the samples collected in the field, is striking. Likewise, when calculating density without including silicic acid, the relative density of lake water is underestimated by 27%.

Hydrothermal sources dominate the major ion and silicic acid content of Crater Lake waters (Collier et al. 1990; Nathenson 1990). In systems where silicic acid is not always proportional to the strong electrolytes in solution, silicic acid will need to be directly determined in addition to the strong electrolytes for accurate assessment of the water column density structure. In biologically productive systems, silicate depletion by diatoms in surface waters and opal dissolution at depth could result in variations in the ratio of silicic acid to the major ions. Increases in silicic acid derived from the dissolution of diatom frustules could provide the necessary stabilization to balance the

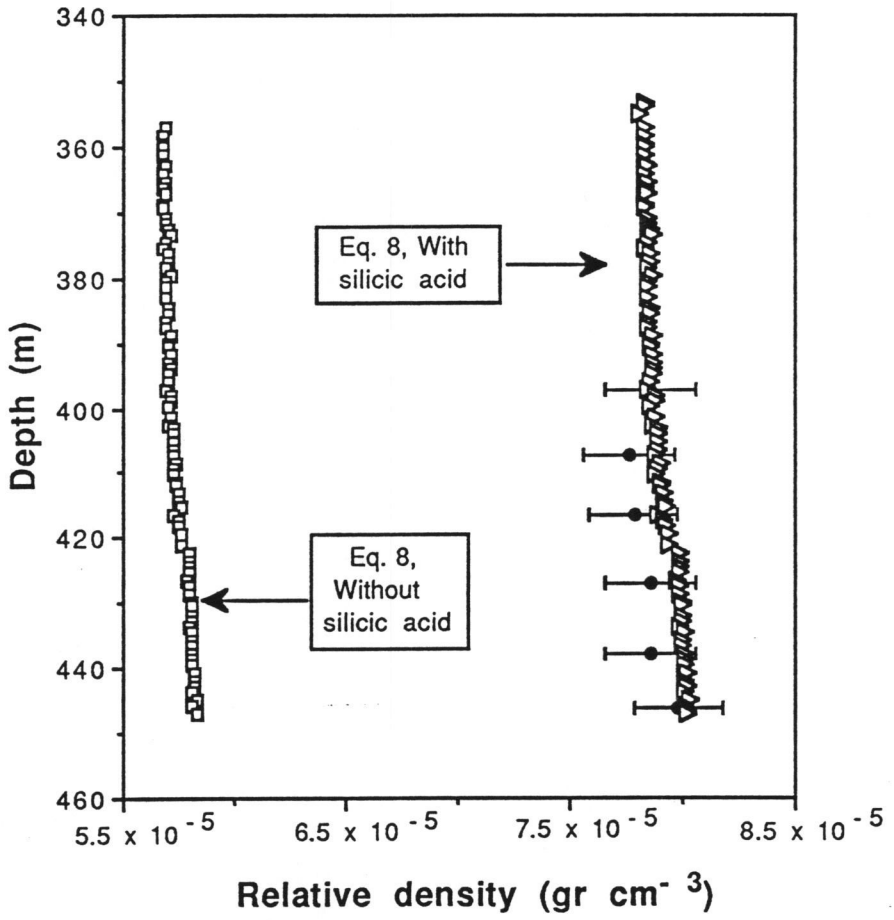

Fig. II.4. The relative density of lake water as a function of depth. The relative density ($\Delta\rho$) is the density of the fluid at 1-atm pressure and 25°C, minus the density of pure water at that temperature and pressure. The $\Delta\rho$ of samples taken in the field (•) are compared to the $\Delta\rho$ based on the hydrographic data and the equation of state (Chen and Millero 1986) (• and Δ). The calculation of the relative density represented by ▫ uses salinity which does not include silicic acid and that represented by Δ uses salinity which does include silicic acid. Hydrographic data was taken at the same time as the samples represented by (•) and the error bars represent ±2 ppm, which is the accuracy of the equation of state (Chen and Millero 1986) and of the density measurement.

observed increases in deep lake temperature of Lake Michigan (Marmorino et al. 1980). Such processes which add or remove silicic acid from the water column will change the ratio of silicic acid to the major ions, and may also affect the stability of a water column if that water column is not otherwise strongly stabilized (i.e. by a thermal gradient in the summer thermocline).

To investigate the stability of a water column, precise determination of the salinity and silicic acid content of the water column may be necessary. The approach described here makes it possible to determine the precise density structure of a water column. This approach is particularly applicable to large deep lakes where the proportions of the major ions are relatively constant.

FIELD RESULTS: THE PHYSICAL PROPERTIES OF CRATER LAKE

Crater Lake has two semi-enclosed basins, one in the northeastern portion of the lake (North Basin) which has a maximum depth of approximately 590 m and the second in the southwestern section of the lake (South Basin) which has a maximum depth of approximately 485 m. The basins are separated by a sill which is situated between 425 and 450 m depth.

The well-known clarity of the lake and intense surface mixing are factors which allow seasonal heat exchange to occur well below 200 m (Collier et al. 1990). This upper water is aerated twice annually and is generally isohaline and saturated with dissolved oxygen all year round. As the summer thermocline develops, evaporation at the surface results in small increases of salt content in the upper few meters of the lake. This process is observable under calm surface conditions coupled with sunny, cloudless skies which are common in the late summer/early fall.

To a first approximation the deep lake is isothermal (Fig. II.5a) and isopycnal (Fig. II.5b, d); however, inputs of heat and salt into the hypolimnion of Crater Lake create measurable vertical and horizontal heterogeneities in the deep-lake temperature (Fig. II.5c) and salinity structure (Fig. II.2a). These heterogeneities in heat and salt result in vertical and horizontal heterogeneities in the density structure of the deep lake. Although the average of the adiabatic gradient for Crater Lake from 300 to 560 m is 4.7 x 10^{-6}°C m^{-1}, the observed thermal gradient (Fig. II.5c) over this depth range in the North Basin is approximately 2.6 x 10^{-4}°C m^{-1} - nearly two orders of magnitude greater than the adiabatic gradient. This "hyperadiabatic" gradient is balanced by a salinity gradient of 8.8 x 10^{-6} g kg^{-1} m^{-1} yielding an increase in density with increasing depth (Fig. II.5d). These thermal and saline gradients are ubiquitous in the deep lake; however, there are temporal and spatial variations in the magnitude of these gradients. For example, the increase in temperature and salinity in the bottom 50 m of the South Basin is much greater than that observed in the North Basin (Fig. II.6a, b). The combined increase with depth in temperature and salinity results in a stable vertical density gradient (Fig. II.6c, where $\sigma_{(0.45, T)}$ is the density of the water column at a pressure of 450 dbars and the in situ temperature). The higher bottom water temperature and salinity gradients, relative to the North Basin, suggest that the South Basin is a dominant source for hydrothermal inputs as has been suggested by others (Williams and Von Herzen 1983; Dymond et al. 1989; and Collier et al. 1990).

Fig. II.5. (a) Potential temperature (°C), (b) potential density (gr cm^{-3}), (c) temperature, and (d) σ_θ as functions of depth in the North Basin of Crater Lake on 17 July 1989. Note: line demonstrating the adiabatic gradient in panel c and the restricted depth range in panels c and d.

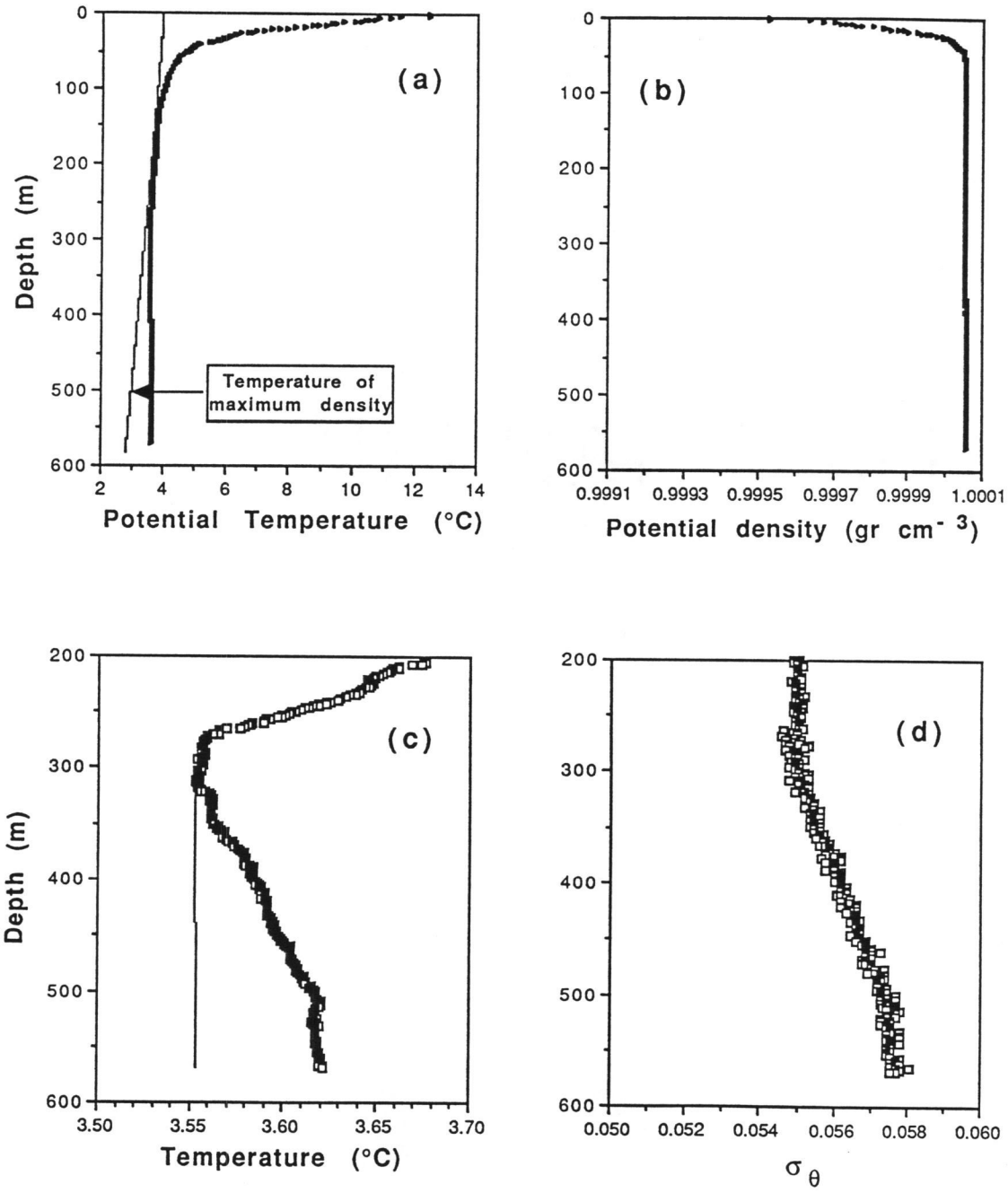
(a)
Depth (m)
Temperature of maximum density
Potential Temperature (°C)
(b)
Potential density (gr cm⁻ ³)
(c)
Depth (m)
Temperature (°C)
(d)
σ θ

Figure II.5

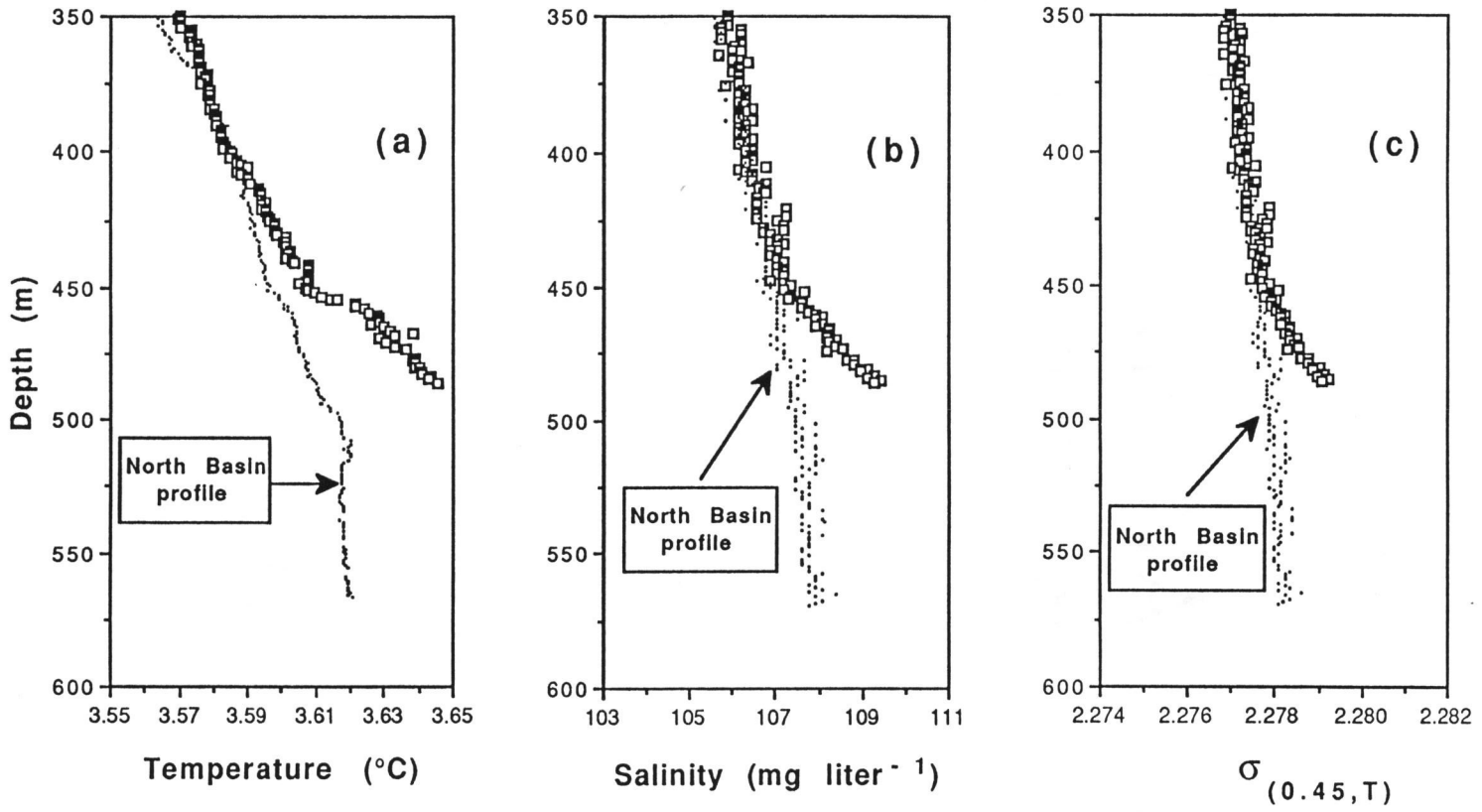

Fig. II.6. (a) Temperature (°C), (b) salinity (mg liter^{-1}), and (c) $\sigma_{(0.45, T)}$ all as functions of depth. $\sigma_{(0.45, T)}$ is the density of the water column at a pressure of 450 dbars and the in situ temperature. Data are taken from the South Basin (□) and North Basin (•) on 17 July 1989

Using Eq. II.1 to evaluate the stability of the hypolimnion of Crater Lake shows that the temperature and salinity gradients combine to yield a statically stable water column. The stability is illustrated by the general increase with depth of σ_θ in Fig. II.5d and $\sigma_{(0.45,\ T)}$ in Fig. II.6c.

The relationship between temperature and salinity (T-S) in the hypolimnion of Crater Lake provides a powerful method for the comparison of the sources and evolution of North and South Basin deep waters.

The bulk T-S properties of the hypolimnion of Crater Lake document the warmer, more saline nature of the South Basin deep water as compared to the North Basin deep water (Fig. II.7). In North Basin waters there is a small increase in salinity below the thermocline as the waters become cooler with depth. The decrease in temperature extends through the mid-water column and reflects an exponential decrease in the mix between surface-warmed water and deep water with increasing depth. The "elbow" feature at the temperature minimum defines a trend for those waters influenced by hydrothermally enriched fluids entering at the bottom of the lake. This influence is observed at a depth of ~350 m. South Basin near-bottom water (1-5 m above bottom) extends from the North Basin bottom water end-member (c), to waters of high heat to salt ratio (a), and to waters of low heat to salt ratio (b). All near-bottom temperature and salinity data collected from the South Basin during 1989 fall between the (a) and (b) T-S "arms" of Fig. II.7. In general, deep waters outside the South Basin have similar T-S characteristics to the North Basin (circles in Fig. II.7). These observations again support the hypothesis that the South Basin is a dominant source of hydrothermally enriched fluids observed throughout the hypolimnion (Williams and Von Herzen 1983; Dymond et al. 1989; Collier et al. 1990).

The lines in Fig. II.7 represent isopycnals (curves of constant density) relative to 465 dbars (474 m) and are calculated from the equation of state presented in Chen and Millero (1977a, b, 1986). These isopycnals illustrate that the density of the near-bottom fluids increases along both T-S arms and that the T-S extrema are vertically stable with respect to background deep water, ('c' in Fig. II.7).

The range of T-S combinations observed near the bottom of the South Basin are incompatible with a simple two end-member linear mixing of near bottom waters. Points along the line extending from (c) to (a) can be accounted for by mixtures of a warm salty end-member with background water. Points falling below this line, however, must be the result of an additional process or multiple end-member mixing. I suggest that small scale double diffusion could lead to curvature in the T-S

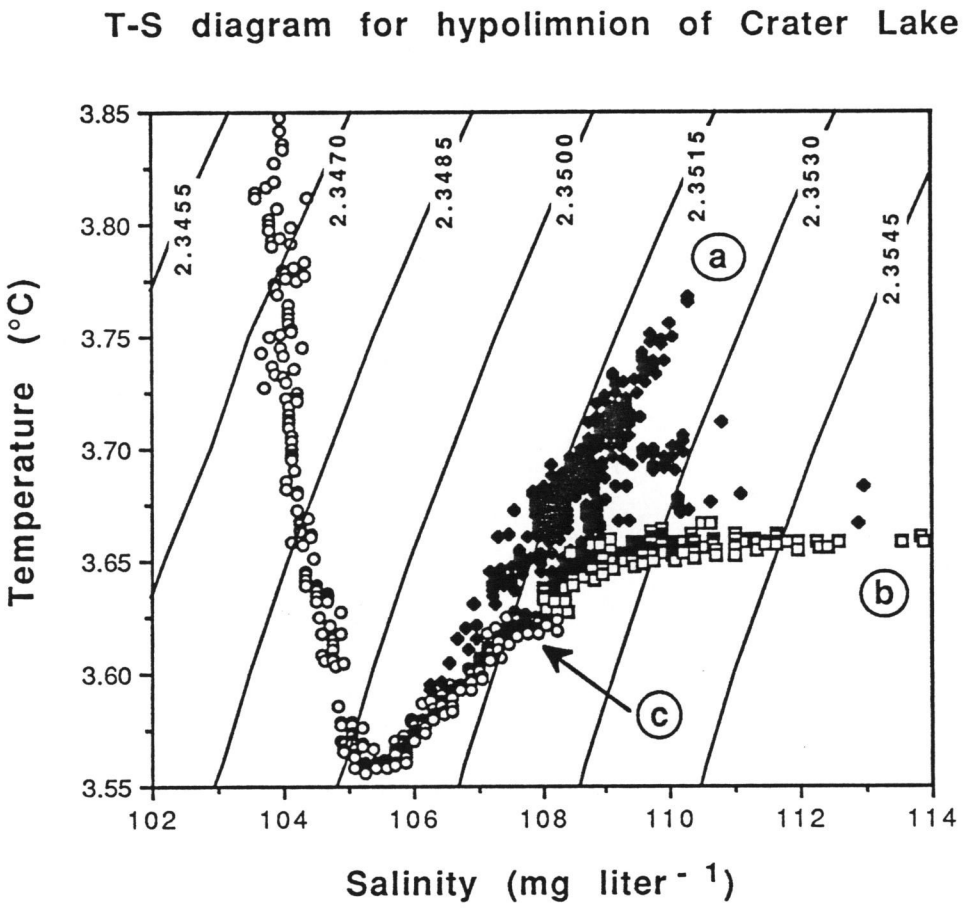

Fig. II.7. T-S diagram of the hypolimnion of Crater Lake. The circles represent North Basin deep water (c) with a bottom depth of 589 m and extending through the water column to a depth of 150 m (approximately 3.75 °C and 104 mg liter^{-1}). South basin deep water is represented by two T-S endmember "arms" where (a) represents water of high heat to salt ratio, and (b) represents water of low heat to salt ratio. Isopycnals are relative to a 465 dbar surface and are calculated using the equation of state of Chen and Millero (1977a, b, 1986).

distribution near the sediment-water interface. This curvature is apparent in the (c) to (b) trend in Fig. II.7. Curvature in the vertical T-S distribution in the ocean has previously been attributed to double diffusion (Ingham 1966; Schmitt 1981) and the theoretical basis for the curvature has been described by McDougall (1983). This mechanism would lead to the differing heat to salt ratios near the sediment-water interface due to the preferential loss of heat relative to salt through molecular diffusion. Heat diffuses two orders of magnitude faster than salt, so the heat to salt ratio of a fluid will decrease with time if diffusive fluxes dominate the evolution of these near-bottom fluids (McDougall 1983). Such a process could be occurring within the sediments/debris that covers much of the bottom of the southeastern portion of the South Basin (Barber and Nelson 1990). Alternatively, this process could be occurring within the water column on small vertical and horizontal scales.

The mechanism for the T-S distribution in the South Basin appears to operate over small spatial scales within the South Basin. If double diffusion were operating throughout the water column we would expect to observe "steplike" features in T and S as suggested by Newman (1976). Such features are not observed.

More elaborate models on the formation of these T-S endmembers will be presented elsewhere in relation to the physical limnology of Crater Lake. It is sufficient for the purposes of this chapter to demonstrate that the use of a precise definition for salinity permits recognition of distinct water sources in a limnological system which has otherwise been described as homogeneous.

In addition to the spatial variations in the T-S properties discussed above, there are also temporal variations in the deep-lake distributions of these properties which identify important mixing processes. These and other mixing phenomena will be examined in more detail elsewhere in a discussion of the overall physics of Crater Lake.

Water column stability is highly dependent on the total salt content when the temperature of the fluid is near the temperature of maximum density. Therefore, defining the temperature-conductivity-salinity relationship in deep lakes is critical to understanding the processes which control the redistribution of heat and salt through the water column.

CONCLUSIONS

In deep, well-mixed lakes, precise and accurate temperature and salinity measurements are essential for characterization of water column physical properties. If silicic acid represents a significant percentage of the total dissolved solids load in a system, it can be an important contributor to fluid density.

Without the high precision measurements employed here, the hypolimnion of Crater Lake would appear vertically and horizontally homogeneous. The data presented here have allowed us to identify active hydrothermal inputs which are responsible for an increase in temperature and salt with depth in the hypolimnion. The temperature and salinity gradients resulting from these inputs generally yield a stable water column. The horizontal heterogeneities in temperature and salinity and the increases in the temperature and salinity gradients near the bottom of the South Basin suggest that this portion of the lake is an area with the largest hydrothermal inputs.

An understanding of the physical processes which control the redistribution of heat and salt in deep lakes is essential to modeling the biogeochemical cycling of solutes in these lakes. The use of deep lakes such as the Great Lakes of North America or Lake Baikal as monitors of global change must include the precise determination of the physical properties of the water column of these lakes. I have outlined a method for the accurate determination of the physical properties of the water column in limnological systems and have demonstrated the utility of this method for Crater Lake, Oregon.

ACKNOWLEDGEMENTS

I acknowledge the generous help of Dennis Barstow at Oregon State University for his assistance with the calibration of the CTD and Mark Buktenica and his crew at Crater Lake National Park. This chapter benefited from comments by Dr. R.E. Stauffer at Limnology and Oceanography and two anonymous reviewers. This research was funded by the U.S. National Park Service under cooperative agreement No. CA 9000-3-0003, CPSU, College of Forestry, Oregon State University.

III. ON THE PHYSICAL LIMNOLOGY OF CRATER LAKE, OREGON: 1. MECHANISMS FOR THE REDISTRIBUTION OF HEAT AND SALT IN THE WATER COLUMN

ABSTRACT

The heat and salt budgets of the hypolimnion in Crater Lake, OR are dominated by subsurface hydrothermal activity. Based on a time-series of CTD data and data from a thermistor chain mooring, the net (conductive and convective) heat flow, due to hydrothermal activity, is estimated to be ~1 W m^{-2} and the corresponding salt flux is ~5 $\mu g\ m^{-2}\ sec^{-1}$. This chapter discusses the observation of these fluxes and the mechanisms and timescales of mixing responsible for the redistribution of these properties through the water column.

The annual vertical exchange of surface water with water from the deep lake occurs during the early winter and to some extent during late spring. This exchange mixes the heat and salt from the deep lake to the surface. Likewise, oxygen rich water from the surface is mixed with deep water, resulting in a net increase in deep lake dissolved oxygen at the time of mixing. This mixing process is not complete, that is, the deep lake does not reach atmospheric saturation with respect to dissolved oxygen at any time during the year. During periods of stratification of the upper water column, the active input of thermally and chemically enriched fluids produces heterogeneities and instabilities in the density structure of the deep lake which drive deep lake mixing. As a result of rapid horizontal and vertical mixing, hydrothermally-derived heat and salt are mixed through the deep lake over timescales of several weeks to months.

INTRODUCTION

Crater Lake, the deepest lake in the United States, is a caldera lake with a surface area of 53.2 km^2, which covers 78.5% of its total drainage basin. It is situated at an elevation of 1882 m above sea level and has a volume of 17.3 km^3 (Phillips 1968). Lake level has been nearly constant since, at least, the turn of the century (Redmond 1990). There are no riverine inputs or outputs to Crater Lake. Water enters the lake primarily through precipitation at a rate of ~4.2 m^3 sec^{-1} with approximately half of that total being removed by seepage (~2.1 m^3 sec^{-1}) and the remaining balance of the water being removed through evaporation (Redmond 1990). The lake has two semi-enclosed basins, one in the northeastern portion of the lake (referred to here as the North Basin) which has a maximum depth of approximately 590 m and the second in the southwestern section of the lake which has a maximum depth of approximately 485 m (South Basin, Fig. III.1).

An understanding of the physical processes which control the redistribution of heat and salt in Crater Lake is essential to modeling the biogeochemical cycling of elements in the lake. There are only a few studies of Crater Lake's physical limnology. Kibby et al. (1968) reported surface current observations as well as the vertical and horizontal distribution of temperature in the upper water column. Radioisotope data from Simpson (1970 a, b) and Volchok et al. (1970) indicate that the characteristic time-scale of deep lake ventilation is approximately one year. Neal et al. (1971, 1972) provided temperature microstructure measurements which demonstrated the hyperadiabatic nature of the thermal gradient of the deep lake. The term "hyperadiabatic" derives from the fact that the thermal gradient below 350 m in the deep lake is at least two orders of magnitude greater than the adiabatic gradient (Fig. III.2.). Williams and Von Herzen (1983) identified two areas of high heat flow along the sediment bottom; one in the North Basin near Merriam Cone (Fig. III.1), and a second in the South Basin where the highest heat flow measurements were recorded. Assuming a homogeneous salinity distribution, they discussed the apparent vertical instabilities and convection that would accompany the observed temperature distribution. Although the work of Williams and Von Herzen (1983) served as a catalyst to the current work, a lack of high precision salt determinations limited their ability to interpret the temperature microstructure of the hypolimnion in Crater Lake. The research outlined in this thesis has provided both the high precision temperature and salinity data which are necessary

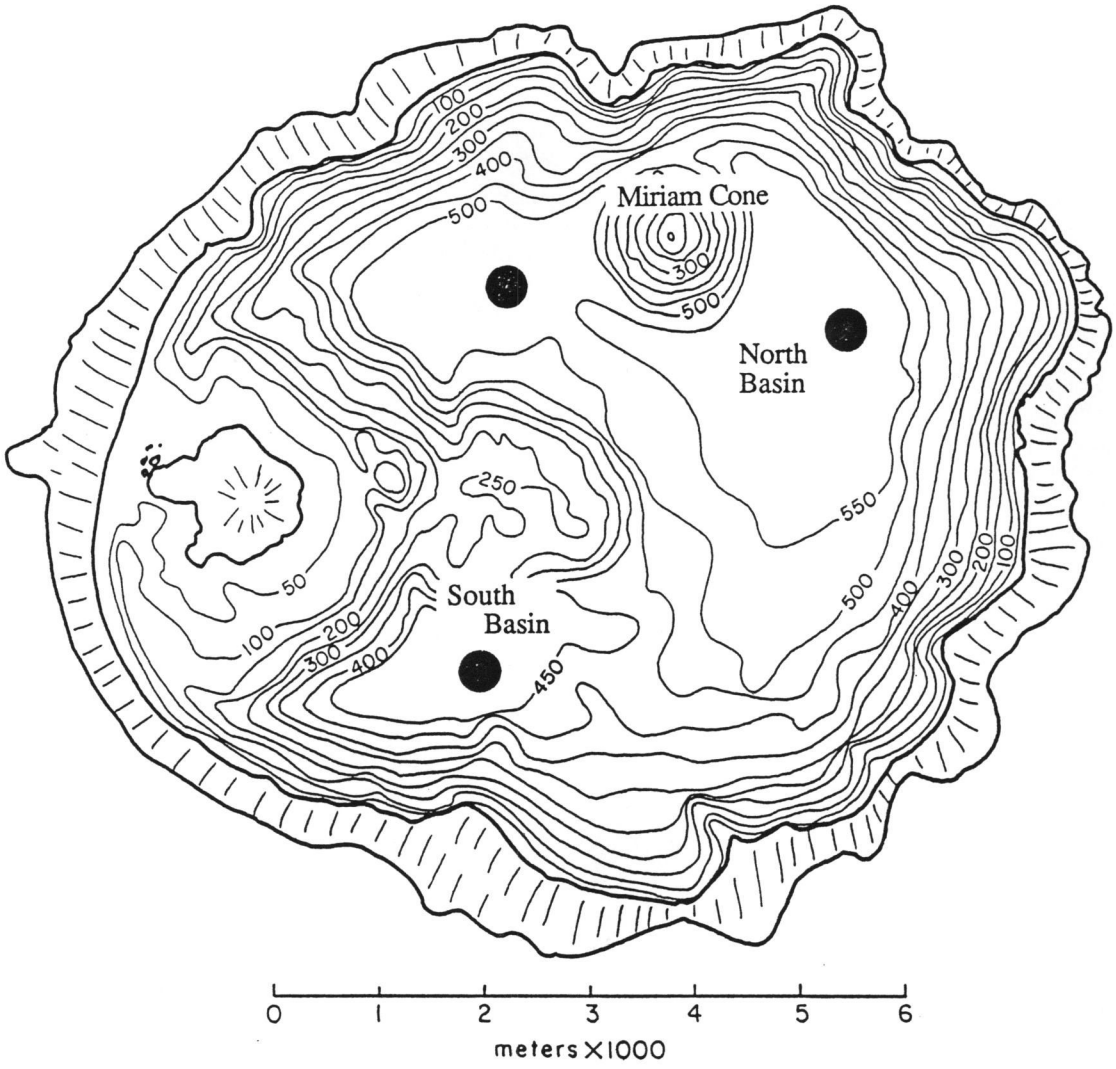

Fig. III.1. Bathymetric map of Crater Lake, OR with geologic features. Large dots represent approximate locations of time series monitoring stations: Station 23 located in the South Basin; Station 13 located in the North Basin; Station 11 located in the northwest portion of the lake. The bathymetry is taken from Byrne (1965).

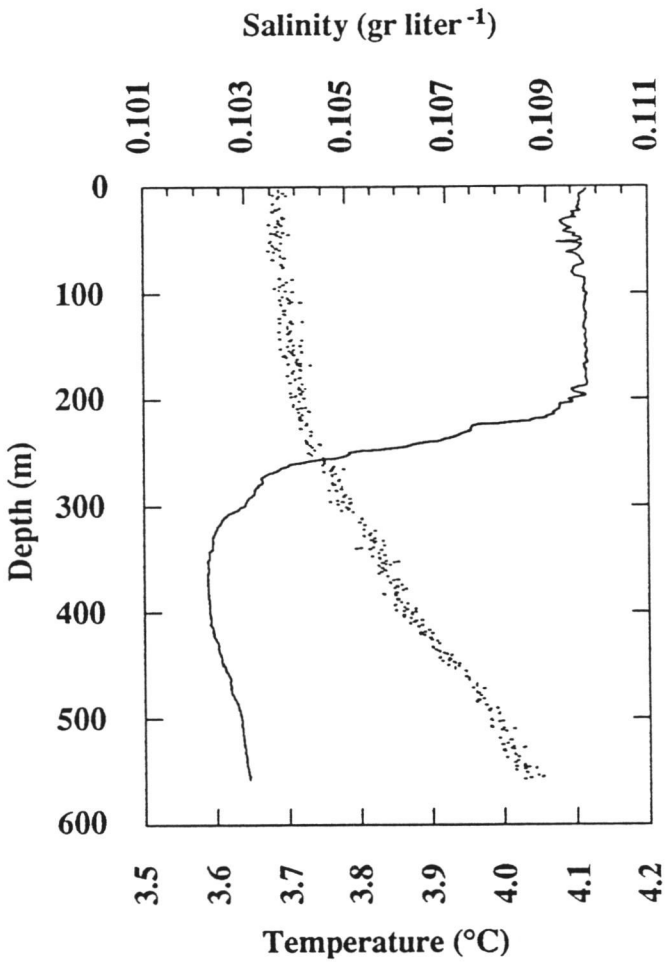

Fig. III.2. Salinity (gr liter^{-1}) and temperature (°C) as a function of depth. Data was taken from the North Basin on 19 January 1990. Note the near-uniform salinity of the upper 200 m and the increase in temperature and salinity with depth below ~350 m.

for the accurate determination of the physical properties and the mixing dynamics of the lake (Chapter II; McManus et al., in press).

Although, to a first approximation, Crater Lake is well mixed with respect to major ions (Collier et al. 1990a; Nathenson 1990; Thompson et al. 1990; Nathenson and Thompson 1990; McManus et al. in press) data presented here document a salinity gradient below 200 m at all times (Fig. III.2). Because of the active input of hydrothermal fluid and the transport of this fluid throughout the deep lake, both the salinity and temperature gradients of the deep water column exhibit spatial and temporal variability. The primary source of the thermally and chemically enriched fluids appears to be located deep within the South Basin (Williams and Von Herzen 1983; Dymond et al. 1989; Collier et al. 1990; McManus et al. in press). Variability in the vertical and horizontal temperature and salinity distribution occurs over timescales of weeks, suggesting that the hydrothermal fluid is mixed relatively rapidly throughout the deep lake.

In this chapter I define the magnitude of the hydrothermally-derived heat and salt fluxes to the deep lake through a time-series of temperature and salinity measurements. In addition, I will discuss how this heat and salt is mixed throughout the deep lake. Toward this end, I will examine mixing processes in the upper lake during seasonal changes in stratification. I will then estimate the degree to which water is mixed from the surface layer to the deep lake during periods of minimum surface stratification, and I will present data which demonstrates the mechanism for deep lake ventilation. Finally, I will discuss how the hydrothermally enriched waters are mixed during periods of maximum surface stratification.

METHODS

Temperature, pressure, and conductivity were measured using a CTD ("conductivity, temperature, depth" recording instrument, SEACAT® model SBE19, Sea-Bird Electronics Inc.) modified for low conductivity waters. The CTD records all data internally at 2 scans per second. Temperature resolution is ±0.0005 °C and, based on laboratory triple point calibrations of the temperature sensor, the absolute accuracy of the temperature sensor was better than 0.001°C from 1987 to 1989. Laboratory calibration of the conductivity sensor using Crater Lake water and subsequent chemical analysis of this water provided sufficient salinity, conductivity, and temperature data to obtain an expression for salinity as a function of in situ conductivity and temperature (Chapter II). Salinities calculated from this expression are ~25% greater than would be predicted from strong electrolytes alone. This is because silicic acid accounts for approximately 25% of the total dissolved solids in the lake. The details of the experiments and further explanation of the affects of silicic acid on the density of Crater Lake water are presented in Chapter II.

The CTD was deployed on a hydrographic wire lowered from the NPS research boat. The time-series of hydrographic data presented in this chapter was collected in the northeastern portion of the North Basin (National Park Service [NPS] station 13), the South Basin, NPS station 23, and in the northwestern portion of the lake, NPS station 11 (Fig. III.1). A time-series of temperature data was also collected using two moored thermistor chains deployed in the South Basin from 3 September 1989 until July 1990. One chain (TC1084) was located at 50-150 m depth, and the other (TC8) extended from 350 m to the bottom (450 m). The chains were equipped with 11 thermistors spaced at 10 meter intervals. Temperature data was recorded every three hours throughout deployment and the thermistors were calibrated at the OSU calibration facility both before and after deployment. The absolute accuracy of the thermistors is ±0.010 °C and the in-field precision, based on daily temperature measurements from the deep lake, is ±0.005 °C.

The dissolved oxygen contents of water samples was determined using a whole-flask Winkler titration method with the modifications of Carpenter (1965 a, b). The overall precision of the oxygen measurement is based on the percent difference between duplicate sample analysis and is better than 0.5%. The equations presented in Benson and Krause (1984) were employed to determine the solubility of dissolved oxygen in

Crater Lake. The mean atmospheric pressure at the lake surface was calculated from the altitude-dependent equation given by Mortimer (1981).

HEAT AND SALT FLUX INTO THE DEEP LAKE

A time-series of CTD data and data from a thermistor chain mooring indicate that there is a consistent input of heat and salt into the deep hypolimnion of Crater Lake. This is demonstrated in the deep lake by the gradual increase in temperature over time observed during periods of surface stratification (Fig. III.3).

Integrated values for the flux of heat and salt are calculated from the time-series of CTD data (McManus et al. 1990). This is accomplished by integrating the area under a vertical profile (either salinity or temperature) and subtracting the area under a profile taken at the same location at an earlier time. For instance, the integrated temperature change between 17 July and 17 August below 350 m (Fig. III.3) is converted to a net heat flux. Each flux calculation represents a volume-weighted average of CTD data from the three monitoring stations (Fig. III.1), and basin volumes were determined from the hypsographic curve presented in Byrne (1965).

The rate of deep lake warming can also be estimated using deep lake temperature data from the thermistor chain moored within the South Basin. This is accomplished in a manner similar to the treatment of the CTD data by calculating the change in temperature between 440 and 350 m during periods of surface stratification. To demonstrate the warming of the deep lake I show an expanded-scale plot of temperature versus time for the thermistor deployed at 410 m (Fig. III.4). The arrows indicate deep lake warming during periods of upper water column stability (fall and late spring/early summer). During winter there is some cooling of the deep waters which is associated with deep lake ventilation; this process will be discussed later in the text.

The results of these calculations for heat and salt flux are presented in Table III.1. The heat and salt flux values are for discrete time intervals during a given year and the flux values represent differences between two profiles separated in time by at least several weeks. My method of calculating the net heat flux yields results which agree with those of Williams and Von Herzen (1983) who reported values between 0.7 and 1.4 W m^{-2}.

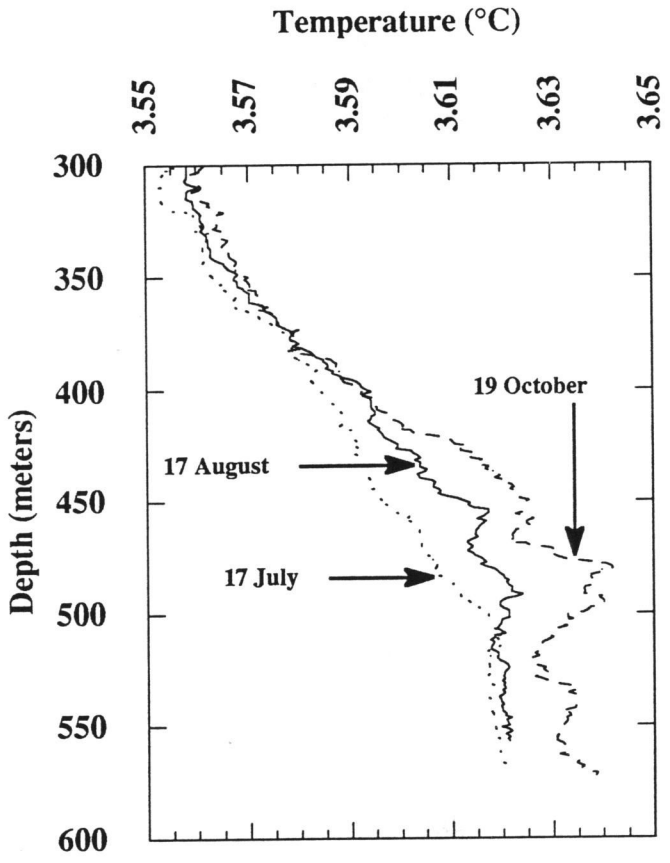

Fig. III.3. Temperature as a function of depth in time series. This CTD data was taken from the North Basin. The data demonstrates the accumulation of heat in the hypolimnion throughout the summer months.

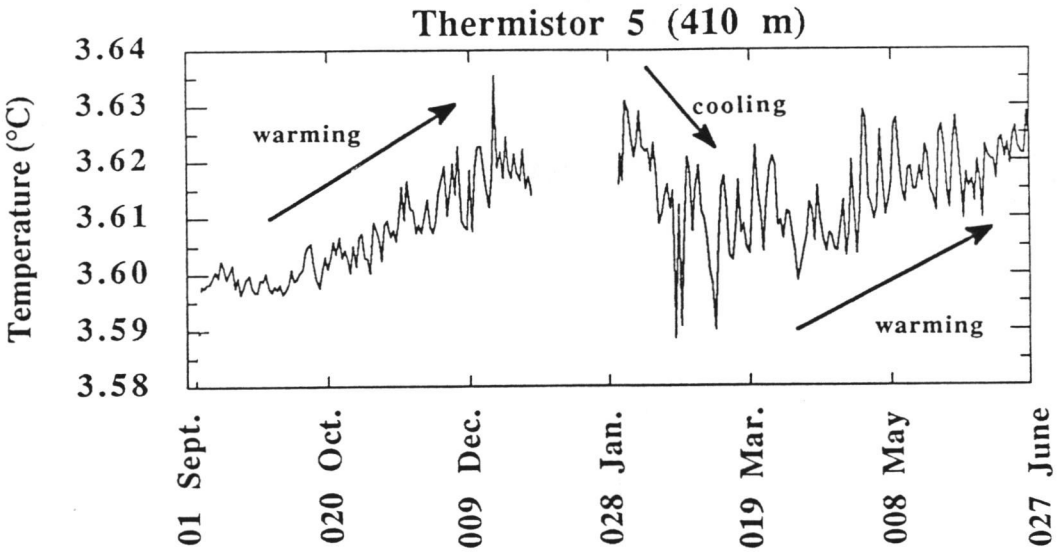

Fig. III.4. Temperature as a function of time from the thermistor at 410 m depth in the South Basin from September 1989 to July 1990. The figure demonstrates the warming due to the constant input of heat from hydrothermal activity and the cooling due to winter mixing. The absence of data apparent in Figure 4 marks a period of time of recorder malfunction.

Table III.1. Heat Flux, Salt Flux, and Fluid Flow

Year/ season**	Method	Heat Flux ($W\ m^{-2}$)	Salt Flux ($\mu g\ m^{-2} \cdot sec$)	Fluid flow ($liters\ sec^{-1}$)
1989/S	CTD	0.9 ± 0.5	4.2 ± 2.5	141±84
1989/F	Thermistor	1.0 ± 0.3	N/A	N/A
1990/Sp	Thermistor	1.2 ± 0.6	N/A	N/A
1990/ES	CTD	0.9 ± 0.2	5.2 ± 3.0	254±146
1990/LS	CTD	1.0 ± 0.4	5.7 ± 3.0	278±146

***S, F, and Sp represent summer, fall, and spring respectively where E and L are early and late respectively.*
For 1989, I used 22.9 km^2 as the surface area of the lake over which the integration was calculated, and for 1990 I used 20.2 km^2.

Fluid flow (Table III.1) is estimated directly from the salt flux values. In calculating the fluid flow, I have assumed that the salinity of the hydrothermal fluid is 0.6 gr kg^{-1} as it enters the South Basin. This salinity value is based on pore water chemistry data (Wheat, unpublished) and the chemical composition of brines which are found at the source of the thermal inputs in the South Basin (Collier et al. 1990b). The estimates of fluid flow are consistent with other values suggested by Nathenson (1990), 80-1900 liters sec^{-1}. Because there may be variations in the end-member composition, the estimated flow rates should only be taken as rough estimates of the net fluid flow associated with these inputs.

Although the annual fluid input due to hydrothermal activity is small compared to the lake volume (17.3 km^3), the fluid flow rate given in Table III.1 (~0.2 $m^3\ sec^{-1}$) is large (~5%) compared to the annual input of water due to precipitation (~4.2 $m^3\ sec^{-1}$, Redmond 1990). Since the hydrothermal fluid is rich in salt relative to precipitation, the input of this high-salinity fluid will have a dominant effect on the salt budget. A more detailed treatment of the geochemical budgets will be presented elsewhere. It is

sufficient for the purposes of this chapter to point out that hydrothermal activity is the dominant source of salt to Crater Lake.

The data presented here represent the first direct observations of the accumulation of heat and salt over time in the deep water column of Crater Lake, OR. Despite the uncertainties in the calculations, the method for estimating heat flux, salt flux and fluid flow confirm and refine the previously reported values.

VERTICAL MIXING OF HEAT AND SALT

During periods of reduced vertical stability of the water column, some deep lake water is mixed with surface water. This mixing results in the exchange of thermally and chemically enriched water from the deep lake with cooler, lower salinity, surface water. Since deep lake water is rich in biochemically important nutrients, particularly dissolved nitrate (Chapter V), this exchange is critical to new biological productivity in the upper 200 m. Such exchange also carries cooler, oxygen rich waters from the surface to the hypolimnion. Therefore, changes in the dissolved oxygen content of the deep lake provides an estimate of the degree to which surface-to-bottom exchange has occurred. For example, if at any period the entire lake were to reach atmospheric saturation with respect to dissolved oxygen, it could then be concluded that all of the waters have come into contact with the surface during a single mixing period.

In the following sections I will examine three stages of vertical mixing in Crater Lake; the breakdown of the seasonal thermocline, inverse stratification, and the mixing of surface water with deep water, which takes place during a minimum in water column vertical stability.

Breakdown of the seasonal thermocline

Most temperate lakes undergo three stages of cooling; the breakdown of the seasonal thermocline, isothermal overturn, and inverse stratification (Carmack and Farmer 1982). The breakdown of the thermocline is characterized by a decrease in the surface density gradient and an increase in the depth of the surface mixed layer. In many deep lakes, continued wind mixing and cold-water convection results in an isothermal water column near the temperature of maximum density. This is followed by surface restratification due to continued cooling of the surface. However, for very deep lakes like Crater Lake, the full water column is rarely isothermal. This is due to the fact that the temperature of maximum density decreases at a rate of approximately 0.02 °C bar^{-1} (~0.002 °C m^{-1}). Thus, waters near their density maximum at the surface will not be able to undergo free convection to the lake bottom. The maximum depth of complete mixing in deep lakes is therefore influenced by the in situ physical properties of lake water which influence the depth of free convection, as well as wind forcing.

The upper water column of Crater Lake begins to undergo destratification in early fall as the density of the surface water increases due to cooling. As the

Fig. III.5. Upper water column thermistor data demonstrating the change in temperature over time. Thermistors were spaced at 10 m intervals between 50 and 150 m; here we show the 50, 100, and 150 m thermistor as examples. During the breakdown of stratification, warm water from above is mixed with ambient (cooler) water resulting in a net increase in water temperature (arrows).

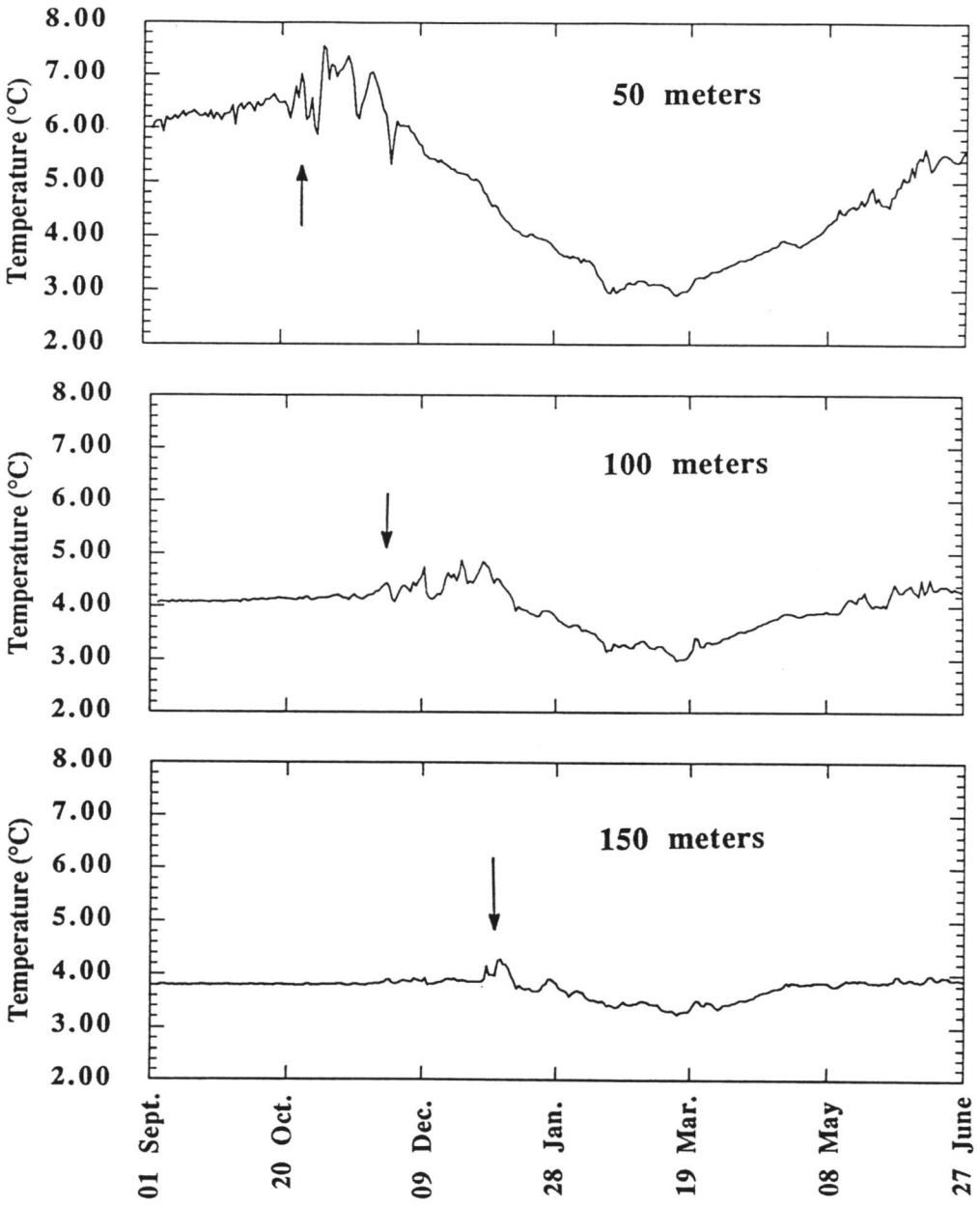
50 meters
100 meters
150 meters
Temperature (°C)
8.00
7.00
6.00
5.00
4.00
3.00
2.00
01 Sept.
20 Oct.
09 Dec.
28 Jan.
19 Mar.
08 May
27 June

Figure III.5

thermocline breaks down, mixing of the surface water with water below causes an initial increase in temperature at depth (i.e. arrows in Fig. III.5). This mixing is driven by wind mixing at the surface and convection of the surface water as it cools. The increase in temperature is seen at 90 m by late December (Fig. III.6a). By mid-January this warming signal has penetrated to >150 m (Fig. III.6b). At this time, at least the entire upper 150 m are isothermal and the mixed layer reaches depths of, at least, 200 m (Fig. III.2) during this period.

The rate of penetration of the mixed layer also reflects the stronger stratification initially present in the upper 100 m as compared to the 100-150 meter depth range. Between 50 and 90 m, the base of the mixed layer descends through the water column at a rate of approximately 1 m day^{-1} until it reaches ~90 m (Fig. III.5 and III.6). The rate of mixed layer deepening from 100 m to 130 m increases to ~8 m day^{-1}. Although the data are inadequate to accurately determine the descent rate below this depth, the rate appears to be between 10 and 20 m day^{-1}. In Babine Lake, Carmack and Farmer (1982) found the mixed layer penetration rate to be ~0.4 m day^{-1} at the surface and found it to increase to rates as high as 20 m day^{-1} during the later stages of mixed layer deepening. It is surprising that the rate of mixed layer formation in Crater Lake, a sheltered near-circular lake with a maximum fetch of 10 km, is similar to that in Babine Lake, which is 150 km in length, 4 km in width, and has a maximum depth of 230 m. The similarities between the two lakes emphasize the importance of convection during the breakdown of the seasonal thermocline and formation of the winter mixed layer in freshwater systems.

Inverse stratification

After the initial mixing, which results in an increase in temperature at the deeper levels of the thermocline, continued winter cooling causes a gradual decrease in the temperature of the upper water column. During the winter of 1990 this cooling continued until mid-March (Fig. III.5). By early April water column warming was occurring at depths >50 m. Once the temperature profile crossed the T_{md} in mid-April, thermocline development began.

Since the surface waters are still colder than the T_{md} in early April, initial warming produces parcels of water of greater density which drive convection. This process is demonstrated by temperature profiles obtained with the CTD from early May 1989 (Fig. III.7). The surface waters are heated during the day, forming convective

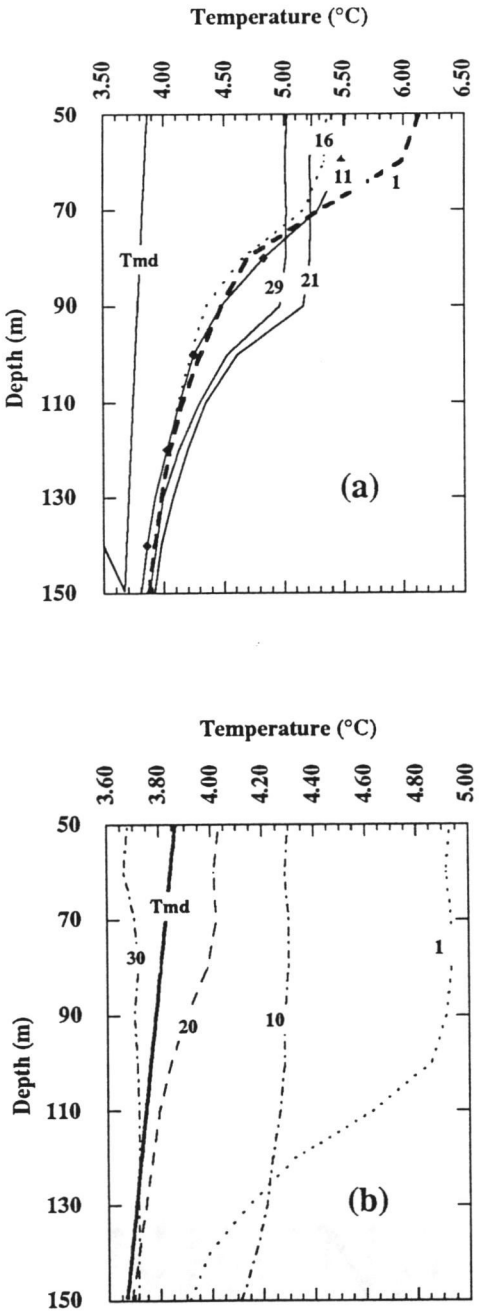

Fig. III.6. Temperature as a function of depth in the upper part of the water column for (a) December and (b) January. Data are taken from the thermistor chain between 50 and 150 m and demonstrates the results of the breakdown of thermal stratification in the upper 200 m.

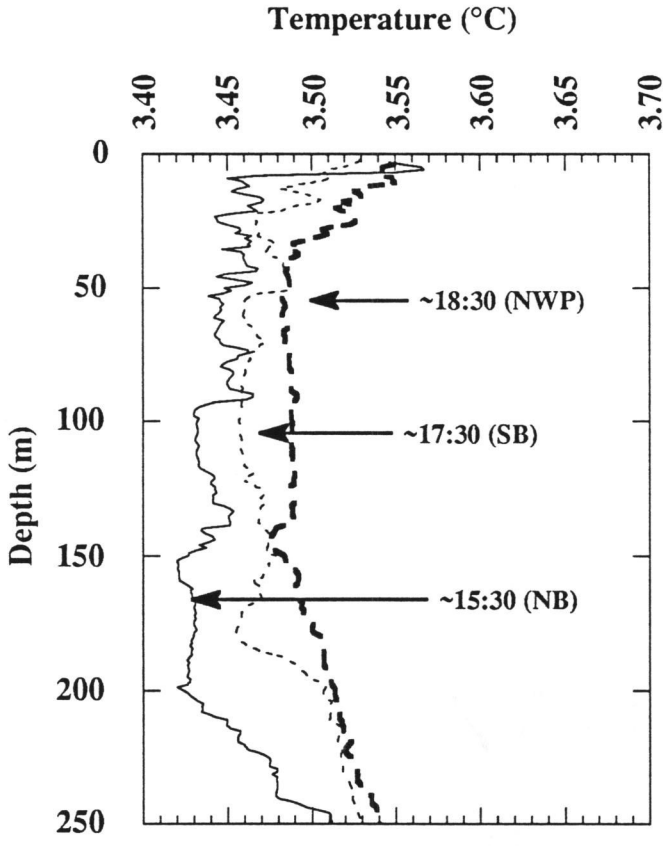

Fig. III.7. One day time series of temperature vs. depth for Crater Lake taken in May 1989. The figure demonstrates convective warming in the late afternoon (solid line), the gradual slowing of the convection by early evening (dotted line), and the near-uniform temperature profile by sunset (heavy dashed line). NB represents North Basin; SB South Basin; and NWP represents the northwest portion of the lake.

cells which sink throughout the course of the day (solid line Fig. III.7). This continued process warms the entire water column through which convection may occur leaving a warmer column of near-uniform temperature water at the end of the day (dashed line Fig. III.7). The three profiles in Fig. III.7 were taken from the three different monitoring stations (Fig. III.1) on 11 May and some of the differences are due to horizontal variations in mixing and heating. Therefore, the net warming apparent between the three profiles can not be used to estimate a one-dimensional heat input into the upper lake.

Spring heating of the water column results in a cycle of warmer temperatures during the day and cooler temperatures at night in the thermistor record of the upper water column (Fig. III.8). The maxima in daily water temperature at 50 m during the month of April are recorded at 1300 and the minima between 0100 and 0500. As the temperature of the upper lake approaches the temperature of maximum density at 50 m (~April 20), the upper water column becomes nearly isothermal at about 3.9°C (Fig. III.8). After this point (~1 May), rapid warming of the surface waters leads to a stratified water column, thereby isolating the deeper waters as suggested by the near-constant water temperature at 100 m until approximately 10 May. After approximately 10 May, large variations in the daily water column temperatures are observed. These fluctuations are probably driven by a combination of storms, surface driven convection due to cooling, strong horizontal thermal gradients, and other upper water column mixing processes.

Of particular importance with respect to this work is the relative speed with which the water column undergoes restratification in the spring. Once the upper waters are restratified, mixing between the upper and deep lake can no longer occur. Storms occurring during periods of minimum stability, i.e. while the water column temperature is closest to the T_{md} as is seen on 10 May, may provide the impetus for deep mixing, as is discussed in the following section. Climate variability will therefore influence deep mixing in the spring, as well as during the fall/winter.

A more detailed study of the upper water column-atmosphere interactions should include thermistors which extend to the surface as well as detailed meteorological data. In addition future modeling efforts should accurately represent convection as well as shear induced mixing. For the purposes of this work it is important to point out that the upper 200 m of the water column in Crater Lake is well-mixed twice annually (winter and late spring). During these periods of mixing, both CTD measurements and thermistor data indicate that the upper 200 m of the water column is isothermal.

Fig. III.8. April - May expanded scale thermistor chain data (TC1084). Data is from 50 (top) and 100 meters (bottom). The temperature of maximum density (Tmd) was calculated from the equation of state for fresh water(Chen and Millero 1986).

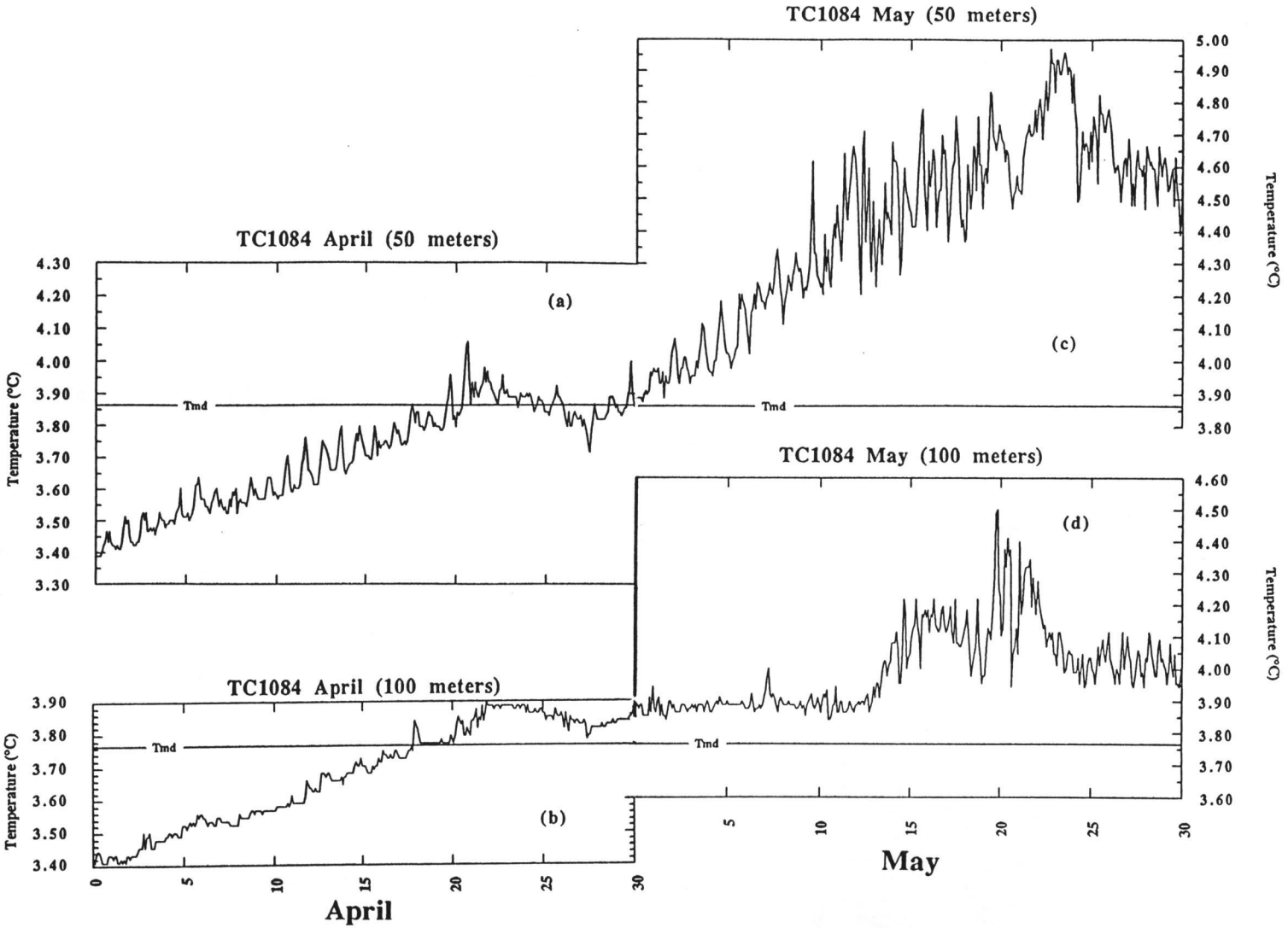
TC1084 May (50 meters)
TC1084 April (50 meters)
(a)
(c)
Tmd
Tmd
TC1084 May (100 meters)
(d)
TC1084 April (100 meters)
(b)
Tmd
Tmd
Temperature (°C)
Temperature (°C)
Temperature (°C)
Temperature (°C)
April
May

Figure III.8

It is remarkable that the mixed layer in Crater Lake achieves such great depths. The similarities in the rate of mixed layer deepening for Crater Lake and Babine lake appear to be a function of convective mixing. In addition, the fact that fresh water has a density maximum which is between 3 and 4 °C in the upper 200 m has an influence on mixing in deep lakes (Weiss et al. 1991).

Mixing of surface water with deep lake water

A time-series of dissolved oxygen data, CTD data, and thermistor chain data all indicate that some exchange of surface water (defined here as water from the upper 200 m) with deep water occurs in Crater Lake at least once a year. The data suggest that this annual mixing process is likely to be incomplete.

Dissolved oxygen is a useful tool for the study of mixing processes in lakes. The details of the oxygen budget of the deep lake will be discussed in Chapter V; however, it is sufficient for the purposes of this chapter to point out that deep oxygen consumption can occur by two processes. Dissolved oxygen is consumed by the decomposition of particulate organic material raining out of the euphotic zone. Also, in Crater Lake, reduced chemical inputs from hydrothermal activity contribute to the depletion of dissolved oxygen in the deep lake.

Convective mixing during the winter and spring tends to saturate the upper water column with dissolved oxygen (e.g. April oxygen profile in Fig. III.9). Because annual mixing of deep lake water with well-oxygenated surface water is the only mechanism that will increase the dissolved oxygen contents of the deep lake, changes in deep lake dissolved oxygen serve as a semi-quantitative measure of the extent of vertical mixing in Crater Lake.

Data collected from September 1988 and April 1989 demonstrate an increase in dissolved oxygen, measured at 550 m, of nearly 10 μmol liter^{-1} (Fig. III.9). Likewise, from January 1990 to July 1990 another increase in deep lake dissolved oxygen is observed, indicating that the ventilation process was again repeated during the winter and possibly spring of 1990. This mixing is, however, incomplete, leaving the deep lake undersaturated with respect to atmospheric saturation of dissolved oxygen at all times sampled. Mass balance calculations indicate that for the 1988-89 field season 30-45% of deep lake water was exchanged with aerated surface water. This implies a characteristic time scale of deep lake ventilation between 2 and 4 years.

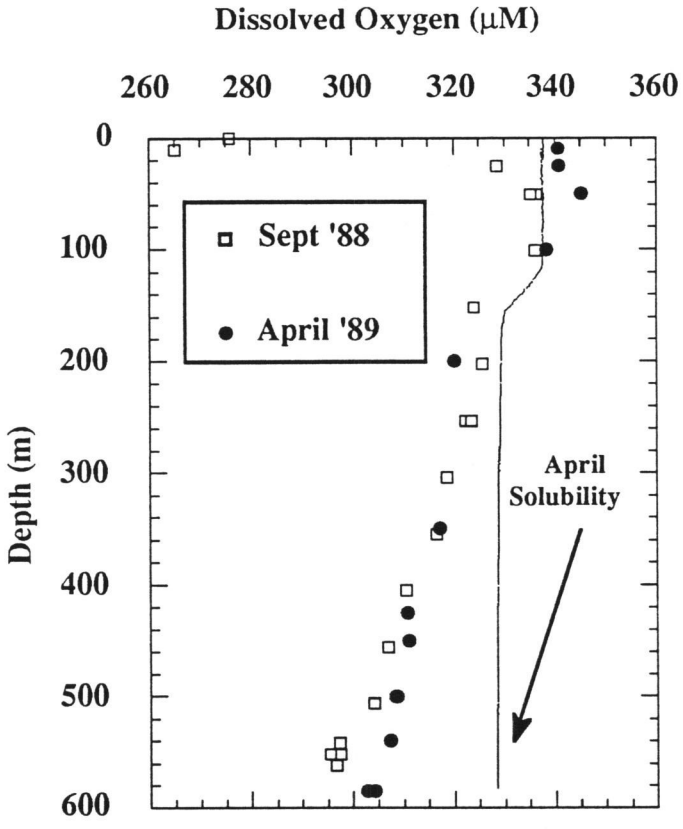

Fig. III.9. Expanded-scale dissolved oxygen as a function of depth for September 1988 and April 1989. Note that the measured dissolved oxygen is always within ~15% of the saturated value. The increase in oxygen from fall/winter to spring/summer can be seen for the deep lake. The line of oxygen solubility is for April and is calculated from equations presented in Benson and Krause (1984). Solubility is calculated with respect to atmospheric saturation of dissolved oxygen at the in situ temperature.

CTD data collected at the same time as the dissolved oxygen data and thermistor chain data also provide evidence for the exchange of surface water with water from the deep hypolimnion. A one dimensional approximation of the heat budget in the deep North Basin from January 1990 to July 1990 (Fig. III.10) indicates that a net loss of heat (225 kcal m^{-2}) occurred between January 1990 and July 1990 in North Basin deep water (> 475 m). This calculation simply represents the difference in the heat contents of the deep North Basin between January and July 1990. This loss of heat is due to the transfer of the warmer deep water upward, providing further evidence for exchange between surface and deep waters. These findings are also consistent with the deep water cooling evident in the thermistor chain data collected from the South Basin (Fig. III.4).

The deep lake thermistor chain data imply that deep lake vertical mixing lasted approximately one month during the winter of 1990 (Fig. III.4). Most of the thermistors in this chain recorded the maximum in deep lake temperature in early February. After this time the deep lake underwent cooling until it again began to warm. Water column cooling occurs during a period of reduced upper water column stability which is due to a reduction in stratification as described in the previous sections. During a minimum in water column stability cold waters from the upper 200-300 m exchange with the deeper warmer waters.

There are two phases of deep lake mixing which are illustrated in Fig. III.11 (a) a turbulent diffusion phase, and (b) a sudden or episodic convective mixing phase. The gradual decrease in temperature between 1 February and 20 February, over the depth interval 350 to 420 m is a result of mixing the colder water from above with the deeper warm water and can be modeled with a turbulent diffusion model:

$$F_H(z,t) = \int_0^z \rho C \left(\partial T[z,t]/\partial t\right)_z \, dz \qquad \text{(III.1)}$$

and

$$F_H(z,t) = -\rho C \, K[z,t] \left(\partial T[z,t]/\partial z\right)_t \qquad \text{(III.2)}$$

In eqn. III.1 and III.2, F_H is the heat flux, $\partial T/\partial z$ and $\partial T/\partial t$ are the slopes of the temperature versus depth and temperature versus time relationships respectively (Li 1973), and ρ and C are the density and the specific heat capacity respectively. The vertical diffusion coefficient (K[z,t]) evaluated from this data is 1.5 - 2 x 10^{-3} m^2 sec^{-1}.

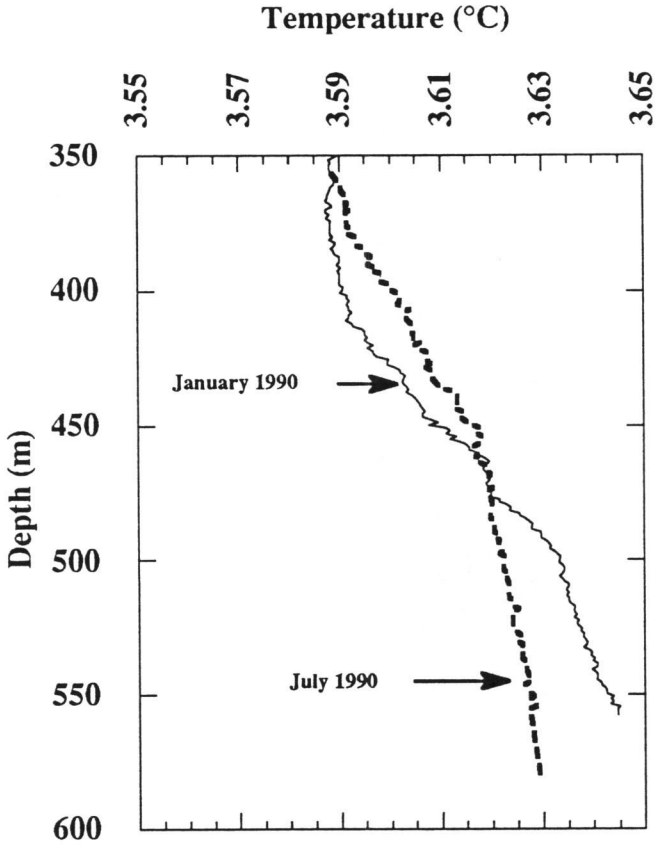

Fig. III.10. Temperature as a function of depth for January 1990 and July 1990. The cooling of the deep water column due to the exchange of surface water with deep lake water during the winter results in a lower total heat content of the deep water measured in July 1990.

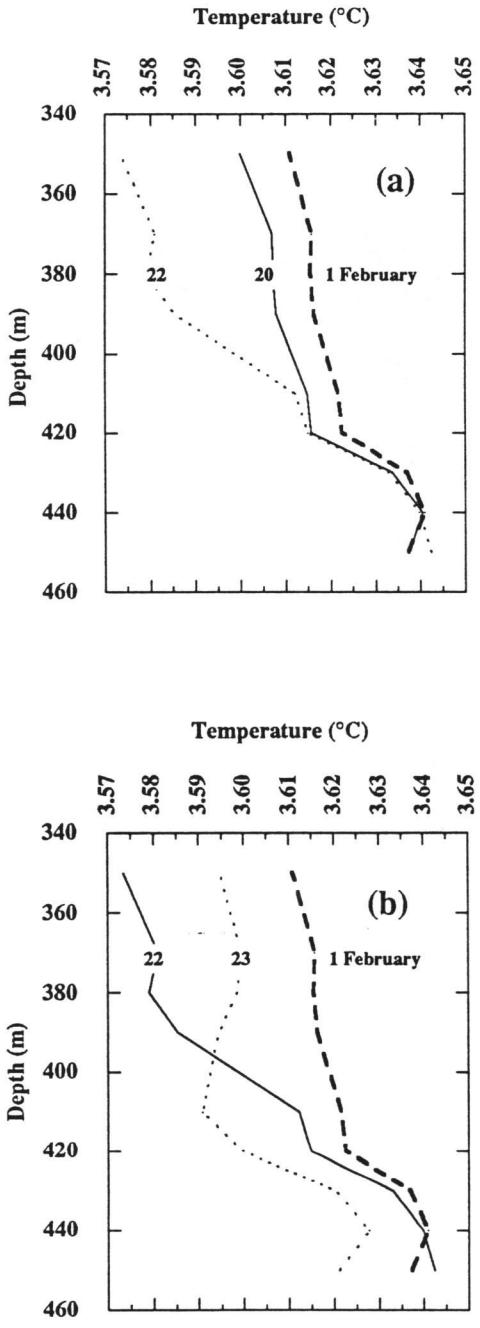

Fig. III.11. (a) Temperature as a function of depth for 1, 20, and 22 February. (b) Temperature vs depth for 1, 22, and 23 February. In (a) the diffusion of cold water from above dominates the mixing process from 1 February to 20 February. This is followed by the development of an unstable deep water column due to the accelerated (sudden) mixing of cold water from above.

I will compare this diffusion coefficient to the effective diffusion coefficient calculated for the hypolimnion during periods of high surface stratification, later in this chapter.

I hypothesize that the majority of the exchange between surface and deep water occurs via a mechanism which is similar to that proposed by Farmer and Carmack (1981), Carmack and Farmer (1982), Carmack et al. (1989), Carmack and Weiss (1991), and Weiss et al. (1991). This mechanism relies on the effects of pressure on the temperature of maximum density and has therefore been termed "thermobaric instability" (Carmack et al. 1989; Carmack and Weiss 1991). Since the temperature of maximum density decreases with increasing pressure, colder water overlying warmer water becomes "conditionally unstable" with respect to water immediately below. Wind forcing and/or internal waves displace a water parcel vertically to a depth where its temperature is closer to the temperature of maximum density than the ambient water at that depth. Once the parcel is displaced, it will continue to descend through the water column, because of its greater density relative to the surrounding water, until it reaches a point of neutral stability.

A requirement for the deep penetration of a water parcel is that $\Delta S\ \Delta z^{-1}$ (the vertical salinity gradient) is approximately equal to zero or is negligible compared to the temperature and pressure effects on the density of adjacent water parcels. In Lake Baikal, U.S.S.R., where the results of this process have been dramatically demonstrated, this requirement is satisfied (Carmack et al. 1989; Carmack and Weiss 1991; Weiss et al. 1991; Falkner et al. 1991). There, surface water descends through the water column to near-bottom depths with a well-preserved surface signature in temperature, dissolved oxygen, and other geochemical tracers (Carmack and Weiss 1991; Weiss et al. 1991). In Crater Lake between the depths of 200 and 400 m, the approximation of $\Delta S\ \Delta z^{-1} = 0$ may hold; however, the gradual increases in salinity below this depth range will increase the density of the ambient fluid making exchange of the colder, less salty fluids (upper waters) with the warmer, saltier fluids more difficult.

Using estimates of the salinity gradient obtained from January 1990 CTD data and the thermistor data presented in Fig. III.11a, the densities, relative to 400 dbars, of the waters above 390 m are calculated to be more dense than the waters below 400 m. The temperature profile for the following day shows that there has been some apparent exchange between the colder water from above and the warmer water below, resulting in colder waters now underlying warmer water (Fig. III.11b). In the subsequent days there are rapid changes in the vertical temperature distribution in this part of the water column, eventually resulting in a stable density gradient. It is also apparent from the

figure that the near-bottom waters have not been mixed to the same degree as the waters above 420 m. The net effect of mixing dense cold waters from above with warm, salty waters from below, is that any instability-driven mixing decreases in effectiveness with increasing depth in Crater Lake due to the resisting force of the salinity gradient. In addition, the surface temperature and oxygen signal will simply decrease as it is mixed with ambient waters during its decent to the deep lake.

It is reasonable to expect that the magnitude or effectiveness of this type of mixing will vary from year to year. As surface waters cool below the temperature of maximum density, the upper waters become restratified. The rate of cooling and restratification of the upper water will influence the "completeness" of deep water ventilation. This ventilation is more likely to occur during the winter mixing phase rather than in the spring. Although thermally-driven convection will also occur during spring warming, calmer weather conditions at Crater Lake typically dominate during spring. Thus, heating of surface water occurs fairly rapidly thereby making vertical exchange less likely or less efficient during this period. Year to year climate variations will therefore affect the extent of annual vertical exchange. This has recently been demonstrated by McCormick (1990) who finds that circulation models coupled with global climate models predict that during warmer years, Lake Michigan may not completely turnover and a permanent thermocline may form in the deep regions of the lake.

The oxygen and temperature data presented here suggest that the annual exchange of surface water with deep water is a critical process for the vertical redistribution of heat and salt in the lake. It is difficult to predict the annual magnitude or extent of this mixing process in the water column without a yearly time-series of data. It is likely that a comprehensive model of surface-to-bottom exchange is impossible without detailed meteorological data as well as water column chemistry and temperature data. Pearle et al. (1975) used the appearance of nitrate enrichments in the surface water to estimate the timing of turnover; unfortunately, this approach can not be applied to the Crater Lake system without nitrate data collected more frequently throughout the year. Crater Lake's inaccessibility makes this method difficult. Some enrichments in surface nitrate have been observed during early April in the upper isothermal layer (G. Larson 1988); however, it is not clear if these observed surface enrichments are due to bottom water upwelling, atmospheric inputs, or some combination of the two.

TRANSPORT OF HEAT AND SALT THROUGH THE DEEP LAKE

In this section I examine the processes of heat and salt transport through the hypolimnion during periods of surface stratification. Because Crater Lake is a bottom heated, salt stabilized system I will first explore double diffusive convection as a possible mechanism for the vertical transport of heat and salt through the water column. In determining the significance of double diffusion, I examine the theory behind the evaluation of double diffusive fluxes, how this flux is associated with layering, and compare the theory with the observations of Crater Lake. It is found that double diffusion can not account for the heat and salt flux observed through the water column in Crater Lake. Having evaluated the significance of double diffusion within Crater Lake, I will suggest alternative mixing mechanisms that can account for the necessary horizontal and vertical mixing.

Analysis of the significance of double diffusive convection in the water column

In cases where the vertical gradients of temperature (T) and salt (S) both increase with depth "staircase" features in T and S are often observed (Newman 1976). These staircase features are turbulent layers, where T and S are well-mixed vertically, which are separated by sharp density interfaces above and below each layer (Turner 1965). The fluxes of heat and salt across these density interfaces rely on molecular diffusion (Huppert 1971; Marmorino and Caldwell 1976; Padman and Dillon 1989).

The evaluation of double diffusive convection is dependent upon the differing molecular diffusivities between heat and salt in lake water and the density ratio;

$$R\rho = \frac{\beta \Delta S_z}{\alpha \Delta T_z} \qquad \text{(III.3)}$$

(Kelley, 1990) where $\beta = \rho^{-1}(\partial\rho/\partial S)$, $\alpha = -\rho^{-1}(\partial\rho/\partial T)$, and ΔS_z and ΔT_z are the observed salinity and temperature gradients respectively. Although the increase in temperature with increasing depth provides a destablizing force on the density profile in Crater Lake, the density profile is statically stable. This is because increases in salt with depth provide sufficient stabilization for the density to increase with increasing depth (i.e. $R\rho > 1$).

Reformulation of the double diffusive flux laws and their components is the subject of on-going research (see Kelley 1990). For the purposes of this study I will employ the traditional 4/3 flux law of Turner (1973);

$$\alpha F_T = c(g\kappa/\nu)^{1/3}(\alpha\Delta T)^{4/3} \qquad \text{(III.4)}$$

and

$$\beta F_S = \alpha F_T \gamma \qquad \text{(III.5)}$$

where F_T (°C m sec^{-1}) is the vertical flux of temperature associated with double diffusion and is easily converted to heat flux F_H (W m^{-2}) by $F_H = \rho C_p F_T$, where ρ is the density and C_p is the heat capacity of the fluid, F_S is the vertical flux of salt (g m^{-2} s^{-1}), g the gravitational constant, κ the thermal diffusivity, ν the kinematic viscosity, c is the thermal flux factor which is an empirically derived quantity and is a function of the density ratio, and γ is the diffusive flux ratio which is also empirically determined as a function of the density ratio ($R\rho$). The variation of γ with the density ratio expresses the changes in the ratio of salt diffusivity to thermal diffusivity with increased mechanical mixing. Kelley (1988, 1990) points out that the 4/3 flux law of Turner (1973) could overestimate the actual property flux by 34%, this will prove to be of little consequence to the arguments developed here. I employ Kelley's (1990) formulations of c and γ for calculating diffusive fluxes where:

$$\gamma = \frac{R\rho + 1.4(R\rho - 1)^{1.5}}{1+14(R\rho - 1)^{1.5}} \qquad \text{(III.6)}$$

and

$$c = 0.0032 \exp\left(\frac{4.8}{R\rho^{0.72}}\right) \qquad \text{(III.7)}$$

Table III.2 presents data showing the heat flux over time as measured by the CTD and the flux that is calculated by the 4/3 flux law (Model F_H). Heat (temperature) fluxes are calculated from the CTD by integrating the area under a vertical temperature profile and then subtracting the area under a profile taken at the same location at an

earlier time. Since no obvious "step-like" features are evident for any prolonged period in the water column of Crater Lake, the criterion used for application of the flux law was that the temperature gradient, over the depth interval chosen, was relatively constant in time.

Table III.2 Calculation of Heat Flux based on CTD data and model

Time period (1989)	Depth Range (meters)	CTD Flux (F_H) (W m^{-2})	Model (F_H) (W m^{-2})
May-June	409-544	0.63	0.025
June-July	400-500	0.46	0.024
July-Aug	400-500	1.20	0.038
Aug-Sept	400-500	0.14	0.028
Sept-Oct	400-500	2.00	0.026

Comparison of the fluxes derived from the CTD data with the calculated flux data (Table III.2) shows that double diffusive convection does not account for the observed heat flux through the water column. For example, in Table III.2 we see that between May and June from 409 to 544 m (the depth interval over which the temperature gradient remained relatively constant) there was a net heat flux of 0.63 W m^{-2} as measured by the CTD; however, based on the thermal gradient and equation III.4, I calculate a double diffusive heat flux of 0.025 W m^{-2}.

Alternatively, double diffusive fluxes can be related to the thickness of the convecting layers (Turner 1973; Kelley 1984). It is therefore useful for the purposes of this chapter to estimate the height that these layers would need to be if double diffusion were the only acting mechanism for the vertical transport of heat and salt through the water column. The parameterization of the layer thicknesses are carried out according to Kelley (1984, 1988) where the intrinsic layer thickness scale is;

$$H_o = \left(\frac{\kappa_T}{N}\right)^{1/2} \qquad \text{(III.8)}$$

and the layer thickness is given by

$$H = GH_o = G\left(\frac{\kappa_T}{N}\right)^{1/2} \qquad \text{(III.9)}$$

where G is the scaled layer thickness and is a function of the density ratio (R_ρ), the Prandtl number ($Pr = \nu/\kappa$), and the Lewis number ($Le = \kappa_S/\kappa_T$). The results presented here show that if double diffusive convection were responsible for the fluxes in the deep lake, the layer thicknesses should range between 1 and 30 m (Table III.3).

Rearranging equation (III.4) yields an expression for ΔT between two "steps" as a function of the prescribed flux [i.e. $\Delta T \propto (F_T)^{3/4}$]. The prescribed flux ($F_T$) is based on the CTD data from Table III.2 which has been rewritten in Table III.3 as Flux $(CTD)_{obs.}$. This relationship allows us to estimate the ΔT (the change in temperature between the layers) required for transport of heat by double diffusion in Crater Lake. Also, both ΔT and H (the layer thickness) are related to each other through dimensional analysis where the layer thickness is dependent on the change in temperature at the interface (ΔT) divided by the temperature gradient ($\Delta T/\Delta z$). For the calculation of the layer thicknesses (H_{model} in Table III.3) I use the calculated ΔT and the observed temperature gradient ($(dT/dZ)_{obs.}$). The modeled layer thicknesses (H_{model}) and ΔT's (ΔT_{model}) presented in Table III.3 reflect reasonable estimates of what would be observed if double diffusion were the dominant mechanism for the transport of heat and salt through the water column in Crater Lake. Also, the calculated layer thicknesses agree with those predicted by Eq. III.8 and III.9. It is likewise important to point out that the CTD does have the resolution to detect these features if they were occurring on these scales in the lake, and that no step-like features are observed in the bulk water column of the lake.

Table III.3 ΔT and Layer Thicknesses based on Observed Fluxes

Time period (1989)	Flux $(CTD)^*_{obs.}$ ($°C\ m\ s^{-1}$)	$(dT/dZ)_{obs.}$ ($°C\ m^{-1}$)	ΔT_{model} (°C)	H_{model} (meters)
June-July	10.9×10^{-8}	0.00024	0.0024	10.1
July-Aug	28.5×10^{-8}	0.00032	0.0052	16.5
Aug-Sept	3.3×10^{-8}	0.00042	0.0006	1.4
Sept-Oct	47.6×10^{-8}	0.00027	0.0074	27.4

**For purposes of dimensional consistency I have chosen to express the prescribed flux in units ($°C\ m\ s^{-1}$).*

In summary it is apparent that double diffusive convection, as a mechanism for the transfer of heat and salt through the water column in Crater Lake, underestimates the total heat flux by one to two orders of magnitude. This finding is consistent with the absence of observable "steps" in the T and S profiles. Double diffusion may, however, be important on small spatial and temporal scales, and may contribute to the T-S distribution near the sediment-water interface. This possibility is evaluated more thoroughly in Chapter IV.

Horizontal mixing in the deep lake

When the upper water column of Crater Lake is thermally stratified, deep lake mixing is dominated by horizontal basin-to-basin exchange processes. This mixing is indicated by changes in the vertical distribution of temperature, salinity, and other geochemical tracers (e.g. dissolved gases and trace elements).

CTD data taken from the North Basin in September 1988 demonstrates that the vertical distribution in temperature and salinity may deviate from the normal linear increase with depth (cf. Fig. III.2 with Fig. III.12). These variations in the vertical gradients are referred to here as "microstructure" features. I propose that these features are due to the lateral flow of hydrothermally enriched water from the South Basin. As the South Basin fills with warm, salty water, it will "spill over" into the deeper portions of the lake because of its greater density relative to non-enriched fluids. The sill depth between these two basins is located between 425 and 450 m depth. The sill depth corresponds to the depth of the microstructure features observed in both the South Basin (near the sediment-water interface) and the North Basin (mid-water column) (Fig. III.12a). The presence of warmer waters in both basins at the same depth (~425 m) supports the hypothesis that the fluids originated in the South Basin.

In order to accurately assess the stability of the deep water column in September 1988, $\sigma_{0.5}$ was computed. Where $\sigma_{0.5} = (\rho_{0.5} - 1) \times 1000$ and $\rho_{0.5}$ is the potential density of a fluid referenced to 500 dbars. In deep aquatic systems, σ_θ does not accurately represent the local "stability" of the water column (Fig. III.12d). This is due to the effect of pressure on the density of a fluid, where σ_θ is calculated for 1 atm pressure as opposed to a pressure more representative of two deep parcels of water under consideration (i.e. 500 dbars pressure). Most of the water throughout the water column appears to be statically stable with respect to 500 dbars (Fig. III.12c); however, stability calculations for some individual points within the water column suggest that

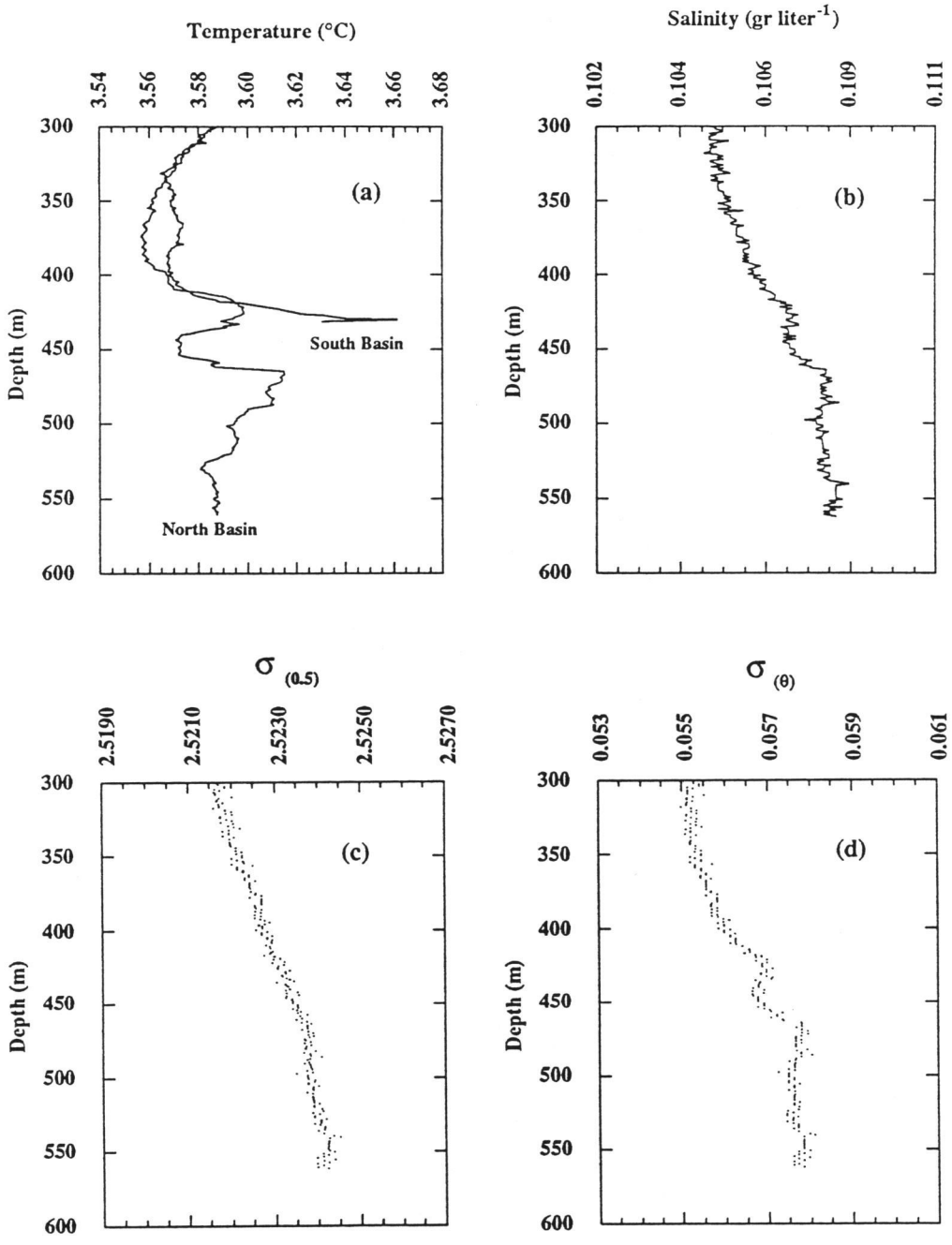

Fig. III.12. Hydrographic data taken 19 September 1988. (a) Temperature as a function of depth for both the South and the North basins, (b) Salinity as a function of depth for the North Basin, (c) $\sigma_{0.5}$ as a function of depth for the North Basin, (d) σ_θ as a function of depth for the North Basin. Densities are calculated from equations presented in Chen and Millero (1986).

there are some unstable parcels of water. These parcels are unstable over vertical distances of 5-10 m. Since changes in the vertical density structure on this scale approach the resolution of our instrument, there is significant uncertainty associated with classifying the "stability" of parcels of water over this depth range. The thermal structure of the deep lake shown in Fig. III.12a tends to change shape over periods of hours; further, such structure may be gone upon revisitation to the lake after a period of weeks. These additional observations suggest that these features are indeed unstable and transient.

^{222}Rn and Fe (dissolved and particulate) measurements further illustrate the basin to basin exchange process. Water with high ^{222}Rn and Fe contents overlay water of lower ^{222}Rn and Fe content in the North Basin (Fig. III.13). These single profiles exhibit the net effect of horizontal exchange. Both ^{222}Rn and Fe are time-dependent tracers of the South Basin hydrothermally enriched water. Iron is highly reactive in well-oxygenated environments and will only be found at high concentrations near reduced sediments or hydrothermal vents. Radon is a radioisotope with a half-life of ~3.8 days. It too should only be found in close proximity to a hydrothermal vent or the sediments in Crater Lake. The horizontal transport of iron from the South Basin leads to a maximum in dissolved and particulate Fe between 450 and 500 m in the North Basin (Fig. III.13a). ^{222}Rn also exhibits a deep-water maximum at ~475 m in the North Basin (Fig. III.13b). The net effect of the proposed horizontal movement of waters from the South Basin to the North Basin is that "younger" (^{222}Rn enriched) waters overlay the "older" (^{222}Rn depleted) waters in the North Basin.

Although the water column features representative of horizontal mixing have been observed at various times throughout the summer the most dramatic features are consistently observed in late summer/early fall (September-October). These periods of more intense horizontal exchange have larger thermal anomalies in the North Basin than those typically observed during the summer. Since September and October are periods where the lake is thermally stratified, and since wind forcing tends to be minimal at this time of year, surface disturbances can not supply the necessary forcing for the initiation of this mixing process.

Based on the fluid inflow and composition estimates, and on the observed near-bottom salinities of South Basin waters, I estimate that the South Basin could "fill-up" with a mixture of hydrothermal and ambient fluid on the scale of several weeks to months. The horizontal exchange process proposed here is not necessarily a continuous process. Consequently, the non-steady state nature of this mixing process in the deep

Fig. III.13. (a) Dissolved and particulate iron as a function of depth from the North Basin (data from Collier et. al., 1990). (b) ^{222}Rn as a function of depth for the North and South Basin. Although not on the graph, the deepest ^{222}Rn value from the particular South Basin hydrocast shown on the figure was 35 dpm 100 liters^{-1}.

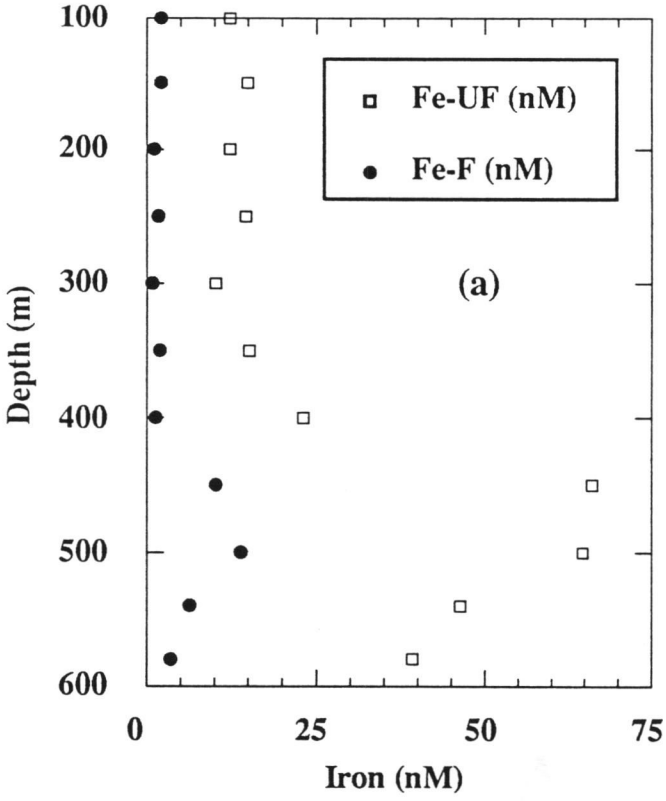

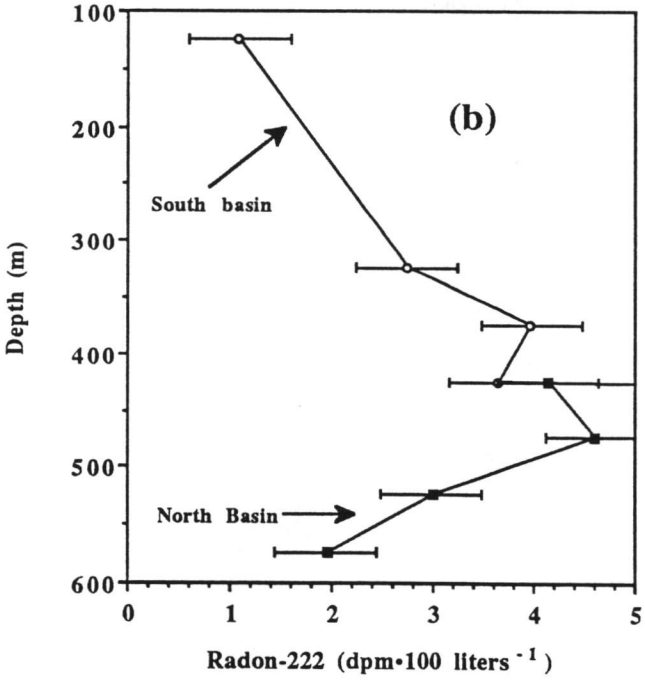

Figure III.13

lake results in the relatively large uncertainty (1σ) in the net heat and salt flux estimates which are based on a few individual vertical profiles (Table III.1).

Vertical mixing processes in the deep lake

In addition to horizontal advection playing a large role in the transport of heat and salt through the deep lake, I propose that turbulent diffusion coupled with vertical convection, transport heat and salt through the hypolimnion. Although the mechanism which initiates turbulence in Crater Lake is not known, I base this hypothesis on two observations: (1) because the calculated effective vertical diffusivities for both heat and salt in Crater Lake are the same order of magnitude (10^{-4} m^2 sec^{-1}) and are many orders of magnitude larger than the molecular values (10^{-7}-10^{-9} m^2 sec^{-1} for heat and salt respectively), the mixing process can not simply be driven by molecular diffusion (or double diffusion); (2) there are small-scale vertical thermal instabilities in the water column which do not appear to be due to the horizontal transport of heat and salt described in the previous section.

The effective diffusivities for heat (K_{eT}) and salt (K_{eS}) can be modeled according to a simple diffusion model (see equations III.1 and III.2 for the development);

$$F_T = K_{eT}\left(\frac{dT}{dz}\right) \qquad \text{(III.10)}$$

and

$$F_S = K_{eS}\left(\frac{dS}{dz}\right) \qquad \text{(11)}$$

where F_T and F_S are the measured flux of temperature (°C m s^{-1}) and salt (g m kg^{-1} s^{-1}) respectively (for dimensional simplicity I use F_T as opposed to F_H -- the heat flux). These measurements are again based on a time-series of CTD measurements (Table III.1). My calculations reveal that the effective diffusivities for heat and salt are approximately 6 to 8 x 10^{-4} m^2 sec^{-1}. If molecular diffusion was an important mechanism for the transport of heat and salt through the water column, the calculated effective diffusivity for heat would be two orders of magnitude larger than the effective diffusivity for salt. The effective diffusion coefficient calculated here for the summer-

fall period is approximately a factor of two smaller than the diffusion coefficient calculated (earlier in the text) for diffusion during the month of February ~2 x 10^{-3} m^2 sec^{-1}. This observation suggests that the intensity of deep lake mixing during the winter is slightly greater than during the summer, which is not surprising since the overall stability of the upper water column is greater during the summer. However, at all times, turbulent diffusion processes will obviously be smaller in magnitude than the instability-driven convection from the upper lake described earlier in the text.

Observations of small temperature inversions through the mid-water column suggest the presence of small, buoyant "plumes" (Fig. III.14). Salinity profiles lack the sensitivity of the temperature profiles and do not show this effect. Therefore the stability of these thermal features can not accurately be calculated; however, the data suggests that they are transient features which are occasionally observed in the mid-to-deep lake. These "plumes" could be caused by either of two processes (or some combination of the two). The plumes may be caused by direct inputs of buoyant water into the South Basin. Alternatively, they may be generated by conductive heating or double diffusive development of thermally and chemically enriched waters resting at the sediment-water interface. These processes could eventually lead to instability and formation of thermal convection cells that vertically mix the excess heat and salt.

An alternate convective mechanism for mixing heat and salt through the water column, is suggested as a large temperature anomaly in the middle of the water column (Fig. III.15a). This temperature anomaly was measured in the South Basin of Crater Lake on 11 September 1987 and is greater than 0.1°C between 225 and 275 m, relative to the North Basin profile. This corresponds to a total heat anomaly of 9600 kcal m^{-2}, which is a factor of five to ten larger than typical near-bottom thermal anomalies measured in the South Basin (Chapter IV). Shown with this data (Fig. III.15a) are temperature profiles taken from the South Basin approximately 6 hours earlier (solid line) and the North Basin approximately 3 hours earlier (dotted line). Although the two South Basin profiles are from the same general location, they may be separated in space by as much as 500-1000 m. T-S diagrams (Fig. III.15b-d) of the three hydrocasts (below 100 m) illustrate the dramatic change in the characteristics of the large thermal anomaly. However, the T-S diagrams of all the CTD data show some influence of the warmer, more saline water, suggesting that the heat and salt seen in SBE028 may be spreading horizontally along a constant density surface.

This large thermal anomaly is hydrostatically stable with respect to 250 dbars and is buoyant relative to 450 dbars. This suggests that perhaps the water column

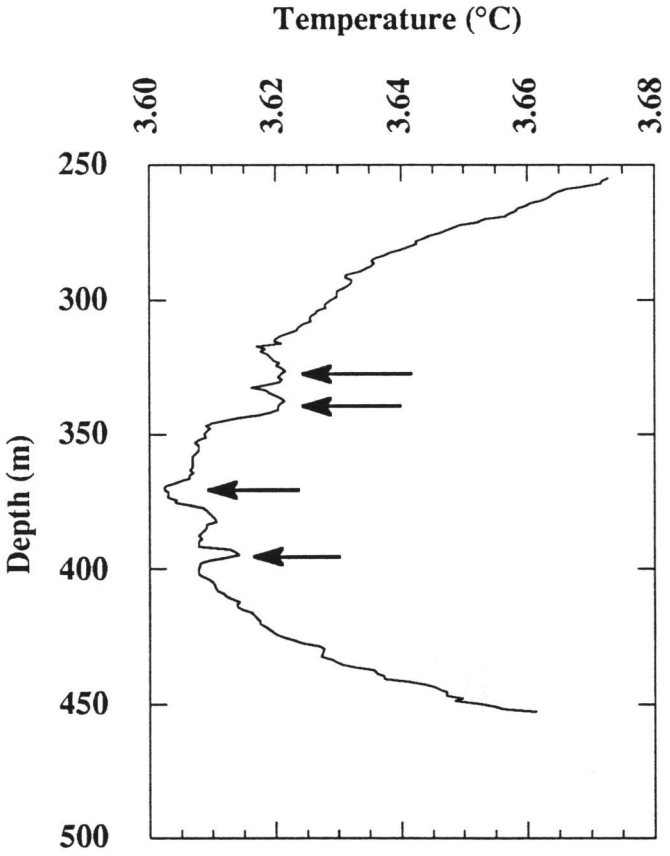

Fig. III.14. Examples of vertical instabilities (arrows). Data is from 18 September 1990 from the South Basin.

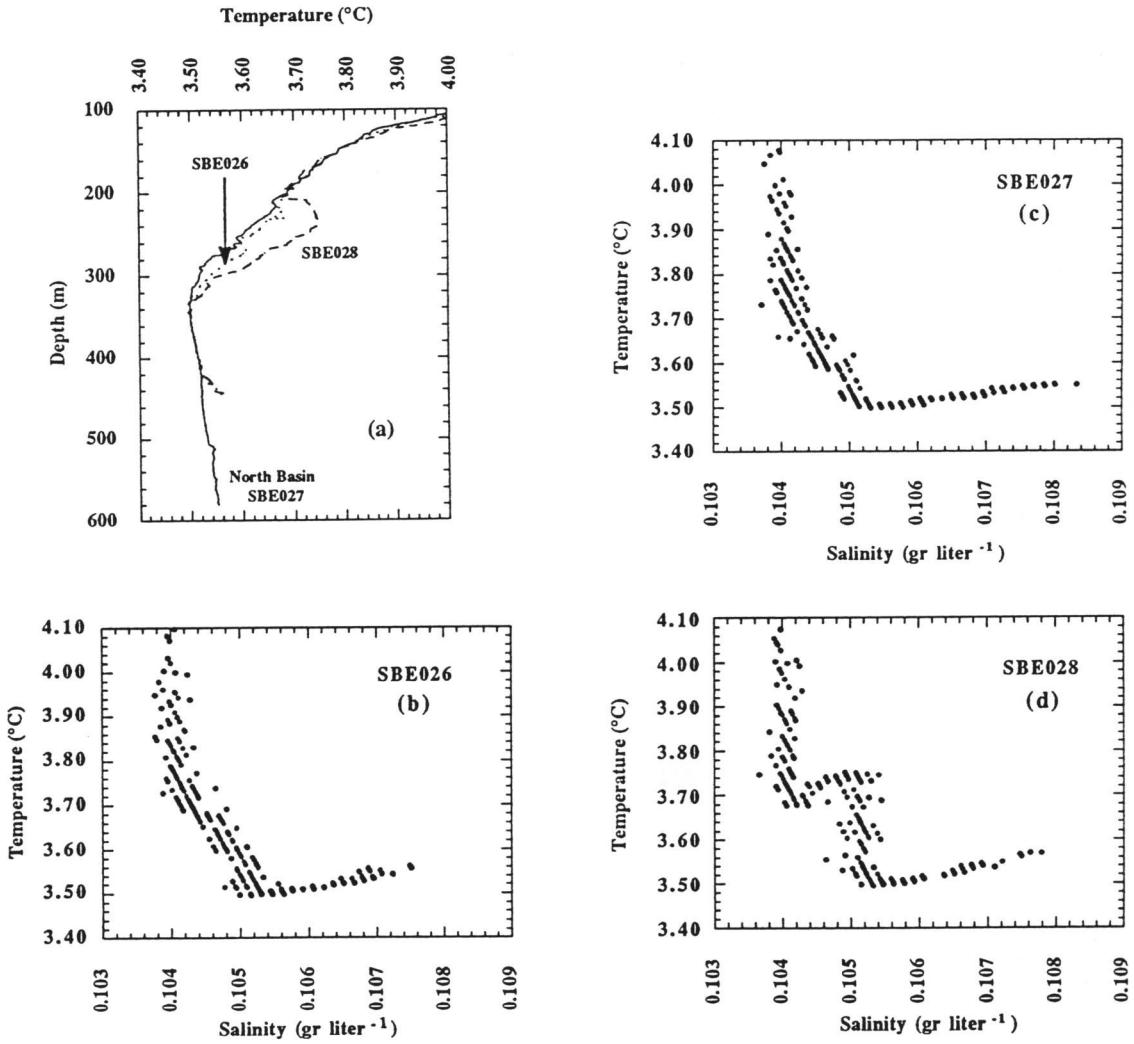

Fig. III.15. (a) Temperature as a function of depth for SBE026 (South Basin), SBE027 (North Basin), and SBE027 (South Basin). (b-d) T-S diagrams for the three hydrocasts. The data shows the T-S anomaly in all three hydrocasts, but is particularly striking for SBE028.

anomaly represents a "plume" which originated at the sediment-water interface and has risen to neutral buoyancy. Alternatively, there could be a source of thermally and chemically enriched water along the caldera wall at this depth, which I have not observed to date.

Although there is also a potential for enhanced mixing along the sides of the basin, first order calculations suggest that such mixing will be insignificant compared to the other mechanisms. To constrain this calculation it was assumed that all the measured heat transport occurs along the side of the caldera and will subsequently be transported to the interior of the lake. In order for mixing along the sides of the basin to be responsible for the transport of a property (heat or salt) at our measured flux rates (Table III.1), the rate of vertical exchange along the sides would need to be unreasonably large.

Calculations presented here suggest that vertical mixing in the deep lake is dominated by turbulent diffusion rather than by molecular or double diffusion. However, the mechanism which initiates turbulence in Crater Lake is not known. Horizontal advection followed by vertical mixing and vertical convection also play a role in the vertical redistribution of heat and salt through the water column. As would be expected, our calculated diffusion coefficients for the deep lake are larger than values for the region just below the thermocline (50-150 m) in Crater Lake (10^{-5} - 10^{-6} m^2 sec^{-1}). Also, the range in diffusion coefficients calculated for the deep lake (6-20 x 10^{-4} m^2 s^{-1}) compares well with the range for the deep ocean (O[1-100 x 10^{-4} $m^2 s^{-1}$]) as derived from ^{222}Rn-depth profiles (Sarmiento et al. 1976). This comparison illustrates the importance of turbulence in the redistribution of heat and salt in the hypolimnion.

The physical processes described here appear to be directly tied to the active input of thermally and chemically enriched waters and because of these processes the deep lake remains relatively well mixed.

THE OVERALL INFLUENCE OF HYDROTHERMAL ACTIVITY ON THE PHYSICS OF THE WATER COLUMN

The hypolimnion of Crater Lake is only marginally stable. This is reflected by the buoyancy frequency (N), which for the hypolimnion of Crater Lake is $O(10^{-4}\ sec^{-1})$ (Collier et al. 1990; McManus et al. in press). The turbulent diffusion coefficient ranges between 10^{-4} and $10^{-3}\ m^2\ sec^{-1}$, which reflects relatively rapid vertical exchange throughout the deep lake.

Without the input of heat into the hypolimnion there would be no destabilizing force acting on the water column. Alternatively, if Crater Lake were conductively heated from the bottom (due to the fact that it rests in a caldera), yet there were no saline fluid inputs, the lake would be expected to undergo thermal convection (Williams and Von Herzen, 1983). Mixing in this case would be more rapid than observed.

If there were no change in the salinity gradient, it may, in principle, be easier to develop the thermobaric instabilities due to a lack of a salinity gradient. The surface signal carried by this mixing process could then be carried all the way to the bottom as in Lake Baikal (Carmack et al. 1989; Carmack and Weiss 1991;Weiss et al. 1991). Since the instability of the water column relies on wind shear or seiching or both (Carmack and Weiss 1991;Weiss et al. 1991), it is likely that the ventilation of the deep lake would be more dependent on the severity of winter storms, as in Lake Tahoe (Pearl et al. 1975). Also because of the relatively small fetch of the lake, wind forcing may be less significant in Crater Lake than in Lake Tahoe or Lake Baikal and will make wind-dependent mixing more difficult.

Although it is difficult to precisely ascertain the net effect of hydrothermal activity on the physics of Crater Lake, there are a variety of unique physical features of the water column which can only be attributed to the active input of heat and salt near the bottom of the lake. Any change in the hydrothermal activity could only alter lake mixing. The active inputs of hydrothermal fluids generate both vertical and horizontal density instabilities which contribute to the rapid horizontal and vertical mixing of deep lake water. It follows then, that hydrothermal activity is important to the relatively rapid vertical mixing that occurs in Crater Lake, OR (characteristic time-scale of deep lake mixing ~2 years). This mixing returns biologically important nutrients from the deep lake to the surface lake at least once a year. Without such nutrients - principally dissolved nitrate - the new production which relies on these nutrients would be lower.

CONCLUSIONS

My estimates of the deep lake heat budget of Crater Lake are consistent with the previous estimates of Williams and Von Herzen (1983). Because the methods employed within this chapter are independent from those of Williams and Von Herzen (1983), who used sediment heat flow measurements, the agreement between the two data sets supports the estimate of heat flow made in this chapter. The data presented here provide the first direct observations of the accumulation of heat and salt in the deep lake and lead to direct estimates of these fluxes.

Dissolved oxygen data, thermistor chain data, and CTD data all indicate that annual vertical mixing is significant in the hypolimnion of Crater Lake. Data presented here also indicate that this exchange process is incomplete, resulting in undersaturation of dissolved oxygen at all times in the hypolimnion. Due to the increase in density with depth in the lake, the degree of vertical mixing decreases with increasing depth.

During periods of surface stratification, mixing is dominated by turbulent diffusion and horizontal advection rather than molecular diffusion, although the forcing mechanism of the turbulence is not known.

ACKNOWLEDGEMENTS

Mark Buktenica, John Salinas, and Scott Stonum from Crater Lake National Park provided day and night field support for this research and their efforts are greatly appreciated. In addition, the logistical assistance of Gary Larson at OSU College of Forestry allowed much of this work to be accomplished. This research was funded by the U.S. National Park Service under cooperative agreement No. CA 9000-3-0003, CPSU, College of Forestry, Oregon State University.

IV. ON THE PHYSICAL LIMNOLOGY OF CRATER LAKE, OREGON: 2. BEHAVIOR OF THERMALLY AND CHEMICALLY ENRICHED FLUIDS AT THE SEDIMENT-WATER INTERFACE

ABSTRACT

The eastern portion of the South Basin of Crater Lake, Oregon is a region of active hydrothermal input. Although, to a first approximation, there is a linear relationship between excess heat and salt in this basin, there are small variations in the heat to salt ratio near the sediment-water interface. Detailed mapping of the South Basin near-bottom temperature and salinity distribution has allowed the development of constraints which identify the possible modes of entry for the enriched fluids into the deep lake. Mixing between a hydrothermal end-member fluid and ambient South Basin water form a mixture which is more dense than either fluid. The variation in the near-bottom temperature and salinity distribution is non-linear, suggesting that small-scale double diffusion or conductive cooling of a hydrothermal end-member or both of these processes may be occurring at or below the sediment-water interface.

INTRODUCTION

Crater Lake, Oregon, located in the southern Oregon Cascades, rests within the collapsed caldera of the andesidic volcano Mt. Mazama. Although volcanism has occurred as recently as 4000 years BP within the caldera system, the lake's morphology is primarily a result of a climatic eruption that occurred ~6850 years BP (Bacon and Lanphere, 1990). With over 400 k years of volcanic history, it is not surprising to find hydrothermal activity within the lake system.

The chemistry and physics of the deep water column in Crater Lake are dominated by the active inputs of thermally and chemically enriched (hydrothermal) fluids (Williams and Von Herzen 1983; Collier et al. 1990a, b; Chapter II; Chapter III). Using high precision temperature and salinity measurements, the South Basin has been identified as a region of active hydrothermal inputs (Collier et al. 1990a; Chapter II). This basin has thermal and saline gradients which are typically one to two orders of magnitude larger than the gradients from the rest of the lake.

The eastern portion of the South Basin appears to be the region of primary fluid input. It was here that Williams and Von Herzen (1983) reported measurements of heat flow as high as 5 W m^{-2}. Much of the recent research efforts (Collier et al. 1991) have therefore focused on this portion of the South Basin and the findings from this location support the hypothesis that the South Basin is a region of active hydrothermal venting.

Bacterial mat communities have been documented in the eastern portion of the South Basin (Dymond et al. 1989). These mats are composed primarily of iron and manganese reducing bacteria (Dymond et al. 1989). Dense saline pools have also been found resting along the lake floor in this portion of the lake (Collier et al. 1990b, 1991). Both the fluids surrounding the bacterial mats and within the saline pools have anomalously high temperatures and salinities (Dymond et al. 1989; Collier et al. 1990b). Therefore, these features are assumed to represent locations of active hydrothermal input.

The active input of hydrothermal fluids affects the density structure of the deep lake which, in turn, influences the horizontal as well as the vertical mixing rates (Chapter III). The magnitude of the heat flux, salt flux, and fluid flow associated with hydrothermal venting is approximately 1 W m^{-2}, 5 μg m^{-2}, and 200 liters sec^{-1} respectively (Chapter III). The heat flow estimates agree with those of Williams and Von Herzen (1983) who reported values between 0.7 and 1.4 W m^{-2}. In this chapter I will focus on the distribution of heat and salt within the South Basin, and discuss the

effect that these properties have on the physics of near-bottom waters in this basin. The observations of the distribution of heat and salt presented within this chapter constrain the modes of input and the evolution of the water at the bottom of the South Basin in Crater Lake.

METHODS

Crater Lake has two semi-enclosed basins; the South Basin which has a maximum depth of ~485 m, and the North Basin which has a maximum depth of ~590 m (Fig. IV.1a). The bathymetry of the eastern portion of the South Basin is, in part, influenced by debris flows and avalanches from the caldera walls (Barber and Nelson 1990). Because of the course nature of this material, the sediments that cover the basement in this section of the South Basin tend to be porous.

During August of 1988 and 1989 a series of dives were carried out using the one-manned submersible Deep Rover (Dymond et al. 1989). One of the goals of these dives was to identify the magnitude and nature of hydrothermal inputs to the deep lake (Collier et al. 1991). Toward this goal, the distribution of heat (temperature) and salt have been surveyed in the eastern-portion of the South Basin of Crater Lake. From this survey, a detailed record of the bathymetry of this portion of the lake has also been obtained (Fig. IV.1b).

Temperature, conductivity, and pressure were measured in situ using a conductivity, temperature, depth profiler ("CTD", SEACAT® model SBE19, Seabird Electronics, Inc.). The resolution of the temperature and salinity measurements, based on CTD calibrations in 1987 and 1989, is better than 0.001 °C for temperature and ±0.0002 gr liter^{-1} for salinity (Chapter II). Salinity and density were calculated from in situ conductivity and temperature using direct calibrations (Chapter II) and an equation of state for lake water (Chen and Millero 1986). Much of the data presented here was collected with the profiler attached to a hydrographic cable which was lowered from the lake surface. Additional near-bottom temperature and salinity data were collected with the CTD mounted on the submersible.

Navigation of the CTD profiles was accomplished with a microwave ranging system (Motorola Mini-Ranger) that had a precision of ±5 m. An orthogonal coordinate system was established relative to Eagle Point, located at the southern end of the caldera (Fig. IV.1a).

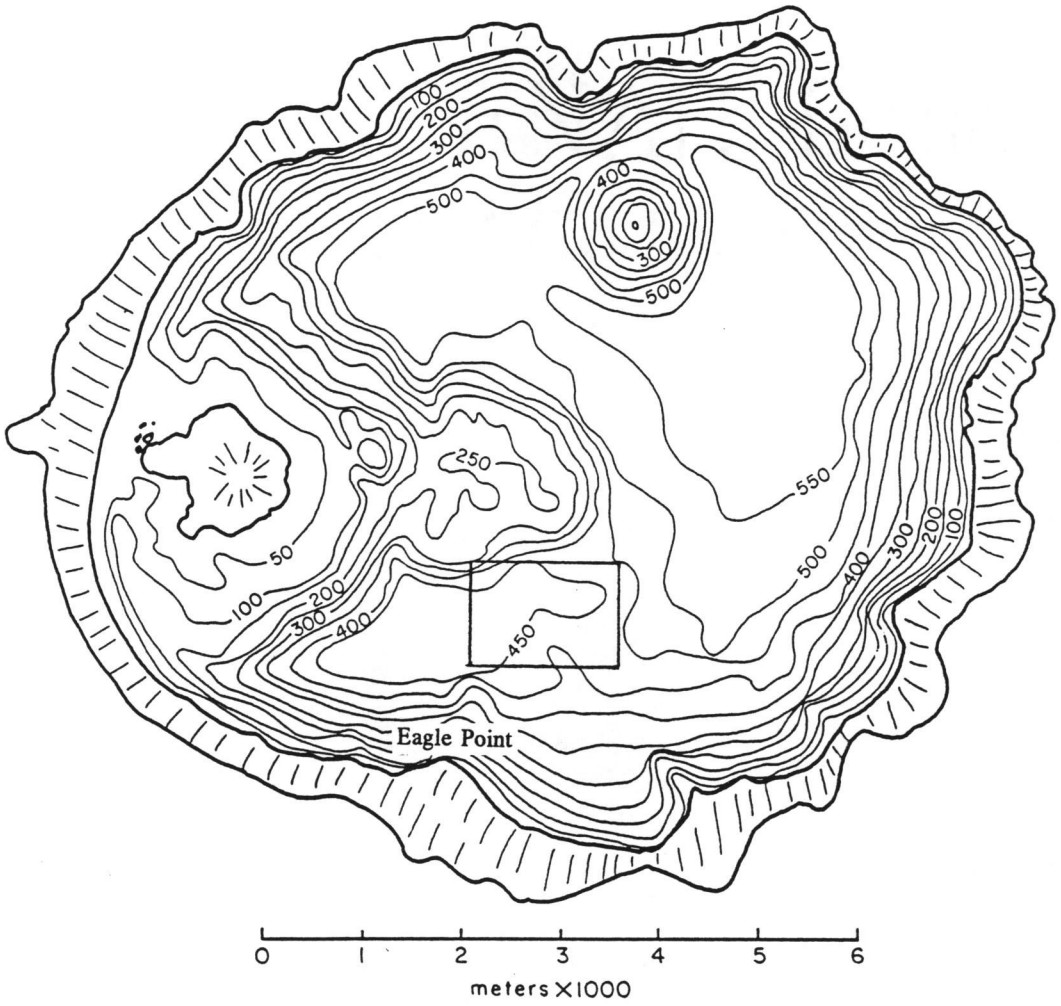

Fig. IV.1. (a) Batymetric map of Crater Lake, OR. Bathymetry from Byrne (1965). Boxed area shows region represented in Fig. IV.1b.

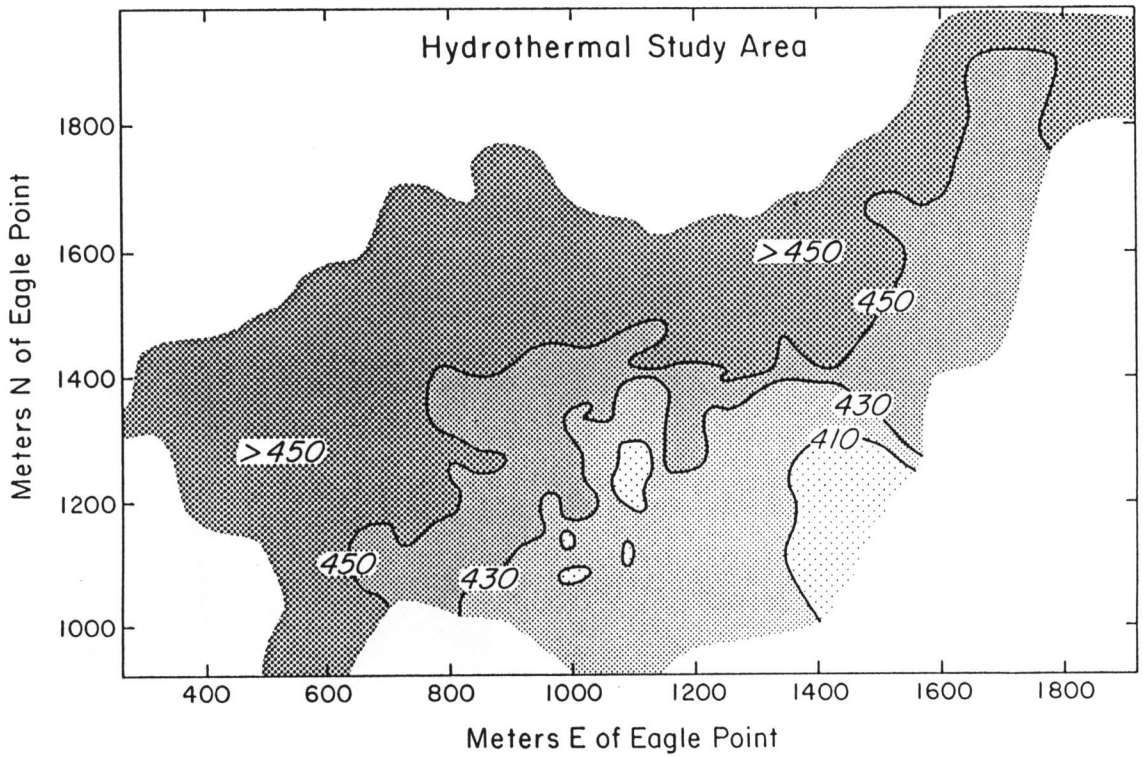

Fig. IV.1. (b) Expanded-scale bathymetric map of the eastern portion of the South Basin.

RESULTS

T-S properties of the deep lake

The vertical temperature gradient in Crater Lake is at all times "hyperadiabatic" (Neal et al. 1971, 1972). The term hyperadiabatic derives from the fact that the thermal gradient below 350 m in the deep lake is approximately two orders of magnitude greater than the adiabatic gradient (Fig. IV.2a). This increase in temperature with depth is due to the active input of hydrothermal fluids.

The lake is horizontally well mixed with respect to temperature and salinity as is demonstrated by the similarity among the three T-S profiles taken from different areas of the lake (Fig. IV.2b). Data to the left of the temperature minimum in Fig. IV.2b represent the T-S characteristics from 150-275 m on 17 July 1989. This temperature minimum deepens as the summer progresses due to the turbulent transport of heat from the surface. By mid-to-late August this temperature minimum is at approximately 300 m.

Although the lake is generally well-mixed, the South Basin contains the most extreme end-members in water column temperature and salinity (Fig. IV.2). Vertical gradients in temperature (Fig. IV.2a) and salinity are always much greater below 400 m in this basin than in the rest of the deep lake, suggesting that this basin is the primary source of hydrothermal fluids to the deep lake. Therefore, the primary focus of this chapter will be on the spatial distribution of heat and salt within the deep South Basin and the behavior of these anomalous South Basin fluids.

CTD data from South Basin submersible dives (Fig. IV.3) illustrate the heterogeneous nature of the near-bottom waters in this basin. Three T-S "trends" are apparent in Fig. IV.3a: (H) water with a high heat to salt ratio (high temperature-low salinity); (I) water with an intermediate heat to salt ratio (high temperature-high salinity); (L) water with a low heat to salt ratio (low temperature-high salinity). The background deep lake water (BK) as described in Fig. IV.2 lies at the intersection of these various components of South Basin water. All water column temperature and salinity data collected in 1989 from the South Basin lie somewhere between the (H) and (L) "arms" in Fig. IV.3a.

The temperature and salinity signals plotted as a function of time during one of the 1989 dives further demonstrates the near-bottom heterogeneity in the distribution of heat and salt (Fig. IV.3b). Here, the temperature and salinity signals do not always

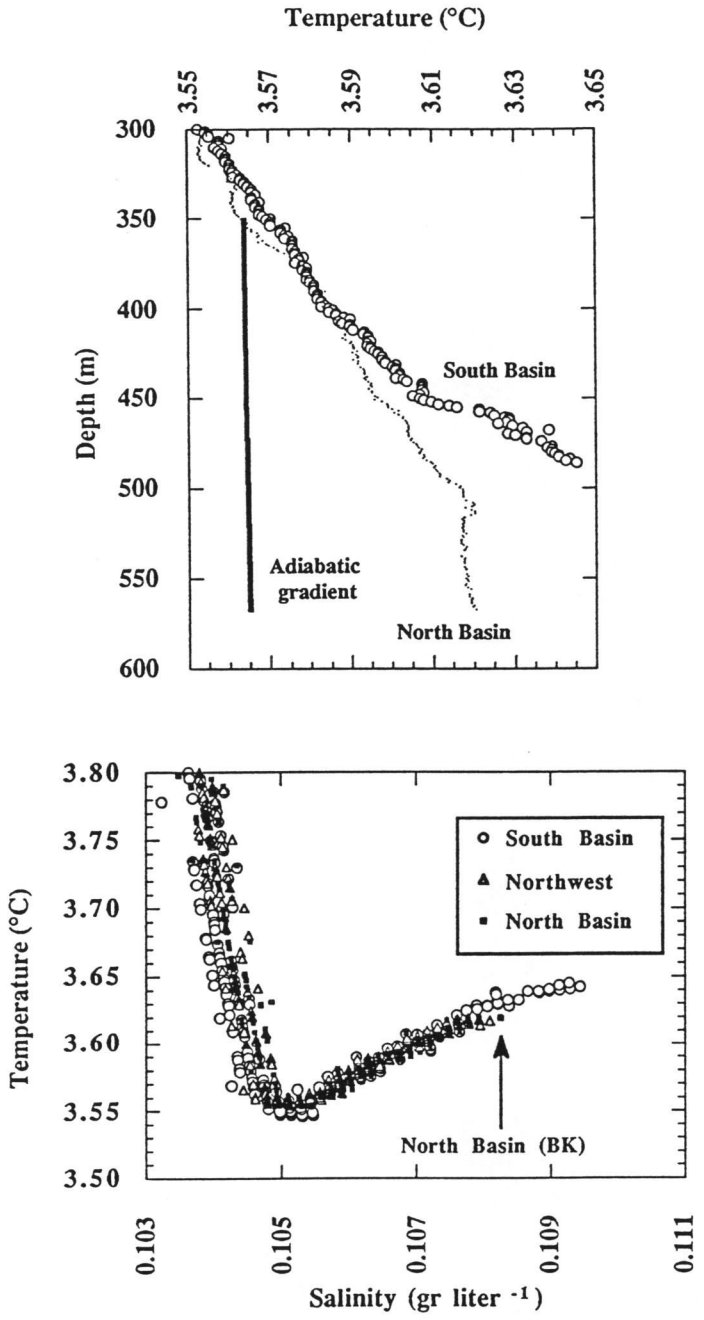

Fig. IV.2. (a) Temperature as a function of depth in the North and South Basins of Crater Lake. Note the line showing the adiabatic gradient below 350 m. (b) T-S diagram of our three monitoring stations in Crater Lake for depths greater than 150 meters. Note the overlap of the three profiles with the exception of the deeper South Basin (Stn. 23) water. The South Basin deep waters can be seen to be warmer and saltier than the deep waters from the rest of the lake.

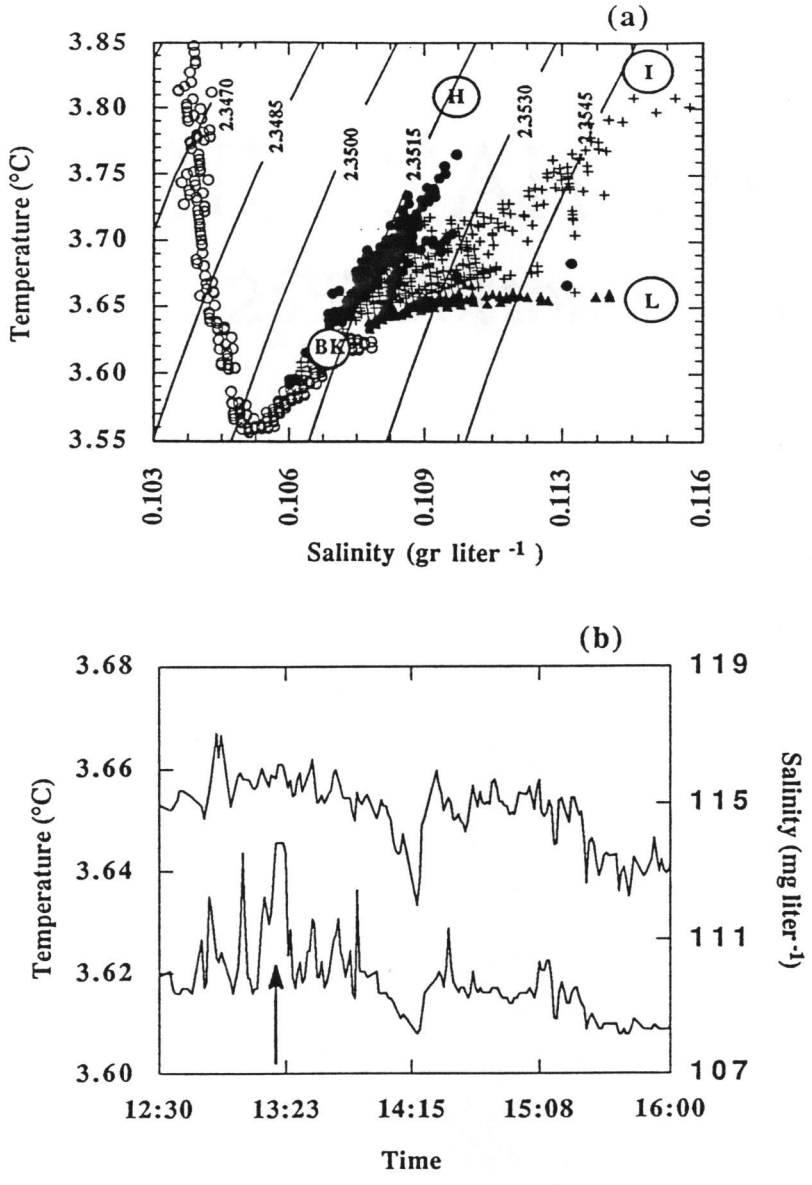

Fig. IV.3. (a) T-S diagram of the deep South Basin of Crater Lake. Figure shows three T-S trends: (H), a high heat-to-salt ratio; (L), a low heat-to-salt ratio; (I), an intermediate heat-to-salt ratio; as well as background deep lake water (BK). Curves are isopycnals calculated for a reference pressure of 465 dbars from the equation of state presented in Chen and Millero (1986). (b) Temperature (bottom) and salinity (top) as a function of time collected during a submersible dive in 1989. The variation in temperature and salinity over time do not necessarily correspond (arrow in figure) due to the varing heat-to-salt ratios. Most CTD data is collected within 3 m of the lake bottom.

covary as shown by the arrow in Fig. IV.3b. These T-S changes illustrate spatial variation in the heat to salt ratio which may be due to a variety of mixing processes as discussed below.

The spatial distribution of heat and salt in the South Basin

To examine the spatial variability of temperature and salinity within the South Basin, a series of CTD sections across the basin was collected. I have integrated a total of 66 navigated profiles, collected during the 1987, 88, and 89 field seasons, to construct maps of the "excess heat" (kcal m^{-2}) and "excess salt" (gr m^{-2}) contained within the South Basin (Fig. IV.4). The "excess" property (heat or salt) is defined as the difference between the South and North Basin vertical property profiles over the same depth range. For example, the vertically integrated heat content in the North Basin is subtracted from the vertically integrated heat content in the South Basin over the same depth range in Fig. IV.2a. This calculation method focuses only on the localized anomalies which are observed within the South Basin which are greater than the general heating/salting effect seen throughout the rest of the deep lake.

The maxima in the vertically integrated heat and salt seen at the right-hand side of Fig. IV.4 are in the same vicinity as the high heat flow measurements reported by Williams and Von Herzen (1983). In addition, these maxima are located over bacterial mat assemblages (Dymond et al., 1989). The high values on the west end of the figures reflect the larger volume of warm, salty water in the deeper portions of the South Basin. As the hydrothermal fluids enter the eastern portion of the basin, they appear to move down-slope to the deeper parts of the basin. In addition, it is possible that there are other sources of hydrothermal fluids in the deeper regions of this basin.

The excesses of heat and salt (Fig. IV.4) are reasonably well correlated (Fig. IV.5) which is consistent with a common carrier, the hydrothermal fluid. For reasons I will discuss later in the text, the mixture of hydrothermal fluid and ambient South Basin water generally yields a mixture that is more dense than either fluid. Because the mixtures of ambient water and hydrothermal water are generally the densest waters in the South Basin, the density distribution of the deep South Basin increases with increasing depth in the water column. The hydrothermally enriched fluids, which are entering at a bathymetric high (Fig. IV.1b), will have a tendency to flow down-slope due to their greater density relative to ambient lake water. The result of this down-slope

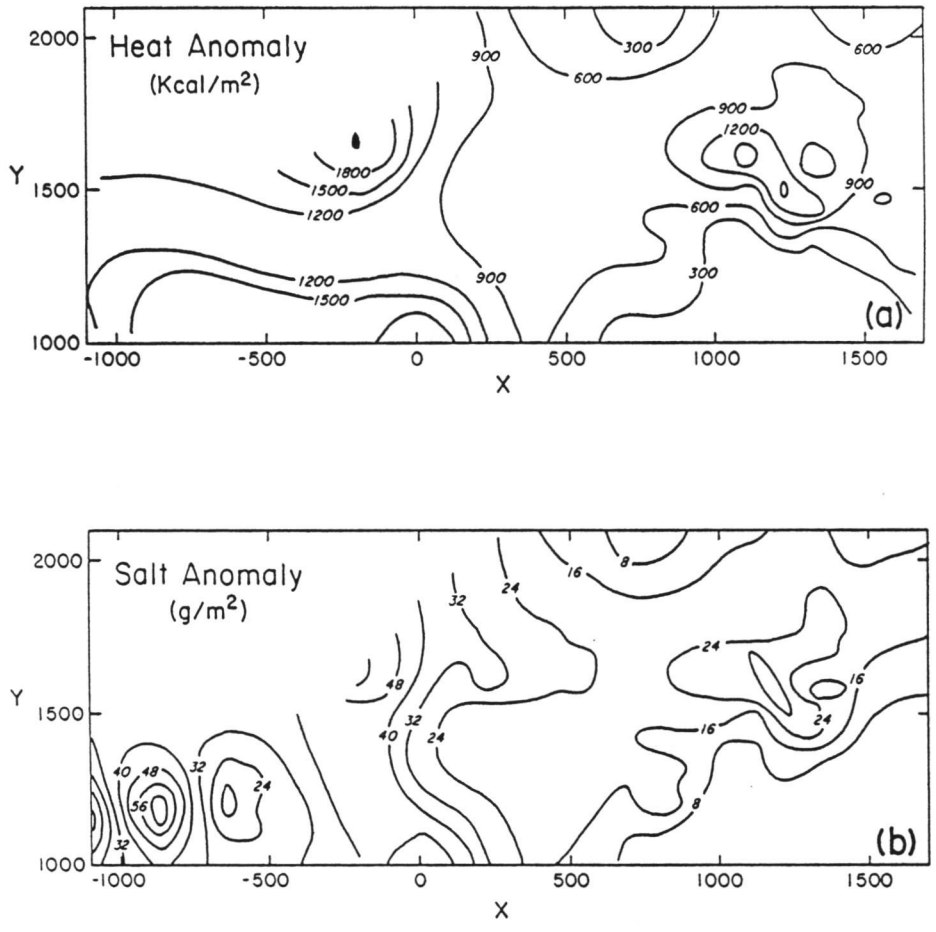

Fig. IV.4. Maps of excess heat (a) in kcal m^{-2} and excess salt (b) in mg m^{-2}. The anomolous heat/salt contents are in excess over the heat/salt contents in the North Basin at the same depths (i.e. difference between the North Basin and South Basin profiles in Fig. IV.2a). X and Y are meters east and north of Eagle Point respectively (as in Fig. IV.1b).

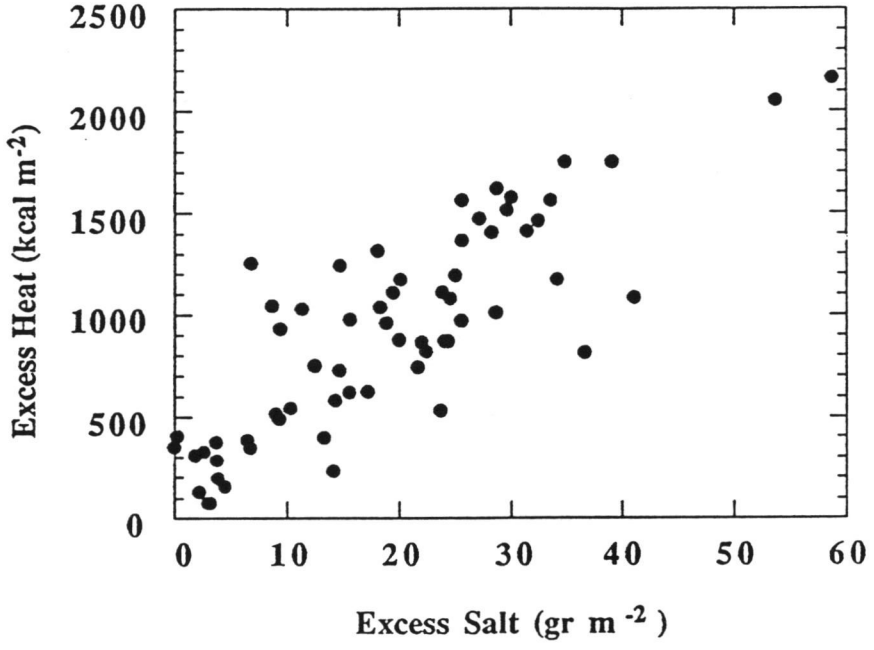

Fig. IV.5. Excess heat as a function of excess salt (from Fig. IV.5). Results suggest that the heat and salt are being delivered by a common carrier, hydrothermal fluid.

movement of fluid is a density profile which is influenced by the bathymetry (Fig. IV.6).

Near-bottom currents were measured approximately 1 meter above bottom using an S4 electromagnetic current meter. The current meter recorded flow rates during its two week deployment between 0 and 2 cm sec^{-1} with most of the readings between 0.5 and 1 cm sec^{-1}. The current directions were generally in the north-northwest direction throughout the two week deployment, suggesting a flow away and down-slope from the fluid source region. Although this data may represent a gravity current driven by the active input of dense hydrothermal fluid, the data set is insufficient to be conclusive.

Results from a detailed near-bottom survey of temperature and salinity in the eastern portion of the South Basin demonstrate that at bathymetric highs the heat to salt ratio is high and at bathymetric lows the heat to salt ratio is low (Fig. IV.7; see Fig. IV.1b for bathymetry). This survey was carried out with the CTD mounted on the submersible. Despite the first-order correlation between heat and salt (Fig. IV.5) there is clearly a change in the heat to salt ratio with depth in the basin (Fig. IV.7). Consistent with the variation in the heat to salt ratio with the bathymetry, higher temperature hydrothermal features (e.g. bacterial mats Dymond et al., 1989) are observed at bathymetric highs whereas at bathymetric lows, lower temperature features (e.g. saline pools, Collier et al. 1991) are observed.

All the observations presented within this section indicate a relationship between the bathymetry and the near-bottom distribution of temperature and salinity in the South Basin. In the following section I attempt to describe the physical processes which generate the observed distribution of heat and salt within the South Basin.

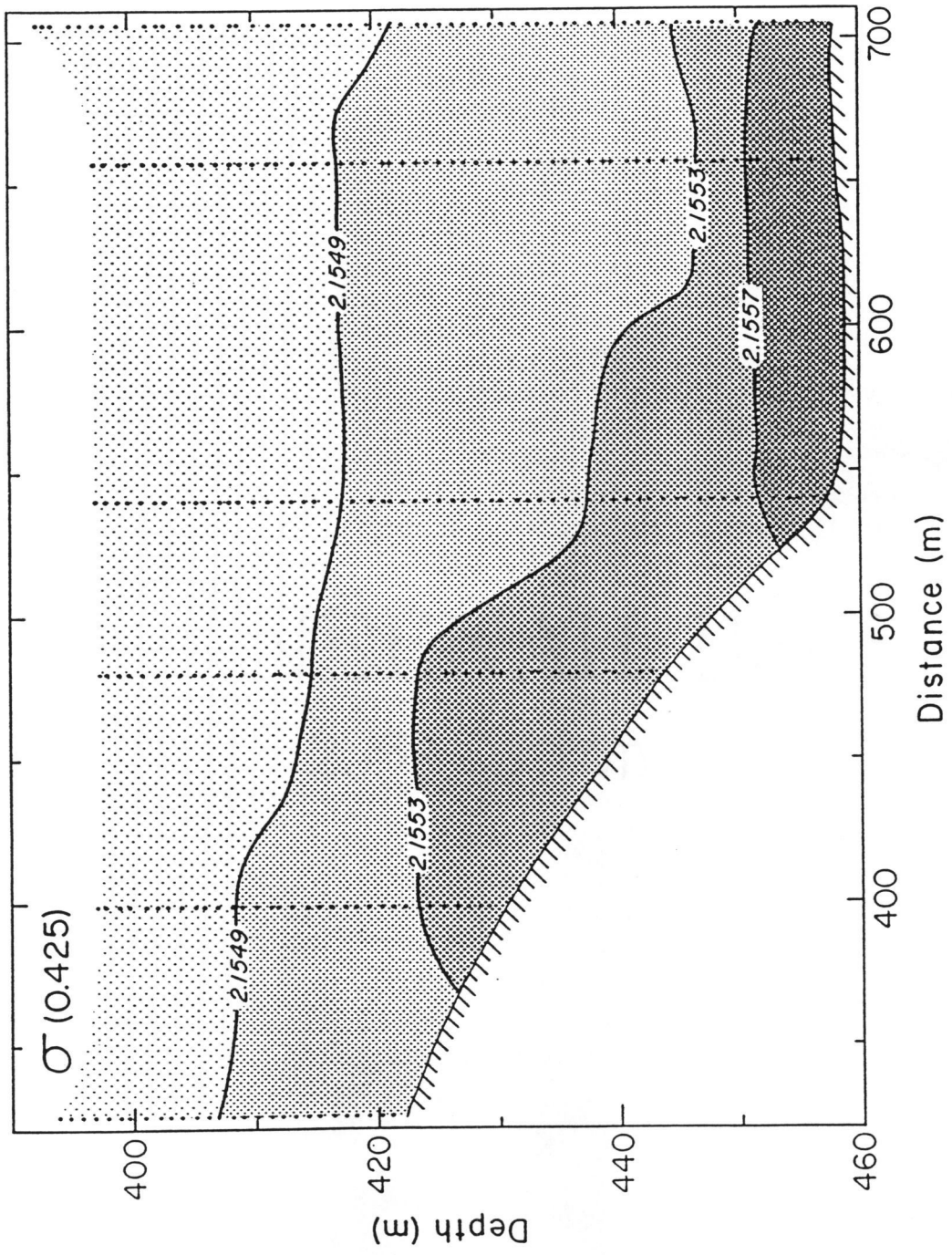

Fig. IV.6. Density contours at a reference pressure of 425 dbars [$\sigma_{(0.425)}$] for a series of hydrocasts. Hydrocasts run along a line from the south to the north in the eastern portion of the South Basin. Depth and distance are in meters.

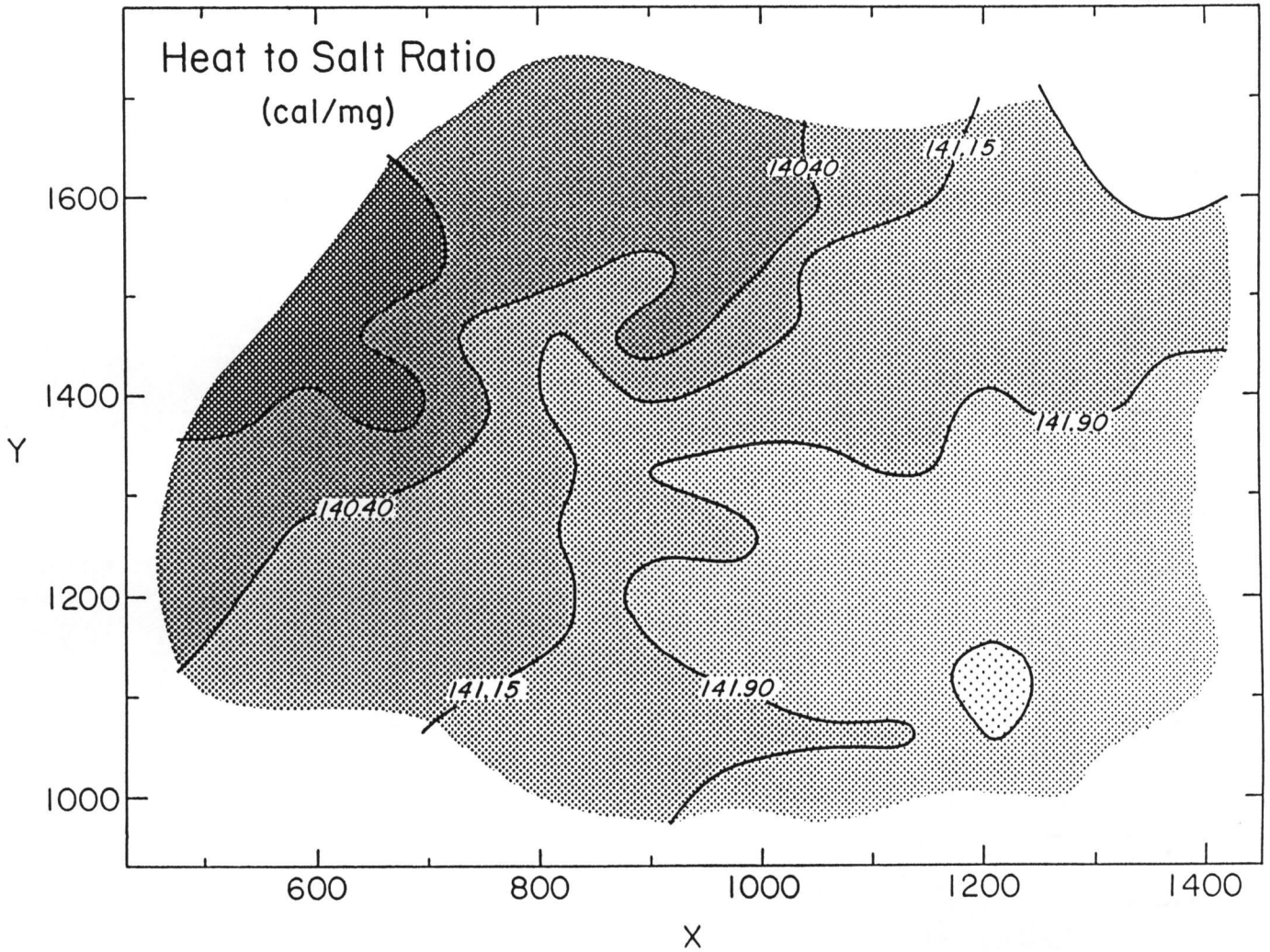

Fig. IV.7. Heat-to-salt ratio of near-bottom waters (~3 meters above bottom) in cal/mg. Data was collected with the CTD mounted on the arm of the submersible *Deep Rover*. X and Y are the same as for Fig. IV.4. The high heat-to-salt ratio fluids correspond to a bathymetric high whereas the fluids having lower heat-to-salt ratios are at bathymetric lows (cf. bathymetry in Fig. IV.1b).

DISCUSSION

Establishing a T-S end-member

In order to understand the mixing behavior and distribution of the hydrothermal fluids in the South Basin, an estimate of the composition of the undiluted hydrothermal end-member is needed. Although the 1989 water column data indicate that the South Basin waters are only slightly enriched in heat and salt over ambient lake water (<20%, Fig. IV.3a), bacterial mats, sediment pore waters, and saline pools sampled in the South Basin were found to have much higher temperatures and salinities than in the water column. Results from both the saline pools (Collier et al. 1990b) and sediment pore waters (Wheat et al. in prep.) suggest that the South Basin hydrothermal end-member salinity is ~0.6 gr kg^{-1} which I assume is the salinity of the hydrothermal end-member.

In choosing the temperature of the hydrothermal end-member it is assumed that buoyancy is the mechanism which delivers fluid to the bottom of the South Basin. Further, it is assumed that there is a single end-member which undergoes a variety of mixing and cooling processes which result in the observed T-S distribution (Fig. IV.3a). I suggest that extrapolation from (BK) along the (H) T-S trend defined in Fig. IV.3a to 0.6 gr kg^{-1} salinity represents the only end-member temperature which satisfies both assumptions and is consistent with the data. From this extrapolation an end-member temperature of ~23°C is obtained (Fig. IV.8). For discussion purposes, I have also extrapolated along the (I) and (L) trends in Fig. IV.3a to a salinity of 0.6 gr kg^{-1} to give the points shown in Fig. IV.8.

If buoyancy is the force which delivers the end-member through the porous media (i.e. sediments) to the lake bottom, then L in Fig. IV.8 is not a legitimate choice for a primary hydrothermal end-member and the low heat to salt ratio fluids found in the deep lake (Fig. IV.3a) need to be explained by another mixing mechanism. Although the extrapolation to a potential end-member represented by (I) in Fig. IV.8 yields a fluid which is buoyant relative to ambient water, no mixture between (BK) and (I) will produce fluids along the (H) trend. End-member (H) is buoyant relative to ambient lake water and I will suggest that (H) can undergo a variety of mixing and cooling processes which will result in any T-S combination apparent in Fig. IV.3a and b.

The possible mechanisms which govern the physics of the hydrothermally enriched fluids as they enter the South Basin are constrained by the observations of the

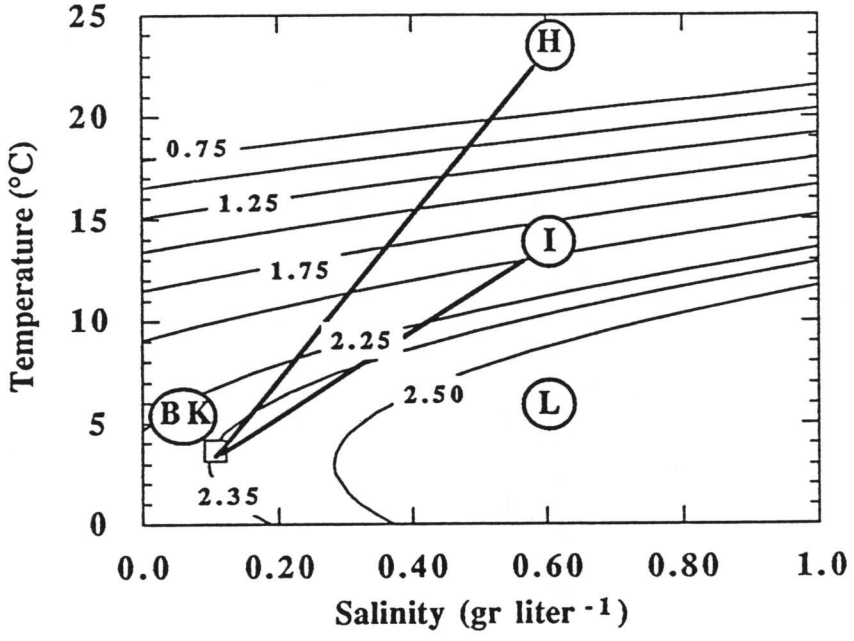

Fig. IV.8. Linear extrapolations of the trends presented in Figure IV.3a to a hydrothermal end-member salinity of 0.6 gr liter^{-1}. Data from Fig. IV.3a is contained within the box in the lower left hand corner of the figure.

heat and salt distribution within the South Basin (Fig. IV.3, 5). These constraints include the observation that; the heat to salt ratio of the near-bottom water in the South Basin is not constant, and it varies with the bathymetry (Fig. IV.7), and high temperature features are generally found at bathymetric highs whereas low temperature features are found at bathymetric lows.

In describing the development of the T-S distribution in the South Basin, two fundamental phenomena of fluid behavior are invoked which occur when fluids of different temperature and salinity mix. In the case where the source fluid enters the system as a buoyant plume, a mixture between the buoyant fluid and ambient fluid may result in a mixture which is more dense than either (Turner and Gustafson 1978; McDougall 1983; McDougall 1984; Campbell et al. 1984; Turner and Campbell 1987). This is demonstrated by the (BK) to (H) line in Fig. IV.4 where starting from (BK) represented by the box located on the 2.35 isopycnal and moving along a mixing line toward (H), the density at first increases along the mixing line and then decreases as the mixture becomes more enriched in (H). Additionally, double diffusion may dominate fluid behavior on small scales. Under the conditions that the buoyant fluid flow and the initial density difference between the buoyant fluid and ambient fluid are small, a buoyant plume may undergo double diffusive loss of heat rather than rapid convection (McDougall 1983).

The density of a mixture of two end-members

Since the mixing line between ambient water and the hydrothermal end-member crosses through a large range of isopycnals which are curves (Fig. IV.4), mixtures of the two end-members BK and H may yield fluids which are more dense than either. If the buoyant hydrothermal end-member were entering at a bathymetric high, then mixing at the sediment-water interface could produce a more dense fluid which could then flow down-slope. This process is suggested by the horizontal density distribution in Fig. IV. 6.

This mixing could also occur within the sediments rather than just in the water column. Fluids may rise through the sediments and mix with pore fluids until they have become neutrally buoyant. Once the density of these fluids becomes greater than lakewater, they may flow down slope within the sediments, and may subsequently exit the sediments deeper in the South Basin.

Although the mixing of two end-members will influence the density of the fluids as they travel along the sediment-water interface or within the sediments, this mixing will not change the heat to salt ratio. In order to change the heat to salt ratio of these fluids, an additional mechanism will need to be invoked.

Double diffusion in the water column and conductive heat loss

The variation in the South Basin heat to salt ratio may be accomplished by double diffusion or through the loss of heat by conduction with surrounding solids.

Double diffusion is a molecular process where heat may diffuse from a fluid faster than the salt due to the differing molecular diffusivities of these two properties. A characteristic of double diffusive convection in environments where warm salty water is underlying cold, fresh water is the formation of sharp steps in T and S separated by well-mixed convective layers (Newman 1976). The deep lake temperature and salinity data lacks any distinct "steps" (Fig. IV.9). This observation leads to the conclusion that double diffusion is not the major transport process controlling the vertical fluxes of heat and salt through the water column. The water column in Crater Lake is dominated by turbulent mixing processes, although the actual forcing mechanism for this turbulence is not known (Chapter III). In spite of the evidence against double diffusion in the water column, I suggest that double diffusive mixing may be operating on fluids near the sediment-water interface and on the fluids contained within the small saline brines.

Several features of the deep South Basin do suggest some degree of double diffusion. The heat to salt ratio varies near the sediment-water interface (Fig. IV.8) and one explanation for this observation is that heat is being lost preferentially over salt from the hydrothermal fluids. If diffusive loss of heat or double diffusion were significant within the system, then there would be curvature in the near-bottom T-S distribution (Ingham 1966; Schmitt 1981; McDougall 1983). The high salinity-low temperature mixtures (trend L in Fig. IV.3a) form a curve rather than a line on the South Basin T-S plot, suggesting that the water in this region has undergone preferential loss of heat over salt.

The calculation of the density ratio provides a quantitative way of evaluating the potential for double diffusion in the lake, where the density ratio R_ρ is defined as follows:

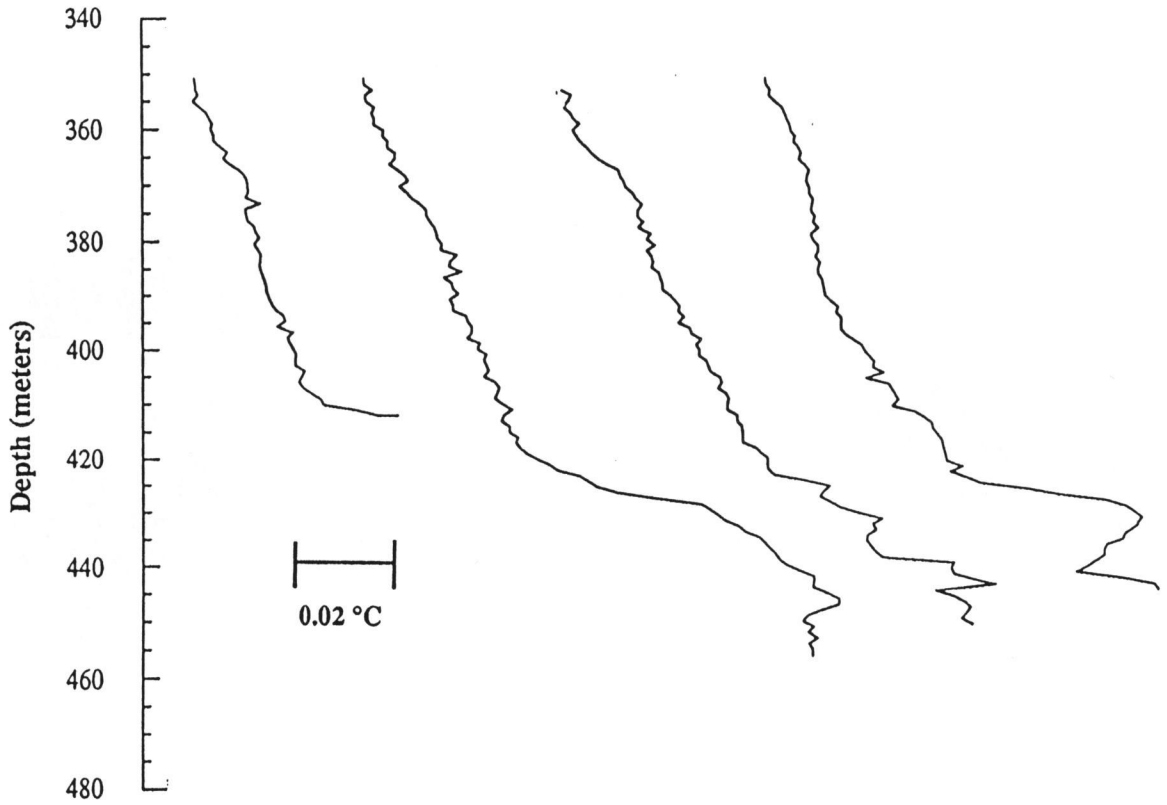

Fig. IV.9. A series of south-to-north temperature profiles from the eastern portion of the South Basin. The temperature at 350 m is approximately 3.56°C for each profile. Note the sharp interfaces near the bottom of the profiles and the lack of any distinct "step-like" features.

$$R\rho = \frac{\beta \Delta S_z}{\alpha \Delta T_z} \qquad \text{(IV. 1.)}$$

where ß = (1/ρ) (∂ρ/∂S), α = - (1/ρ) (∂ρ/∂T), and ΔS_z and ΔT_z are the salinity and temperature gradients respectively. A plot of the density ratio as a function of depth (Fig. IV.10) shows that in the upper portion of the water column the density ratio is high (>2) suggesting that double diffusion is not important as a mechanism for heat and salt transport (Huppert, 1971). However, at depths near the sediment-water interface (0-20 m above bottom) the density ratio approaches 2, and on occasion is less than 2, suggesting that double diffusive convection may be contributing to the loss of heat and salt from these near-bottom fluids.

Finally, although there are no well-mixed "step-like" features apparent in the temperature profiles of Fig. IV.9, irregular features having sharp interfaces are consistently observed which suggest that steps may be forming or are briefly formed and subsequently destroyed by turbulence.

As the hydrothermal fluids move through the sediments covering the South Basin, conductive loss of heat by these fluids to the surrounding solid debris will also change the heat to salt ratio. If a dense mixture of hydrothermal fluid and pore fluids is formed, as previously described, this mixture may loose heat while in contact with the surrounding debris due to conductive cooling. Alternatively, the permeability of the debris flow may vary in conjunction with the bathymetry (i.e. high porosity at bathymetric highs and low porosity at bathymetric lows). The result of such a variation is that at a bathymetric high the end-member fluid will travel through the debris rapidly, thereby retaining its heat to salt ratio. At bathymetric lows, the lower permeability in this region will lead to an increase in residence time of the end-member fluid resulting in more conductive heat loss by the fluid.

Without a more detailed knowledge of the physical properties of the sediments within the South Basin, it is not possible to constrain the importance of conductive heat loss on the hydrothermal fluids. The importance of conductive cooling on thermal waters has previously been suggested by Ingebritsen et al. (1989). They suggest that the differences between observed hot spring discharge temperatures in the Oregon Cascades and temperatures predicted from geothermometry arise from conductive cooling of the thermal water.

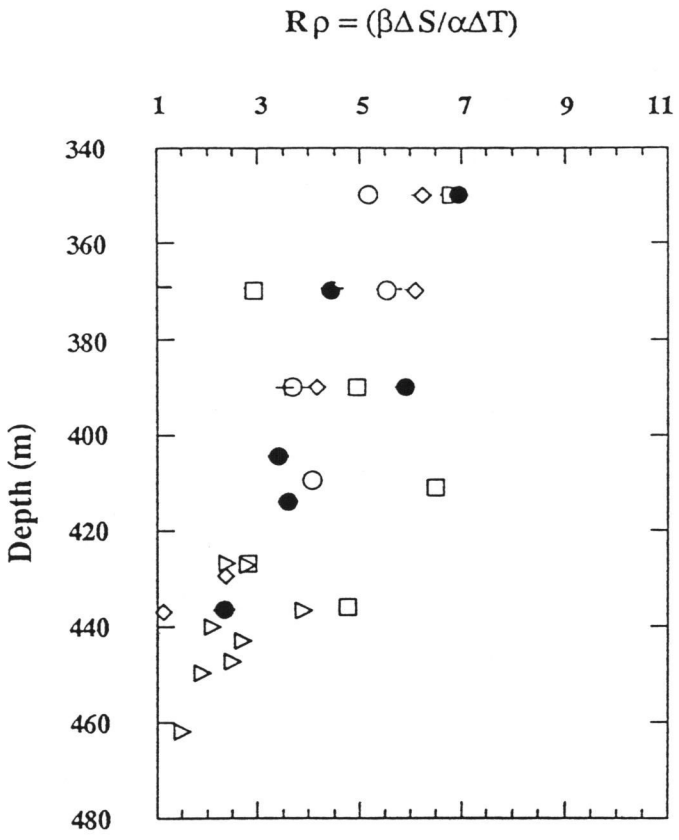

Fig. IV.10. The density ratio versus depth for the South Basin. Calculations of Rρ close to the sediment-water interface suggest that double diffusion may be occurring near the lake floor; however, further up the water column the density ratio is high suggesting that double diffusion is not dominant within the water column. Different shapes represent the different hydrocasts in Fig. IV.9. Above ~420 m, each value in the figure represents an average of three consecutive points at 1 meter intervals which are centered around the point. The deeper Rρ values are calculated for discrete points (not averages) that are dependent on the changes in the vertical temperature gradient. Because these deeper data have much larger gradients in T and S than the upper water column, the confidence in the calculated Rρ is greater in the deeper water column than in the upper water column.

Relationship of brines and bacterial mats to the T-S distribution

The distribution of the bacterial mats and the saline pools are consistent with the observations of the T-S distribution within the South Basin. Higher temperature mats tend to be located at bathymetric highs and rock outcrops, whereas lower temperature mats and saline pools tend to be located at bathymetric lows (Dymond et al. 1989; Collier et al. 1991). Due to their lower temperature, the brines are more dense than ambient water. These low temperature high salinity brines must therefore be maintained through double diffusion or through the input of conductively cooled fluid. At steady state, the flux of fluid into the pool must equal the flux out and the flux of heat and salt from the pool may be accomplished by double diffusive convection. Such a process has been modeled by McDougall (1984), who examined the processes that occur when a fluid of high temperature and high salinity enter into a depression from below.

The varying heat to salt ratios in the South Basin

Both conductive loss of heat and double diffusion would partially explain the observed variation in the heat to salt ratio with the bathymetry and it is likely that a combination of these processes is occurring. In addition, the mixing between a buoyant hydrothermal end-member and ambient lake water will produce a linear T-S distribution and a mixture which is more dense than either. A summary of how the distribution of the fluids of varying heat to salt ratios may be achieved is presented in Fig. IV.11. The lettering on the diagram corresponds to the T-S end-members in Fig. IV.3a and Fig. IV.4.

At (H) (Fig. IV.11) a thermally and chemically enriched fluid rises to the surface through the sediments with a high heat to salt ratio and is buoyant. The mixing of (H) with ambient water produces a mixture which is more dense than either initial fluid and has a high heat to salt ratio. Therefore, the newly formed mixture will flow down slope along the sediment-water interface possibly producing a density distribution as in Fig. 7.

As the water of high heat to salt ratio moves down-slope, any double diffusive loss of heat relative to salt will decrease the ratio of these two properties and further increase the density (I and L, in Fig. IV.11). However, because the scales of mixing suggest that double-diffusive convection is not a dominant mechanism for the redistribution of heat and salt through the bulk water column as is evidenced by a lack of steps in Figure 10 (also Chapter III), the effects of any double diffusive convection on

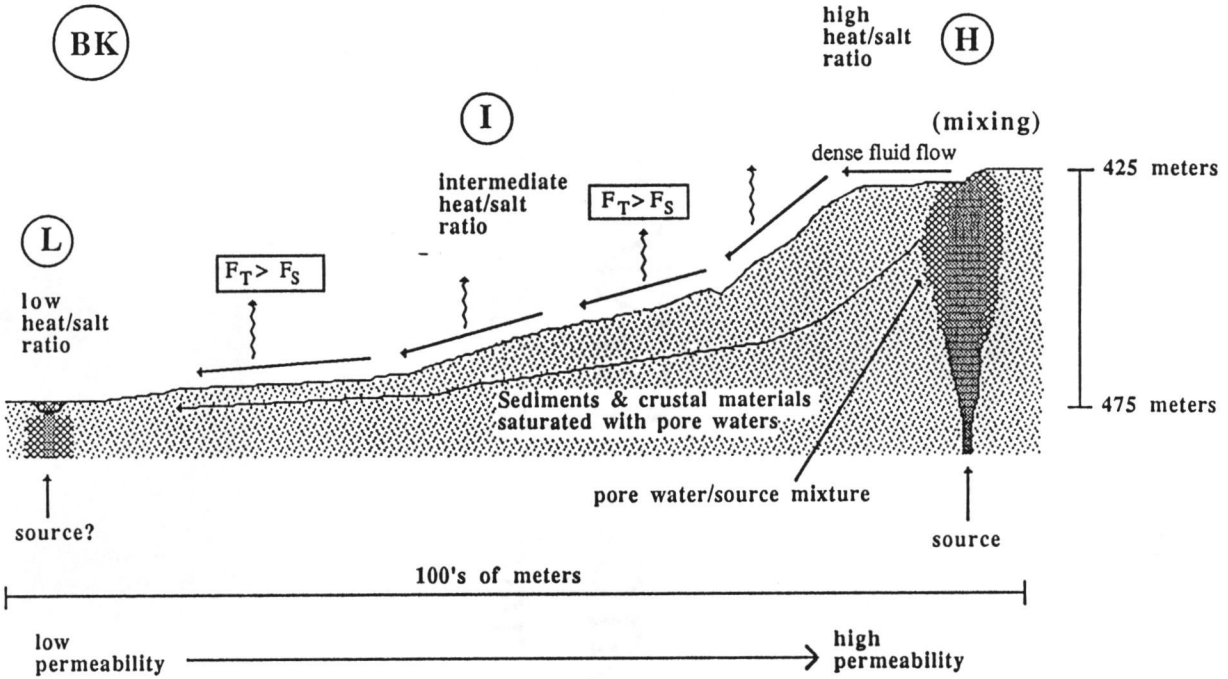

Fig. IV.11. Conceptual model which describes how the varying heat to salt ratios observed near the sediment-water interface in the South Basin (Fig. IV.7) , may be achieved. The lettering on the cartoon corresponds to the lettering in Fig. IV.3a.

the overall T-S properties of the deep lake will be confined to small or local scales near the sediment-water interface. Even if there were preferential loss of heat over salt occurring in the near-bottom regions of the South Basin, turbulent mixing in the water column would tend to mix the steps out. Conductive heat loss by the end-member fluid within the sediments, may also contribute to the observed near-bottom distribution of temperature and salinity. This conductive heat loss may be due to variations in sediment permeability or down-slope movement of the hydrothermal-ambient mixture or both.

Another mechanism for changing the heat to salt ratio of near bottom waters is through chemical reactions of the fluids within the sediments (i.e. mineral dissolution). This would tend to change the heat to salt ratio by increasing the salinity of the pore fluids. However, chemistry data indicate that there are no large systematic changes in fluid chemistry throughout the South Basin (Dymond et al. 1989; Wheat et al. in prep.). In general, changes in fluid composition are primarily due to dilution with lake water and not reaction.

The distribution of heat and salt along the sediment-water interface of the South Basin is partially controlled by the non-linear density behavior of mixtures between South Basin ambient water and hydrothermal end-member water. It is suspected that the varying heat to salt ratios of the near bottom waters in the South Basin are driven by double diffusive and conductive heat loss. However, in order to better understand the processes which lead to variations in the near-bottom heat to salt ratio, a more thorough knowledge of the physical characteristics of the sediments is needed.

CONCLUSIONS

The T-S properties of the hypolimnion reveal that the waters in the South Basin are warmer and saltier than those in the rest of the hypolimnion. The general correlation between excess heat and salt within the South Basin suggest a common carrier -- hydrothermal fluid. Maps of excess heat and salt suggest that the eastern portion of this basin is the dominant region of hydrothermal inputs.

The near-bottom distribution of temperature and salinity in the South Basin indicates that there are a variety of mixing and cooling processes acting upon the hydrothermal fluid. Two end-member mixing between the hydrothermal fluid and ambient water generates fluids having a high heat to salt ratio which is observed in the eastern portion of the South Basin. This mixing produces a fluid which is more dense than either of these two end-members. Preferential loss of heat through double diffusion or conductive heat loss or both, near or within the sediments, generates a variety of heat to salt ratios which result in the curvature of the near-bottom T-S distribution.

ACKNOWLEDGEMENTS

The logistical assistance of Gary Larson at OSU College of Forestry allowed much of this work to be accomplished. James Milestone, Mark Buktenica, John Salinas, and Scott Stonum from Crater Lake National Park provided day and night field support for this research and their efforts are greatly appreciated. The field and analytical efforts of the OSU research team were invaluable. Special thanks are extended to Roberta Conard and Chris Moser. This research was funded by the U.S. National Park Service under cooperative agreement No. CA 9000-3-0003, CPSU, College of Forestry, Oregon State University.

V. USING THE DEEP LAKE OXYGEN BUDGET IN CRATER LAKE, OREGON TO CONSTRAIN MIXING, CARBON FLUX, AND HYDROTHERMAL INPUTS

ABSTRACT

Small temporal and spatial variations in the distribution of dissolved oxygen below 350 m in Crater Lake, Oregon yield information on the mixing time-scales, carbon flux, and the magnitude of hydrothermal activity within the lake.

Based on a time-series of analyses, the consumption rate of dissolved oxygen in the deep lake was observed to be ~4.4 mmol O_2 m^{-2} day^{-1}. This consumption of oxygen is primarily due to the oxidation of organic matter and, to a lesser extent, the oxidation of reduced inorganic species which are introduced to the system via subsurface hydrothermal springs. Assuming a 1.3:1 stoichiometric relationship between oxygen and carbon for the oxidation of organic matter, the consumption rate of dissolved oxygen requires the oxidation of ~3.4 mmol C m^{-2} day^{-1}. Assuming this carbon has its origin in the upper water column, and the amount leaving the euphotic zone can be estimated by the supersaturation of dissolved oxygen, ~40% of the early summer oxygen supersaturation is due to primary biological production. The remainder of the dissolved oxygen supersaturation is primarily due to direct warming of the upper water column from the penetration of solar radiation.

An increase in deep lake oxygen during the winter of 1988-89 indicates that 30-45% of deep lake water was replaced with well-oxygenated surface water. This corresponds to a deep water ventilation rate of 2.5-3.5 years. Considering the concentration of nitrate in the deep lake, this mixing delivers ~5 x 10^6 moles of nitrogen per year to the upper water column.

In the South Basin, where hydrothermal fluids are entering the lake, the distribution of dissolved oxygen is influenced by reduced inorganic species which are introduced with the hydrothermal fluids. Here, the dependence of the oxygen distribution on hydrothermal activity is suggested by linear relationships between dissolved oxygen and temperature and salinity. In addition, the stoichiometric relationship between dissolved oxygen and nitrate is considerably higher in this basin, where $-\Delta O_2:\Delta NO_3$ is ~40, than in the rest of the lake, where $-\Delta O_2:\Delta NO_3$ is ~16.

INTRODUCTION

Crater Lake, Oregon is a deep, well-mixed, oligotrophic caldera lake located at an elevation of 1882 m in the Oregon Cascades. The lake is predominantly precipitation fed (Redmond 1990) and has no significant surface inputs or outputs. The lake's surface area is 53.2 km^2 which represents nearly 80% of the lake's total drainage basin (Phillips 1968; Redmond 1990). Crater Lake has two semi-enclosed basins, one in the northeastern portion of the lake (North Basin) which has a maximum depth of 589 m and one in the southwestern section of the lake (South Basin) which has a maximum depth of approximately 485 m.

The physical and chemical properties of the deep water column are influenced by subsurface hydrothermal inputs (Collier et al. 1990; Chapter II). The South Basin receives the largest flux of hydrothermal fluids; it is here that the strongest gradients in heat and salt are found (Williams and Von Herzen 1983; Chapter IV). Additionally, Dymond et al. (1990) report finding bacterial mat assemblages in this region of the lake which are composed of Fe and Mn oxidizing bacteria, and mark the location of individual spring inputs. As a consequence of the influence of hydrothermal activity in the South Basin, much of the recent research efforts have been focused in this portion of the lake, particularly in the eastern half of the basin ("the hydrothermal study area").

Dissolved oxygen is a sensitive tracer of physical and chemical processes occurring in an aquatic system. Oxygen in excess of atmospheric saturation in the upper water column is caused by photosynthesis, the penetration of solar radiation resulting in in situ warming of the water column, and air bubble injection (Jenkins and Goldman 1985; Emerson et al. 1991). The disappearance (consumption) of dissolved oxygen at depth is typically due to the oxidation of particulate organic matter raining out of the euphotic zone. If the photosynthetic component of the oxygen excess in the upper water column is properly constrained, then this component should have the same value (opposite in sign) as the amount of oxygen consumed.

In temperate lakes, convective mixing of winter-time surface water with deep water results in an increase in dissolved oxygen at depth. This change in oxygen provides a semi-quantitative estimate for the efficiency and timing of deep lake mixing.

The goal of this chapter is to examine the effects of mixing, carbon flux, and hydrothermal inputs on the distribution and budget of dissolved oxygen in the deep water column of Crater Lake, Oregon. The data set for constraining these processes includes dissolved oxygen samples from 1988-1991, which includes a detailed spatial

and temporal data set collected during the 1989 field season, a more limited nutrient data set, estimates of the composition of the hydrothermal fluid, and sediment trap carbon flux estimates (Dymond and Collier, unpublished).

METHODS

Water column samples were recovered using 5 and 20 liter Niskin samplers and 4 liter Van Dorn bottles. Water samplers were deployed from the National Park Service (NPS) research boat equipped with a hydrowire. During the summer 1989 field season, discrete bottom water samples were also recovered using the submersible *Deep Rover* (Dymond et al. 1990).

Temperature, pressure, and conductivity were measured using a SEACAT® model SBE19 (Sea-Bird Electronics Inc.) "CTD". The temperature resolution is ±0.0005°C, and based on calibrations between 1987-1989 the absolute accuracy of the temperature sensor was within 0.001°C. Salinity is determined from in situ temperature and conductivity as described in Chapter II. Density is calculated from the CTD hydrographic data (Chapter II) and is based on the equation of state for waters in the limnological range as presented by Chen and Millero (1986).

Oxygen samples were analyzed by a whole-flask Winkler titration method with the modifications of Carpenter (1965a, b). An alkaline-iodine fixing solution containing sodium azide was used in samples retrieved near hydrothermal springs to remove potential interferences from reduced iron. The overall precision of the oxygen measurement, based on duplicate sample analysis, is better than 0.5%. Oxygen solubility for Crater Lake was calculated as a function of lake surface elevation, temperature, and salinity (Benson and Krause 1984). The mean barometric pressure was calculated from the altitude-dependent equation given by Mortimer (1981). In discussing the mixing of oxygen-saturated water with deep lake water, I assume that the parcel of water from the upper water column has an oxygen content of 328.5 μM which is the saturation value for the temperature (~3.6°C) of the surface mixed layer during winter.

Silicic acid, phosphate, and nitrate were determined using colorimetric methods described in Strickland and Parsons (1965) and modified for an Alpkem rapid flow analyzer. The precision of the silicic acid, phosphate, and nitrate measurements are ~1%, ±0.05 μM, and ±0.025 μM respectively.

Samples for pH and alkalinity measurements were collected in a 100 ml syringe directly from Niskin sample bottles and were kept cold (~4 °C) until analysis. For analysis, the samples were brought to room temperature and then transferred to a "closed" titration flask (Edmond 1970). The pH was then measured at 25 ± 0.5°C followed by an addition of 0.425 grams of purified KCl and the pH was measured again

(Hillman et al. 1986). Alkalinity of the sample was determined using a closed Gran titration procedure (Gran 1952; Dryssen and Sillen 1967; Edmond 1970). ΣCO_2 was calculated from the pH and alkalinity measurements (Stumm and Morgan 1981). The precision of the calculated ΣCO_2 is ~1%.

Sodium was determined by flame atomic absorption spectroscopy according to the high precision methods described in Chapter II. The precision of the sodium analysis for the data presented in this chapter is ~0.75%.

Sediment traps, with a 0.25 m^2 sampling area, designed and built at Oregon State University (Dymond and Collier 1990) were used to collect particles falling through the water column. Three traps were placed on a single mooring at 200, 380, and 580 m depth. The 200 m trap was equipped with a five cup sampler, allowing time-series sampling with a two month resolution. Samples are preserved in situ using a buffered formaldehyde solution.

RESULTS

Hydrography and the vertical distribution of dissolved constituents

The upper water column in Crater Lake, OR is well-mixed twice annually, during the mid-to-late winter and late spring. During this mixing period, a nearly uniform temperature and density profile is produced in the upper 200 m (Fig. V.1). In addition, as a result of this seasonal mixing, the salinity distribution in the upper 200 m is uniform throughout the year (Fig. V.1b). As first described by Neal et al. (1971; 1972), the thermal gradient below 350 m is "hyperadiabatic" (Fig. V.1a), or approximately two orders of magnitude greater than the adiabatic lapse rate. This thermal gradient in the deep water is due to the active input of hydrothermal fluids and is balanced by an increase in salinity (Fig. V.1b), which yields a stable density gradient in the deep lake (Fig. V.1c).

The water column of Crater Lake is nearly saturated with respect to atmospheric saturation of dissolved oxygen throughout the year (Fig. V.2). This is maintained by rapid vertical mixing, coupled with the relatively low carbon flux through the water column of this oligotrophic system (Dymond and Collier 1990). Likewise, there is little horizontal variability in dissolved oxygen (Fig. V.2). In the upper 150 m supersaturation of dissolved oxygen is typically observed throughout most of the year (Fig. V.2). This excess is due to net photosynthetic production in these upper waters and the penetration of solar radiation which causes in situ heating of subsurface waters.

Hydrothermal activity in the South Basin delivers zero-oxygen water which has high concentrations of chemically reduced species. As a consequence of the oxidation of these reduced species after entry to the deep lake and dilution of South Basin water with this zero oxygen spring water, there are near-bottom heterogeneities in the distribution of dissolved oxygen in the South Basin. Hydrothermal activity also influences the distribution of the lake's major solutes. Bicarbonate is the major anion in Crater Lake and the distribution of ΣCO_2 in the South Basin (Fig. V.3a) increases with depth due to hydrothermal activity. The vertical distribution of silicic acid is also influenced by hydrothermal activity (Fig. V.3b). In contrast, the vertical homogeneity of dissolved phosphate (Fig. V.3c) suggests that it does not have a strong hydrothermal source at the bottom and that this nutrient does not limit primary production in the euphotic zone of Crater Lake.

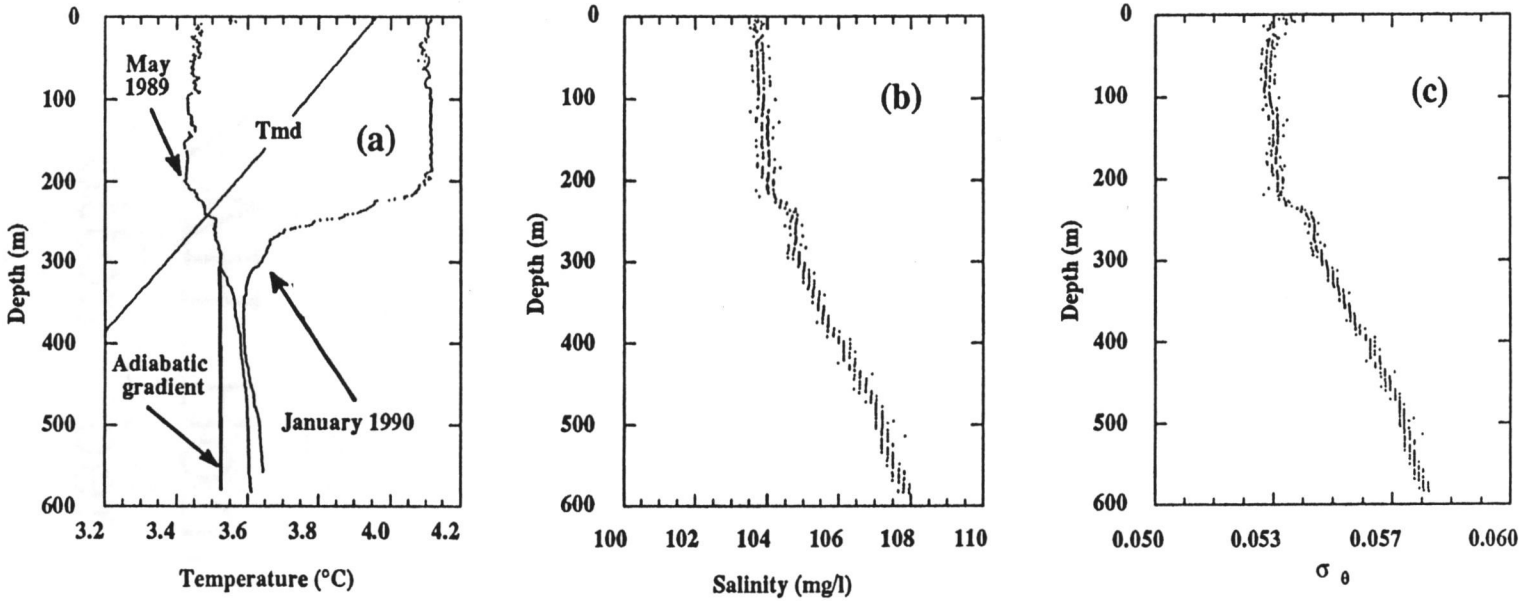

Fig. V.1. (a) Temperature vs. depth for May 1989 and January 1990. The temperature of maximum density (Tmd) and the adiabatic gradient are calculated from a polynomial presented in Chen and Millero (1986). (b) Salinity vs. depth. (c) σ_θ vs. depth. Note the well-mixed nature of the upper 200 m in the water column of Crater Lake and the increase in temperature, salinity, and density with depth below 200 m.

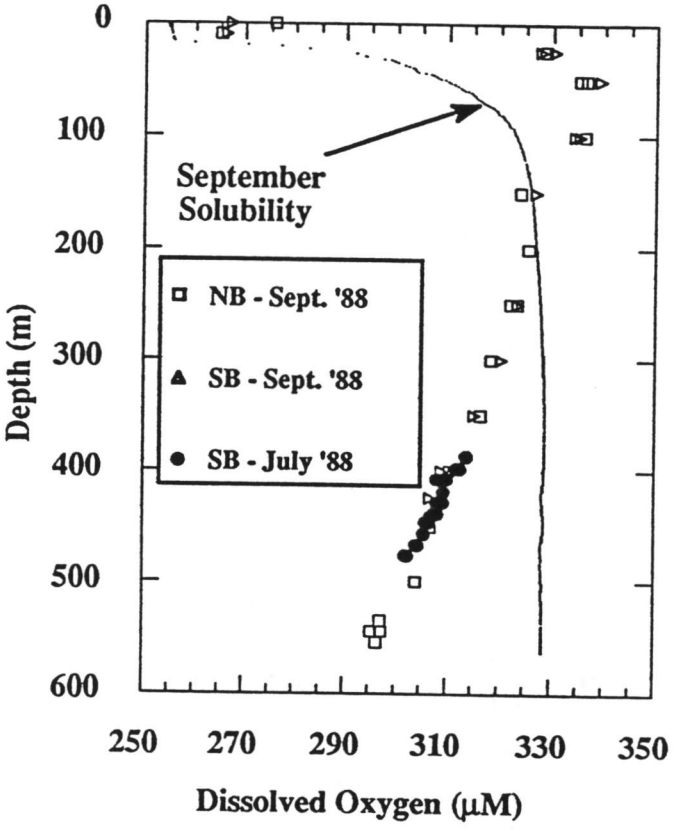

Fig. V.2. Expanded scale dissolved oxygen (μM) as a function of depth for July and September 1988 in both the South Basin (SB) and the North Basin (NB) of the lake. Variations in oxygen solubility are primarily a function of temperature (Benson and Krause 1984).

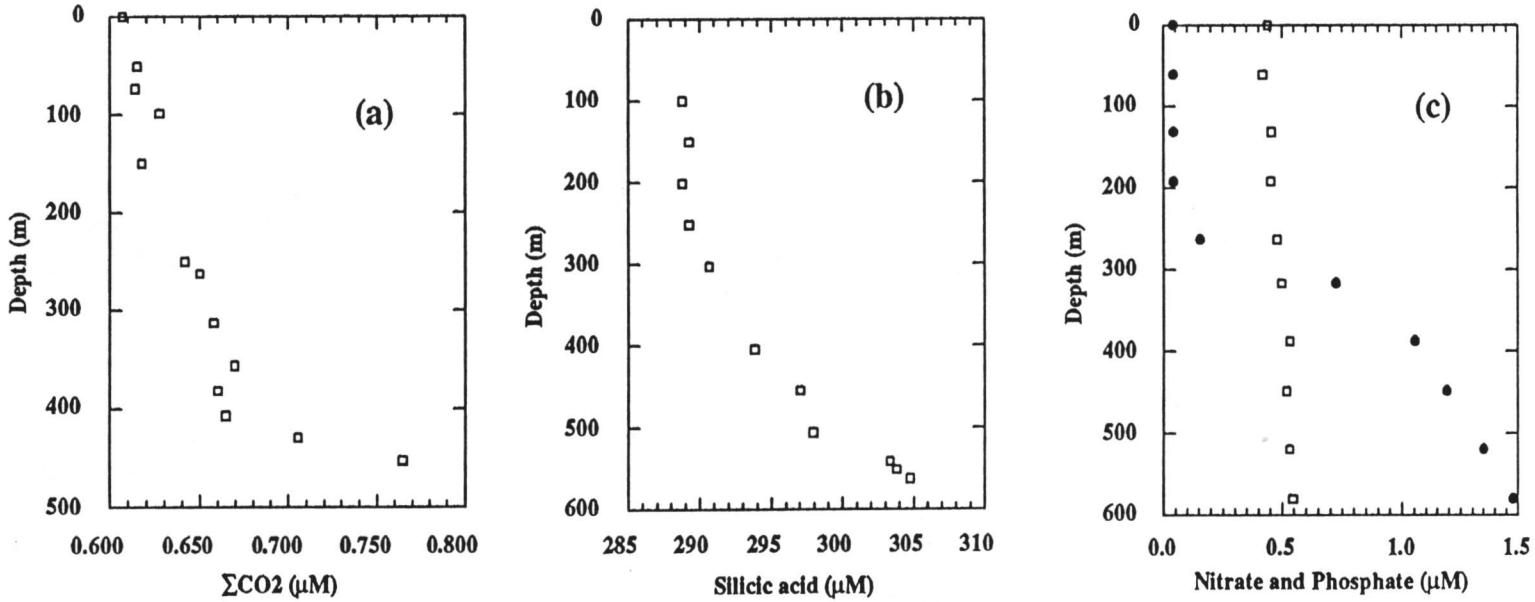

Fig. V.3. (a) ΣCO_2 as a function of depth in the South Basin. (b) Silicic acid and (c) nitrate (filled circles) and phosphate (open boxes) vs. depth in the North Basin. ΣCO_2 is calculated from pH and total alkalinity as described within the text. Both ΣCO_2 and silicic acid are influenced by hydrothermal activity to a much greater degree than either nitrate or phosphate. The silicic acid data was collected in September 1988 and the ΣCO_2, nitrate, and phosphate data were collected during the summer of 1989.

During the summer months, nitrate in the upper 200 m is consistently below 0.05 μM (Fig. V.3c). In addition ammonium levels throughout the water column are typically undetectable (< 0.05 μM). This lack of fixed nitrogen in the upper water column presents a significant limitation to primary production in Crater Lake (Larson 1986; Collier et al. 1990).

Temporal variations in dissolved oxygen

The oxygen cycle in Crater Lake includes the mixing of oxygenated upper water with deep lake water followed by the consumption of oxygen in the isolated deep lake basins due to the decomposition of organic matter and the oxidation of hydrothermally-derived reduced species. A time-series of dissolved oxygen shows that the deep lake (550 m) dissolved oxygen content increased from September 1988 to April 1989 by ~10 μM. This was followed by a decrease in dissolved oxygen of ~13 μM between April 1989 and January 1990. After January 1990 there was another increase in deep lake dissolved oxygen accompanied by a decrease in deep lake temperature due to the partial ventilation of the deep lake with cooler, well-oxygenated surface water (Fig. V.4) (Chapter III).

The rate at which oxygen decreases in the deep lake varies as a function of depth. At a depth of ~300 m there appears to be little or no change in the dissolved oxygen contents throughout the year. The rate of dissolved oxygen decrease at 450 m is 15-20 μmol m^{-3} day^{-1} and the decrease at 550 m is 40-44 μmol m^{-3} day^{-1}.

The integrated change in the deep lake (303 to 557 m) dissolved oxygen inventory measured between June 1989 and January 1990 is -4.4 mmol m^{-2} d^{-1}. Because the data used to calculate the change in the oxygen inventory only covers depths to 557 m, as opposed to the maximum depth of 589 m, and because the respiration rate increases with increasing depth, the estimated respiration rate is a minimum.

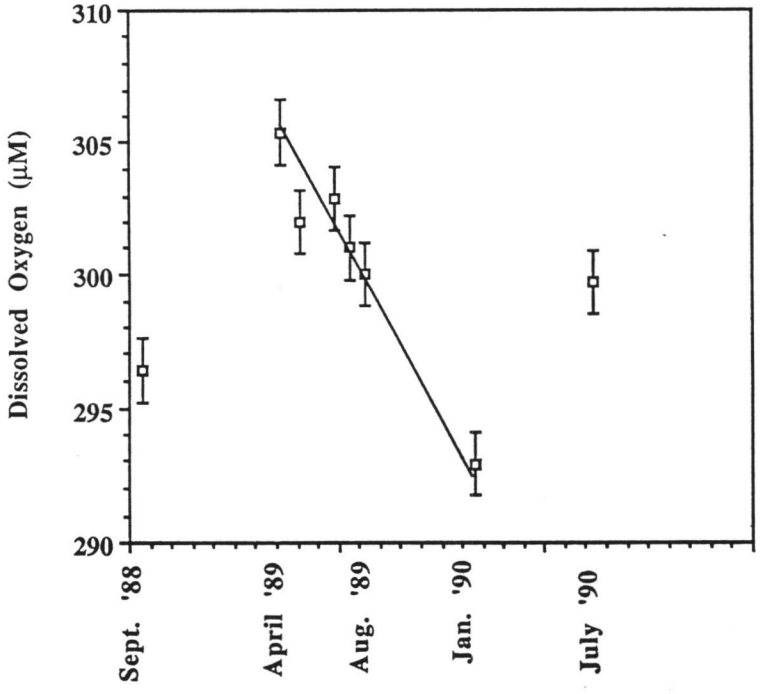

Fig. V.4. Dissolved oxygen at 550 m as a function of time from April 1989 to January 1990. The oxygen cycle in Crater Lake shows an increase in deep lake oxygen due to mixing followed by a decrease due to the consumption of oxygen. The decrease in dissolved oxygen over time in the deep water column is due to the consumption of oxygen by particulate organic material and hydrothermally-derived reduced chemical species. The line demonstrates a consumption rate of dissolved oxygen of approximately 40 μmol m^{-3} day^{-1}.

DISSCUSSION

Mixing

One approach to constrain the extent of deep lake mixing during the winter of 1988-89 is to assume that the dissolved oxygen measurement at 550 m for April (307 μM) is a mixture of air-saturated winter water (328.5 μM) and a deep lake end-member prior to mixing (297.4 μM). Under these assumptions, the deep water in April is comprised of 30% "new" air-saturated water and 70% "old" deep lake water.

Any deep water oxygen depletion occurring after September and before April will change the mixing estimation made above. Extrapolating the deep lake dissolved oxygen consumption rate of ~0.04 μmol liter^{-1} day^{-1} (Fig. V.4) to later in the fall and earlier in the winter suggests that the net change in dissolved oxygen was possibly as high as 16.2 μM O_2 at 550 m. This changes requires a mixture of 45% air-saturated winter water and 55% deep-lake water. Such a mixture implies a deep lake time-integrated ventilation rate of ~2.5 years. The data are insufficient for the same kind of approximations for 1990; however, the data indicate that some exchange has occurred (Fig. V.4). The time scale of vertical mixing calculated here is consistent with the work of Simpson (1970a), who calculated a ventilation rate for Crater Lake on the order of 1 year, and is also consistent with the recent work of Weiss and Lupton (unpublished).

There appears to have also been some mixing between May and June as is indicated by an increase in dissolved oxygen in June relative to May (Fig. V.4). This increase in dissolved oxygen is much smaller in magnitude than the changes seen for the winter mixing period. Although it is difficult to constrain this mixing since the analytical uncertainty is large for such a small change, there was also a small decrease in deep lake temperature further suggesting that some exchange occurred during spring.

In Crater Lake, the mixing cycle occurs each year. Although the annual efficiency of this mixing is unknown (Chapter III), dissolved oxygen data taken in July 1989-91 show that the distribution of deep lake dissolved oxygen is consistent from year-to-year (Fig. V.5). However, this data does not necessarily demonstrate that the mixing process is constant from year to year. Because primary production is dependent on the upwelling of deep lake nutrients, the carbon flux, which results in deep lake oxygen consumption, could be closely coupled to the extent of mixing. This may lead to the observed consistency in deep oxygen profiles from year to year.

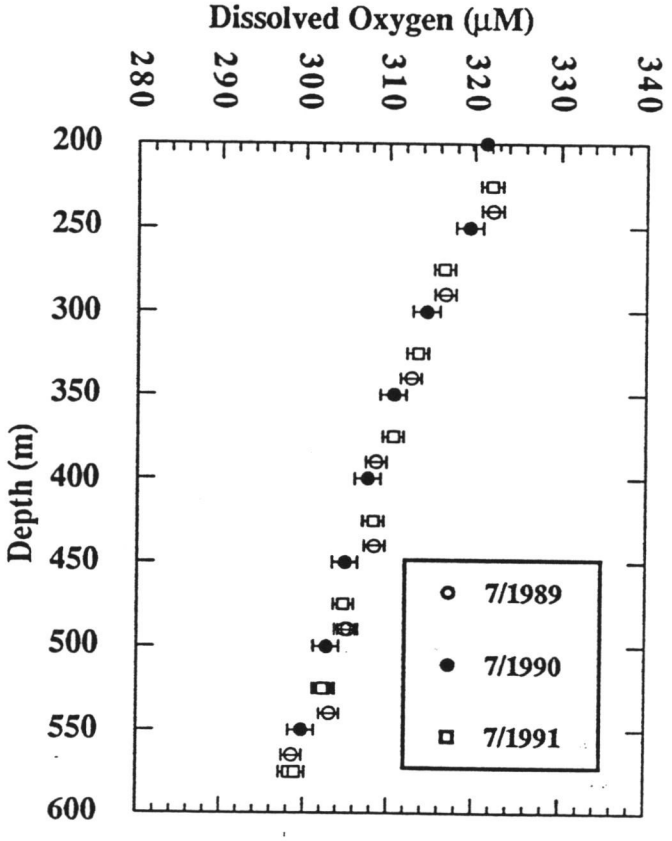

Fig. V.5. Dissolved oxygen as a function of depth for July 1989-1991. Within the analytical precision of the dissolved oxygen measurement, the vertical distribution of dissolved oxygen is consistent from year-to-year.

Dissolved oxygen in the upper water column

Organic matter which rains to the deep lake and is subsequently oxidized has it origins in the euphotic zone of the water column. One method for constraining the flux of organic material out of the euphotic zone is by estimating the amount of excess oxygen generated by primary production (i.e. Jenkins and Goldman 1985).

Supersaturation of dissolved oxygen in the upper water column of aquatic systems is commonly observed and is generated by photosynthesis, the penetration of solar energy which heats subsurface waters in situ, and by air bubble injection. Removal processes for dissolved oxygen include, vertical mixing, respiration, and gas exchange (Jenkins and Goldman 1985; Spitzer and Jenkins 1989). Although I lack the data to constrain all the processes contributing to the upper water column oxygen budget, estimates of the budget can be made which enable the demonstration that there is a sufficient oxygen excess to account for the observed deep lake respiration rate.

Assuming that the rate of oxygen consumption in the deep lake is driven by the oxidation of organic matter, ~700 mmol m^{-2} of carbon are required to account for the oxygen consumed between 26 June and 19 January. This calculation assumes a ratio of $-138O_2$:106C (Redfield 1942; Redfield et al. 1963).

Calculations of excess oxygen presented here encompass the region between the surface and 150 m (the compensation depth). Below 150 m dissolved oxygen is typically less than the saturation value. Although some oxygen consumption is likely to be occurring below this depth, little or no net change in dissolved oxygen is observed from 200 to 300 m between 26 June and 19 January, that is, the supply and removal (respiration) of oxygen are in balance.

If all the supersaturated oxygen (i.e. Fig. V.2) was photosynthetically-derived, this would yield an integrated excess in carbon of ~1150 mmol C m^{-2}. This represents an average value for July 1989-91. Alternatively, considering only the oxygen in excess over the winter saturation value (328.5 μM) an integrated excess of 300 ±100 mmol C m^{-2} is obtained. These estimates are a maximum and minimum respectively. The first estimate assumes that <u>all</u> the supersaturation is due to photosynthesis, which is unlikely to be the case, whereas the second assumes that all the supersaturation produced after spring mixing is due to in situ warming of the water column from the penetration of solar energy, also an unlikely scenario. The actual value will likely lie somewhere between these two extremes.

It is useful to consider what fraction of the upper water column supersaturation is needed to balance the deep lake oxygen deficit. If we consider that the particulate organic carbon, falling out of the euphotic zone (below 150 m), falls to the deep lake which has a smaller surface area, then the carbon values based on oxygen supersaturation should be multiplied by a factor which accounts for the differing surface areas between the upper water column and the deep lake. I account for the smaller lake volume from 300 m to the bottom as compared to 0-150 m by multiplying the calculated carbon inventory value by the ratio of the two volumes (~1.5). The resulting "adjusted" value for the upper limit (1150 mmol C m^{-2}) gives an oxygen-based carbon value of 1700 mmol C m^{-2}. Therefore, the deep lake oxygen budget predicts an oxygen consumption which is ~40% of this value or ~60% of the uncorrected value. This range in the photosynthetic fraction is consistent with that found in the ocean environment (Jenkins and Goldman 1985; Spitzer and Jenkins 1989; Emerson et al. 1991).

The ventilation calculations made earlier in the text are useful for estimating the delivery of a biologically important nutrient (i.e. nitrate) from the deep lake to the upper water column. This would provide another estimate for the amount of particulate organic material raining out of the euphotic zone. For instance, assuming that 40% of the water below 300 m is replaced with water from the upper lake, then nitrate rich water from the deep lake will be delivered to the upper 200 m. The average concentration of nitrate for the deep lake is ~1 μM, therefore this winter mixing delivers ~5 x 10^6 moles of NO_3^- to the upper lake. The resulting productivity from this added "new" nitrogen will return particulate organic material to the deep lake. This carbon flux will consume deep lake dissolved oxygen at a rate of ~5 mmoles O_2 m^{-2} d^{-1} which agrees well with the observed deep lake respiration rate. However, these estimates assume classical stoichiometry between O_2, C, and N which may not be valid for Crater Lake and could therefore make this estimate a minimum.

Without better constraints on the upper water column oxygen budget, one can only state that there appears to be sufficient supersaturation of dissolved oxygen in the upper water column to account for the observed oxygen consumption rate based on a traditional oxygen-carbon stoichiometric relationship.

Particulate organic material systematics

The carbon flux, as measured by sediment traps for the period from July through December 1989 was approximately 0.5 mmole C m^{-2} day^{-1} which is substantially less

than the carbon flux based on the oxygen budget over the same period (3.4 mmol C m^{-2} day^{-1}). Several processes could account for this difference. The 200 m trap shows a carbon flux which is larger than the deeper traps suggesting that decomposition during settling may be important. Assuming the 200 m trap accurately represents the carbon flux through this depth, and because the volume of lake water above 200 m is roughly a factor of three larger than that below 400 m, the sediment flux should increase by approximately a factor of three due to focusing of the raining material. Sediment focusing is a common process in basins which may introduce a bias in interpreting sediment accumulation rates (Lehman 1975). Because Crater Lake is enclosed by steep caldera walls, it may be particularly sensitive to focusing. As particles rain out of the euphotic zone, currents may keep the particles from settling along the caldera walls. Also, resuspension of particles that do settle on the caldera walls could lead to focusing.

Temporal and spatial heterogeneity in primary productivity is another potential mechanism which could account for the discrepancy between the oxygen budget and the observed carbon flux. The May-June period is typically high in particulate organic carbon flux, presumably in response to the very high flux of nutrients from snow melt. Likewise, May is a time of near-daily avalanche events. Since the sediment traps are located in the center of the lake, higher productivity around the edges of the lake coupled with debris flows, could lead to sedimentation around the edges of the deep lake which is not sampled by the traps. Also, the oxygen budget reflects a six month integration of the deep lake processes, whereas the particle flux during most years varies by more than a factor of 10.

The possibility was also considered that most of the organic carbon in the deep lake is in the form of dissolved organic carbon (DOC). Using contemporary analytical techniques (similar to those described by Sugimura and Suzuki 1988), DOC was measured in both deep and shallow water samples. The results from these measurements indicate that the organic carbon pool, necessary for the consumption of oxygen, is probably not in the dissolved form. However, although both deep lake and shallow lake samples gave DOC results which were not statistically different from zero, it is possible that there is a fraction of DOC in Crater Lake, which is undetectable, which contributes to the consumption of deep lake oxygen.

The influence of hydrothermal activity on the deep-lake oxygen budget

Hydrothermal activity delivers anoxic fluid to the deep basins in Crater Lake at a rate of 200 liters sec^{-1} (Dymond et al. 1989; Collier et al. 1991; Chapter III). Reduced elements carried by this fluid consume deep lake oxygen and the input of this zero-oxygen fluid dilutes the oxygen dissolved in the deep lake. Here I will examine the impact of these hydrothermal processes on the oxygen budget of the deep lake.

The dilution of deep lake water with anoxic fluid would change the dissolved oxygen content by <0.1%. This assumes a minimum deep-lake volume of ~9 x 10^8 m^3 (the volume below 300 m) and a hydrothermal fluid flow rate of 63 x 10^5 m^3 yr^{-1} (200 liters sec^{-1}, Chapter III). Therefore, dilution with zero-oxygen water has a negligible effect on the overall oxygen budget of Crater Lake; however, at locations near the source of the anoxic inputs, it is possible that this mixing of zero-oxygen hydrothermal water will affect the local dissolved oxygen distribution. This possibility will be examined below.

The oxidation of hydrothermally-derived reduced elements will also consume some deep lake dissolved oxygen. Based on sediment pore water samples an upper limit estimate for the reduced metal concentrations entering the deep lake is 200 μM for iron and 100 μM for manganese. Assuming that iron and manganese are entering the lake in a reduced form and that exposure to deep lake water will oxidize these species according to the first two reactions given in Table V.1, I can estimate a total oxygen demand associated with these inputs.

At a fluid input rate of 63 x 10^5 m^3 yr^{-1} (Chapter III) the Fe and Mn will consume 4.7 x 10^{11} μmol O_2 yr^{-1}. In the deep lake (below a depth of 300 m) this corresponds to a consumption of ~0.2 μM O_2 yr^{-1} or about 1% of the observed rate of change in dissolved oxygen.

Table V.1. Possible oxygen-consuming reactions associated with hydrothermal inputs.

$Fe^{2+} + 3/2H_2O + 1/4O_2 \rightarrow FeOOH(s) + 2H^+$
$Mn^{2+} + 1/4O_2 + 3/2H_2O \rightarrow \beta MnOOH + 2H^+$
$CH_4 + 2O_2 \rightarrow CO_2 + 2H_2O$
$H_2S + 2O_2 \rightarrow SO_4^{-2} + 2H^+$

Sulfate, measured in hydrothermal end-member samples was found to be as high as 900 μM. Although reduced sulfur (H_2S or HS^-) is often found in hydrothermal

systems, it is unlikely that a significant fraction of the dissolved sulfate entered the lake as H_2S. Two reasons for suspecting that H_2S is not the primary sulfur species are: (1) There was no strong characteristic sulfide odor in any fluid samples which suggests that the concentrations are well below 10 μM. (2) The oxidation of H_2S generates one mole of H^+ for every mole of O_2 consumed and the pH of the deep lake and the pore waters is generally too close to neutral (between 6 and 8) for this reaction to be significant within the water column.

There are only a few methane sample values to constrain the input of this constituent. The results indicate that the deep water column methane concentration is between 10 and 30 nM; likewise, dive samples ranged between 8 and 23 nM. Water immediately above a box core take from within a brine had approximately 6 μM methane, indicating that there is some methane present in the reduced fluid.

Assuming maximum concentrations of 10 μM for both H_2S and CH_4, and assuming the oxidation stoichiometry in Table V.1 then 40 μM O_2 yr^{-1} will be consumed by the incoming fluid. Following the mass balance arguments used for Fe and Mn, this consumption of oxygen by H_2S and CH_4 will account for <1% of the total oxygen deficit. Therefore, the sum of all hydrothermal oxygen demands are less than 2% of the observed loss of oxygen in the deep lake.

South Basin dissolved oxygen distribution

Although hydrothermal activity has a small impact on the overall deep lake oxygen budget, hydrothermal activity strongly influences the local hydrography in the South Basin. Dissolved oxygen depletion is most extreme in the South Basin and the concentration of dissolved oxygen is correlated with the hydrothermal tracers, temperature and sodium. These correlations suggest that the active input of saline fluids may play a role in the oxygen budget (Fig. V.6a, b). In addition, the ΔO_2:ΔNO_3 ratio in this basin is significantly higher than the ratio expected from the oxidation of organic matter which further suggests that particulate organic material is not the only consumer of deep lake oxygen (Fig. V.6c).

Measurements of dissolved oxygen in fluid samples from brines located at the bottom of the South Basin indicate that these brines are anoxic. The minor oxygen contents found in the brine sample in Table V.2 are probably due to bottom water entrainment at the time of collection and not from dissolved oxygen in the brines. The oxygen content of water collected immediately above a pool was also low. Although

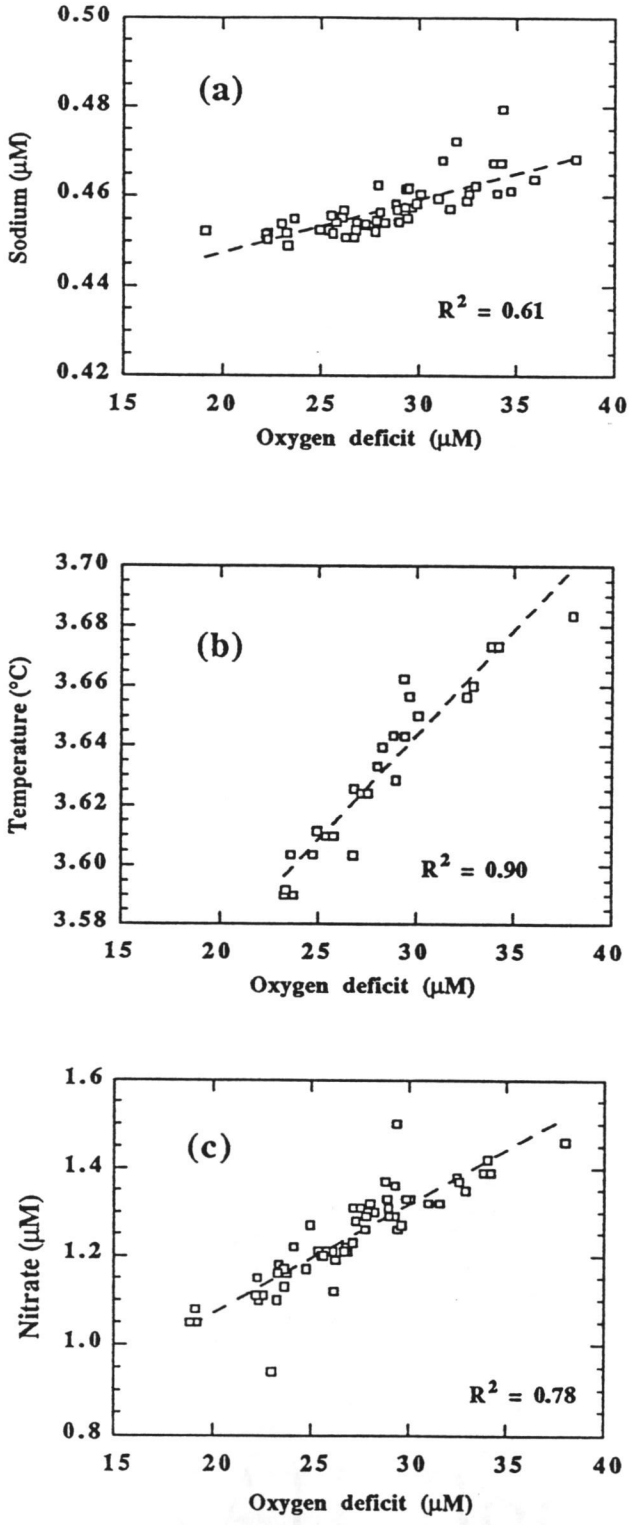

Fig. V.6. (a) Sodium, (b) temperature, and (c) nitrate as a function of the oxygen deficit in the South Basin. The oxygen deficit is defined as the difference between the winter saturation value (328.5 µM O_2) and the measured O_2. Of additional note, $R^2 = 0.93$ for the temperature-salinity relationship and $R^2 = 0.88$ for the salinity-oxygen deficit relationship. The ΔO_2:ΔNO_3 ratio for (c) is ~40.

bacterial mat fluids were always found to contain dissolved oxygen, they were always contaminated with bottom water, and it is unlikely that oxygen is present in the original fluids.

Table V.2. DO and Na concentrations in South Basin submersible samples.

Sample or Dive	DO (μM)	Na (mM)	Comments
CD230 S1	17.7	2.36	"Llao's" Pool
CD223 S1	228.2	1.109	Above "Llao's" Pool
CD230 S3	279.2	0.608	Bacterial mat
CD216 S3	294.2	0.480	Bacterial mat
CD223 S3	294.6	N/A	Above pool
CD229 S2	240.7	N/A	Bottom water
CD230 S2	293.8	0.461	Bottom water
CD228 S2	297.3	0.468	Bottom water
CD226 S2	292.6	0.464	Bottom water
CD222 S2	296.6	0.472	Bottom water

Two trends in the oxygen deficit vs salinity distribution for the South Basin (Fig. V.7) show both the "hydrothermal effect" (dilution and oxidation) and the net effect of the oxidation of organic matter and the interaction of hydrothermal fluids with the rest of the South Basin waters. The bacterial mat sample from CD230S3 lies along a hydrothermal line between the "Llao's Pool" low-oxygen high-sodium end-member and deep lake water (Fig. V.7). As stated above, these hydrothermal fluids have enhanced concentrations of reduced chemical species which consume dissolved oxygen after mixing into the basin. Also, the dilution of deep water with anoxic water will cause a net lowering of the dissolved oxygen content very close to the fluid source. These hydrothermal fluids will also increase the density of near-bottom waters through the addition of salts (Chapter III). Consequently, the ventilation of these fluids occurs to a lesser degree than in other deep waters, which results in lower oxygen contents in the South Basin near-bottom waters.

To quantitatively constrain the influence of hydrothermal activity on the oxygen distribution near the source of the hydrothermally enriched fluid inputs it is assumed that the hydrothermal fluids enter the lake over an area one tenth the size of the hydrothermal study area (eastern portion of the South Basin). Based on the oxygen consumption estimates for the reduced elements from above, and assuming a bottom layer 1 m deep (0.3×10^6 m^3), an oxygen consumption rate of 6.6 μM day^{-1} is obtained. Likewise, this volume will be diluted with anoxic waters by 5.8% per day . Although the effects

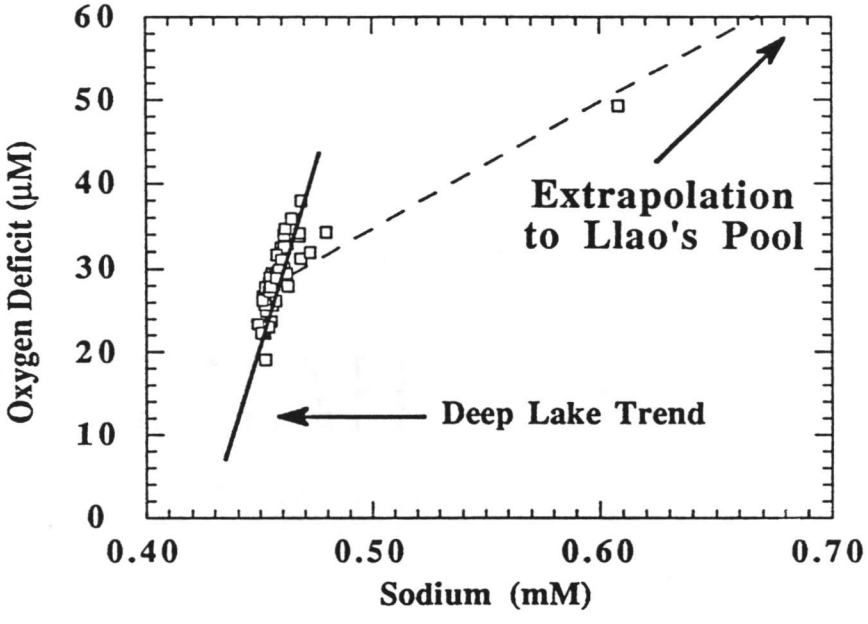

Fig. V.7. Oxygen deficit vs. sodium for all the South Basin samples including specific hydrothermal features. Both an ambient South Basin trend and a hydrothermal trend are apparent in the figure.

of hydrothermal activity on the deep lake oxygen budget are small, these calculations demonstrate the importance of hydrothermal activity on the local oxygen distribution in the deep South Basin.

The linearity between deep lake nitrate and the O_2 deficit (Fig. V.6c) suggests that even within the near-bottom hydrothermal fluids the oxygen deficit is driven by the oxidation of particulate organic matter from the upper waters of the lake. However, as mentioned above, the slope of the line in Fig. V.6c, demonstrates a $-\Delta O_2:\Delta NO_3$ ratio of ~40, which is much higher than that predicted from classical Redfield stoichiometry where $-\Delta O_2:\Delta NO_3 = \sim 9$ (Redfield 1942; Redfield et al. 1963). In fact, there are two $-\Delta O_2:\Delta NO_3$ ratios observed for the deep lake (Fig. V.8), one in the South Basin at depths > 400 m with values between 35 and 40, and another ratio for the rest of the deep lake ~16 which is less-influenced by hydrothermal inputs. The two ratios emphasize the two dominant oxidation processes occurring in the deep lake; the oxidation of organic matter on the oxygen budget of the whole lake, and the oxidation of reduced elements entering the lake.

During the summer of 1989 the C:N ratio was ~15 in the particulate organic material in the 380 and 580 m sediment traps. This is in contrast to the classical C:N ratio of ~7 (Redfield 1942; Redfield et al. 1963). Therefore, both the C:N ratio in particulate material and the $-\Delta O_2:\Delta NO_3$ from the water column ($-\Delta O_2:\Delta NO_3 = \sim 16$) suggest that the stoichiometry between molecular oxygen, carbon, and nitrogen in the particulate organic material is non-classical. It is possible that the atypical stoichiometry between carbon, oxygen, and nitrogen, both in particulate material and in the water column, is due to nitrogen limitation. Non-classical stoichiometry between bio-active elements has been reported for Lake Tahoe, which is also an oligotrophic lake where biological production is nitrogen limited (Imboden et al. 1977).

Based on budget calculations for the hydrothermal study area and the observation that dissolved oxygen in the South Basin is 5-15 μM lower than in the North Basin, it is clear that hydrothermal inputs produce small-scale heterogeneity in the South Basin dissolved oxygen distribution. Further, the distinct $\Delta O_2:\Delta NO_3$ ratio in the deep South Basin compared with that in the rest of the lake (Fig. V.8) indicates that the South Basin is influenced to a much greater degree by hydrothermal activity.

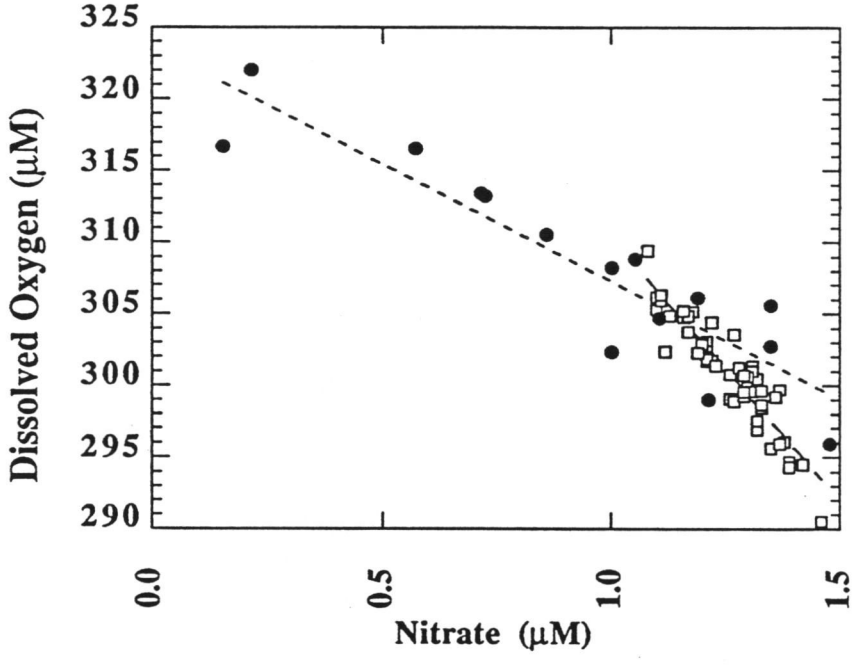

Fig. V.8. Dissolved oxygen vs. nitrate for the entire water column below 250 m. The data shows two relationships; a ΔO_2:ΔNO_3 relationship for the bulk water column (•), and a relationship for the South Basin as in Fig. V.6c.

CONCLUSIONS

The change in dissolved oxygen over time suggests that the flux of particulate organic material out of the euphotic zone is at least 3.4 mmol C m^{-2} d^{-1}. Although not well constrained, the oxygen budget of the upper water column suggests that this is a reasonable carbon flux estimate. Essentially, if ~40% of the early summer supersaturation of dissolved oxygen in the upper water column is due to photosynthesis, then there is sufficient carbon falling out of the euphotic zone, which will ultimately undergo oxidation, to balance the deep lake oxygen budget.

Hydrothermal activity plays a small role in the overall oxygen budget; however, the active input of reduced fluids is shown to influence the local hydrography and bio-active element stoichiometry in the South Basin. Mixing calculations suggest that the deep lake is partially mixed with surface water each year and that it would take 2.5-3.5 mixing cycles to completely ventilate the deep lake.

Oxygen is a powerful tool for assessing net ecosystem processes, and the ratios between the oxygen deficit and the oxidized solutes can provide both source and process information. This chapter demonstrates the importance of using a time-series of geochemical tracers to study geochemical cycles. In the case of Crater Lake, a more detailed atmosphere-lake model is needed to refine the estimates of the budgets of the bio-active elements.

ACKNOWLEDGEMENTS

James Milestone, Mark Buktenica, John Salinas, and Scott Stonum from Crater Lake National Park provided day and night field support for this research and their efforts are greatly appreciated. The field and analytical efforts of the OSU research team were invaluable. Special thanks are extended to Roberta Conard and Chris Moser. This research was funded by the U.S. National Park Service under cooperative agreement No. CA 9000-3-0003, CPSU, College of Forestry, Oregon State University.

VI. SUMMARY OF CONCLUSIONS

Subsurface hydrothermal activity in Crater Lake, Oregon influences the physics and chemistry of the lake's water column. This thesis emphasizes the importance of precise measurements for the characterization of the physical and chemical properties in a well-mixed aquatic system.

The distribution of temperature and salinity in the deep lake indicate that the South Basin is the origin of the high-temperature, high-salinity fluids. The general correlation between excess heat and salt within the South Basin suggest a common carrier -- hydrothermal fluid.

A time-series of measurements has provided direct evidence for the active input of heat (~1 W m^{-2}) and salt (~5 $\mu g\ m^{-2}$) into the deep lake. In addition, the mechanisms and timing of deep lake ventilation have been constrained through the use of a time-series of temperature measurements. The efficiency of annual mixing has been estimated from dissolved oxygen measurements, and it is found that the integrated time scale of deep lake mixing is ~2.5 years. Due to the increase in density with depth in the deep lake, the degree of vertical mixing decreases with increasing depth.

Changes in the near-bottom heat to salt ratio in the South Basin suggest that heat is being lost preferentially over salt in the hydrothermal fluids. This is accomplished through conductive heat loss from the fluid to the surrounding debris, or through double diffusion, or both. Although double diffusive convection may be occurring on small spatial and temporal scales, turbulence is the primary mechanism which transports heat and salt through the water column.

Although it is difficult to ascertain the exact effect of hydrothermal activity on the physics and chemistry of Crater Lake, it is apparent that there are physical and chemical features of the lake which could only be maintained by the active input of hydrothermal fluids. Therefore, changes in the lake's hydrothermal activity will invariably affect the ecosystem.

BIBLIOGRAPHY

Bacon, C.R., and M.A. Lanphere. 1990. The geologic setting of Crater Lake, p. 19-28. *In* E.T. Drake et al., [eds.]. Crater Lake: An Ecosystem Study. AAAS.

Barber, J.H., and C.H. Nelson. 1990. Sedimentary history of Crater Lake Caldera, Oregon, p. 29-40. *In* E.T. Drake et al. [eds.], Crater Lake: An ecosystem study. AAAS.

Benson, B.B., and D. Krause, Jr. 1984. The concentration and isotopic fractionation of oxygen in freshwater and seawater in equilibrium with the atmosphere. Limnol. Oceanogr., 29: 620-632.

Byrne, J.V. 1965. Morphometry of Crater Lake, Oregon. Limnol. Oceanogr. 10: 462-465.

Carmack, E.C., and D.M. Farmer. 1982. Cooling processes in deep, temperate lakes: A review with examples from two lakes in British Columbia. J. Mar. Res., 40, 85-111.

Carmack, E.C., R.F. Weiss, and V.M. Koropalov. 1989. Physical studies of mixing processes in Lake Baikal. EOS 70:1136.

Carpenter, J.H. 1965a. The Chesapeake Bay Institute technique for the Winkler dissolved oxygen method. Limnol. Oceanogr. 10: 141-143.

Carpenter, J.H. 1965b. The accuracy of the Winkler method for dissolved oxygen analysis. Limnol. Oceanogr. 10:135-140.

Chen, C.T., and F.J. Millero. 1977a. Effect of salt content on the temperature of maximum density and on static stability in Lake Ontario. Limnol. and Oceanogr. 22: 140-141.

Chen, C.T., and F.J. Millero. 1977b. The use and misuse of pure water PVT properties for lake waters. Nature 266: 707-708.

Chen, C.T., and F.J. Millero. 1986. Precise thermodynamic properties for natural waters covering only the limnological range. Limnol. Oceanogr. 3: 657-662.

Collier, R., J. Dymond, J. McManus, and J. Lupton. 1990. Chemical and physical properties of the water column at Crater Lake, Oregon, p. 69-79. *In* E.T. Drake et al., [eds.]. Crater Lake: An Ecosystem Study. AAAS.

Collier, R., J. Dymond, J. McManus, R. Conard, C. Meredith, and C.G. Wheat. 1990b. Mass balances and geochemical fluxes derived from hydrothermal activity in Crater Lake, OR. EOS 71:1674.

Collier, R., J. Dymond, and J. McManus. 1991. Studies of hydrothermal processes in Crater Lake, OR. Oregon State University, College of Oceanography Reference #90-7. Submitted to the National Park Service for peer review.

Conway, B.E. 1952. Electrochemical data. Elsevier.

Cox, R.A., F. Culkin, and J.P. Riley. 1967. The electrical conductivity/chlorinity relationship in natural seawater. Deep-Sea Res. 14: 203-220.

Drake, E.T., G.L. Larson, J. Dymond, and R. Collier [eds.]. 1990a. Crater Lake: An ecosystem study. AAAS.

Dryssen, D. and L.G. Sillen. 1967. Alkalinity and total carbonate in sea water: a plea for P-T-independent data. Tellus. 19:113.121.

Dymond, J., and R.W. Collier. 1990. The chemistry of Crater Lake sediments: definition of sources and implications for hydrothermal activity, p. 41-60. *In* E.T. Drake et al., [eds.]. Crater Lake: An Ecosystem Study. AAAS.

Dymond, J., R.W. Collier, and M.E. Watwood. 1989. Bacterial mats from Crater Lake, Oregon and their relationship to possible deep-lake hydrothermal venting. Nature 342: 673-675.

Edmond, J. 1970. High precision determination of titration alkalinity and total carbon dioxide content of sea water by potentiometric titration. Deep-Sea Res. 17:737-750.

Emerson, S., P. Quay, C. Stump, D. Wilbur, and M. Knox. 1991. O_2, Ar, N_2, and ^{222}Rn in surface waters of the subarctic ocean: Net biological O_2 production. Global Biogeochem. Cycles. 5:49-69.

Falkner, K.K., C.I. Measures, S.E. Herbelin, J.M. Edmond, and R.F. Weiss. 1991. The major and minor element geochemistry of Lake Baikal. Limnol. Oceanogr. 36:413-423.

Farmer, D.M., and E.C. Carmack. 1981. Wind mixing and restratification in a lake near the temperature of maximum density. J. Phys. Oceanogr. 11:1516-1533.

Gran, G. 1952. Determination of the equivalence point in potentiometeric titrations. Part II. Analyst. 77:661-671.

Herdendorf, C.E. 1990. Distribution of the World's Large Lakes, In: *Large Lakes*, M.M Tilzer, and C. Serruya [eds.]. Springer-Verlag.

Huppert, H.E. 1971. On the stability of a series of double diffusive layers. Deep-Sea Res. 18:1005-1021.

Ingebritsen, S.E., D.R. Sherrod, and R.H. Mariner. 1989. Heat flow and hydrothermal circulation in the Cascade Range, north-central Oregon. Science. 243:1458-1462.

Imboden, D.M., R.F. Weiss, H. Craig, R.L. Michel, and C.R. Goldman. 1977. Lake Tahoe geochemical study. 1. Lake chemistry and tritium mixing study. Limnol. Oceanogr. 22:1039-1051.

Ingham, M.C. 1966. The salinity extrema of the world ocean. Ph.D. thesis, Oregon State Univ. 123 p.

Jenkins, W.J. and J.C. Goldman. 1985. Seasonal oxygen cycling and primary production in the Sargasso Sea. J. Mar. Res. 43:465-491.

Kelley, D.E. 1984. Effective diffusivities within oceanic thermohaline staircases. J. Geophys. Res. 89:10,484-10,488.

Kelley, D.E. 1988. Small-scale turbulence and mixing in the ocean, *In:* J.C.J. Nihouc and B.M. Jamart [eds], Proceedings of the 19th international liege colloquium on ocean hydrodynamics, Elsevier Oceanography Series. 46:481-502.

Kelley, D.E. 1990. Fluxes through diffusive staircases: A new formulation. J. Geophys. Res. 95:3365-3371.

Kibby, H.V., J.R. Donaldson, and C.E. Bond. 1968. Temperature and current observations in Crater Lake, Oregon. Limnol. Oceanogr. 363-366.

Larson, G. L. 1986. Crater Lake Limnological Program. 1985 Annual Report, National Park Service Cooperative Studies Unit. Oregon State University.

Larson, G. L. 1987. A review of the Crater Lake limnological programs, p. 58-69. *In* T. P. Boyle [eds.], New Approaches to Monitoring Aquatic Ecosystems. ASTM.

Larson, G.L. 1990. Status of the ten-year limnological study of Crater Lake, Crater Lake National Park. *In* E.T. Drake et al., eds., Crater Lake: An Ecosystem Study. pages 7-11. AAAS.

Lehman, J.L. 1975. Reconstructing the rate of accumulation of lake sediment: the effect of sediment focusing. Quat. Res. 5, 541-550.

Li, Y.-H. 1973. Vertical eddy diffusion coefficient in Lake Zurich. Hydrologie. 35:1-7.

Marmorino, G.O., and D.R. Caldwell. 1976. Heat and salt transport through a diffusive thermohaline interface. Deep-Sea Res. 23:59-67.

Marmorino, G.O., S.C. Danos, and J.S. Maki. 1980. Temperature fine-structure of Lake Michigan hypolimnion. Limnol. Oceanogr. 25: 680-699.

McCormick, M.J. 1990. Potential Changes in thermal structure and cycle of Lake Michigan due to global warming. Trans. Am. Fish. Soc., 119:183-194.

McDougall, T.J. 1983. Double-diffusive plumes in unconfined and confined environments. J. Fluid Mech. 133: 321-343.

McManus, J., R. Collier, and J. Dymond. 1990. Heat and salt flux in Crater Lake, OR as deduced from water column CTD measurements. EOS 71:1674.

McManus, J., R. Collier, C-T. A. Chen, and J. Dymond. 1992. Physical properties of Crater Lake, OR: A method for the determination of a conductivity and temperature dependent expression for salinity. Limnol. Oceanogr. (In press).

Mortimer, C.H. 1981. The oxygen content of air-saturated fresh waters over ranges of temperature and atmospheric pressure of limnological interest. Mitt. int. Ver. Limnol. 22:1-23.

Nathenson, M. 1990. Chemical balance for major elements in water in Crater Lake, Oregon, p. 103-114. *In* E.T. Drake et al. [eds.], Crater Lake: An ecosystem study. AAAS.

Nathenson, M. and J.M. Thompson. 1990. Chemistry of Crater Lake, Oregon, and nearby springs in relation to weathering. *In* E.T. Drake et al. [eds.], Crater Lake: An ecosystem study. AAAS.

Neal, V. T., S. J. Neshyba, and W. W. Denner. 1971. Temperature microstructure in Crater Lake, Oregon. Limnol. Oceanogr. 16:695-700.

Neal, V.T., S.J. Neshyba, an W.W. Denner. 1972. Vertical temperature structure in Crater Lake, Oregon. Limnol. Oceanogr. 17: 451-454.

Nelson, C. H., A. W. Meyer, D. Thor, and M. Larsen. 1986. Crater Lake, Oregon: A restricted basin with base-of-slope aprons of nonchannelized turbidites. Geology 14:238-241.

Newman, F.C. 1976. Temperature steps in Lake Kivu: A bottom heated saline lake. J. Phys. Oceanogr. 6: 157-163.

Padman L. and T.M. Dillon. 1989. Thermal microstructure and intenal waves in the Canada Basin diffusive staircase. Deep-Sea Res. 36:531-542.

Pearl, H.W., R.C. Richards, R.L. Leonard, and C.R. Goldman. 1975. Seasonal nitrate cycling as evidence for complete vertical mixing in Lake Tahoe, California-Nevada, Limnol. Oceanogr. 20:1-8.

Phillips, K.N. 1968. Hydrology of Crater Lake, East Lake, and Davis Lakes, Oregon. U.S. Geol. Surv. Water-Supply Pap.,1859-E, 60pp.

Powell, T., and A. Jassby. 1974. The estimation of vertical eddy diffusivities below the thermocline in lakes. Water Resources Res. 10:191-198.

Redfield, A.C. 1942. The processes determining the concentration of oxygen, phosphate and other organic derivatives within the depths of the Atlantic Ocean. Pap. Phy. Oceanogr. Meteorol. 9(2):22 p.

Redfield, A.C., B.H. Ketchum, and F.A. Richards. 1963. The influence of organisms on the composition of seawater, p. 26-77. In M.N. Hill [ed.], The sea, v.2. Interscience.

Redmond, K. 1990. Crater Lake climate and lake level variability, p. 127-141. *In* E.T. Drake et al., [eds.]. Crater Lake: An Ecosystem Study. AAAS.

Robinson, R.A., and R.H. Stokes. 1955. Electrolyte solutions. Academic Press.

Sarmiento, J.L., H.W. Feely, W.S. Moore, A.E. Bainbridge, and W.S. Broecker. The relationship between vertical eddy diffusion and buoyancy gradient in the deep sea. Earth and Planet. Sci. Lett. 32:357-370.

Schmitt, R.W. 1981. Form of the temperature-salinity relationship in the Central Water; evidence for double-diffusive mixing. J. Phys. Oceanogr. 11, 1015-1026.

Simpson, H.J. 1970a. Tritium in Crater Lake, Oregon. Jour. Geophys. Res. 75(27):5195-5207.

Simpson, H.J. 1970b. Closed basin lakes as a tool in geochemistry. Ph.D. Thesis, Columbia University.

Snoeyink, V.L. and D. Jenkins. 1980. Water chemistry.

Sorensen, J.A., and G.E. Glass. 1987. Ion and Temperature dependence of electrical conductance for natural waters. Anal. Chem. 59: 1594-1597.

Spitzer, W.S. and W.J. Jenkins. 1989. Rates of vertical mixing, gas exchange and new production: Estimates from seasonal gas cycles in the upper ocean near Bermuda. J. Mar. Res. 47, 169-196.

Strickland, J.D.H. and T.R. Parsons. 1972. A manual of sea water analysis, 2nd ed.; Fish. Res. Board of Canada Bull. 167.

Stumm, W., and J.J. Morgan. 1981. Aquatic Chemistry, 2nd ed. Wiley.

Sugimura, Y. and Y. Suzuki. 1988. A high-temperature catalytic oxidation method for the determination of non-volatile dissolved organic carbon in seawater by direct injection of a liquid sample. Mar. Chem., 24:105-131.

Thompson, J.M., L.D. White, and M. Nathenson. 1987. Chemical analyses of waters from Crater Lake, Oregon, and nearby springs. U.S. Geological Survey Open-file report 87-587.

Thompson, J.M., M. Nathenson, and L.D. White. 1990. Chemical and isotopic compositions of waters from Crater Lake and nearby vicinity, *In* E.T. Drake et al., [eds.]. Crater Lake: An Ecosystem Study. AAAS.

Turner, D.A., M. Whitfield, and A.G. Dickson. 1981. The equilibrium speciation of dissolved components in freshwater and seawater at 25°C and 1 atm pressure. Geochim. Cosmochim. Acta. 45: 855-881.

Turner, J.S. 1965. The coupled turbulent transports of salt and heat across a sharp density interface. Int. J. Heat Mass Transfer. 8:759-767.

Turner, J.S. 1973. Buoyancy Effects in Fluids. Cambridge.

Volchok, H.L., M. Feiner, H.J. Simpson, W.S. Broecker, V.E. Noshkin, B.T. Bowen, and E. Willis. 1970. Ocean fallout-the Crater Lake experiment. J. Geophys. Res. 75:1084-1091.

Weiss, R.F., E.C. Carmack, and V.M. Koropalov. 1990. Deep water renewal and biological production in Lake Baikal. Nature 349:665-669.

Williams, D.L. and R.P. Von Herzen. 1983. On the terrestrial heat flow and physical limnology of Crater Lake, Oregon. Jour. Geophys. Res., 88:1094-1104.

APPENDIX

APPENDIX A

Major and trace element data from Crater Lake

Major and trace element data are presented for the water column and caldera wall springs from 1987 and 1988. The method of analysis for the major elements is described in Chapter II. Manganese, was analyzed by direct injection of the sample (99 μliters) into a graphite furnace AAS (Perkin-Elmer, 5000).

Table A.1. 1987 Hydrocast Data

Sample	Depth	T (°C)	[Na] (mM)	[Ca] (mM)	[Mg] (mM)	[K] (mM)	[Li] (μM)	[SiO2] (μM)	[Mn] (nM)
6.1	446.1	3.610	0.475	0.173	0.113	0.0456	6.7	302	17.82
6.3	427.0	3.592	0.471	0.170	0.113	0.0452	6.7	299	11.27
6.4	416.7	3.537	0.463	0.168	0.112	0.0445	6.5	297	2.78
6.5	407.5	3.530	0.452	0.169	0.111	0.0445	6.4	295	3.13
6.6	397.2	3.514	0.463	0.168	0.111	0.0442	6.4	294	1.03
7.1	385.3	3.508	0.460	0.168	0.111	0.0442	6.4	294	0.37
7.2	375.8	3.506	0.456	0.168	0.110	0.0441	6.4	294	0.49
7.3	350.9	3.501	0.451	0.168	0.111	0.0438	6.4	287	0.59
7.4	325.7	3.499	0.445	0.167	0.110	0.0437	6.4	292	0.33
7.5	300.9	3.514	0.456	0.166	0.109	0.0434	6.4	290	0.75
7.6	276.4	3.552	0.457	0.167	0.110	0.0435	6.4	290	0.51
18.1	418.5					0.0439	6.5	296	1.31
18.6	404.1	3.514	0.454	0.168	0.111	0.0442	6.4	296	1.05
18.2	433.5	3.517	0.455	0.168	0.110	0.0441	6.6	297	0.63
18.3	449.2	3.520	0.455	0.168	0.111	0.0441	6.6	297	1.16
18.5	464.1	3.521	0.451	0.168	0.111	0.0438	6.4	296	2.84
19.4	476.7	3.522	0.455	0.170	0.111	0.0441	6.6	298	0.55
20.1	486.7	3.612	0.473	0.178	0.119	0.0451	6.6	309	5.10
20.2	471.0	3.575	0.469	0.172	0.114	0.0445	6.5	302	2.50
20.3	456.8	3.553	0.453	0.171	0.112	0.0444	6.5	299	1.98
20.4	441.2	3.530	0.455	0.170	0.111	0.0440	6.5	297	0.78
20.5	427.0	3.526							
20.6	411.3	3.520	0.452	0.168	0.111	0.0438	6.5	298	0.75
21.6	456.5	3.591	0.462	0.172	0.114	0.0448	6.6	302	5.64
21.5	440.8	3.571	0.465	0.172	0.111	0.0446	6.5	298	8.26
26.1	443.3	3.558	0.458	0.171	0.111	0.0443	6.5	298	2.76
26.2	435.2	3.544	0.468	0.171	0.112	0.0441	6.4	293	1.85
26.3	424.9	3.530	0.462	0.171	0.111	0.0440	6.4	293	1.86
26.4	414.2	3.523	0.455	0.170	0.111	0.0441	6.4	293	1.18
26.5	405.4	3.524	0.441	0.169	0.111	0.0439	6.4	292	1.19
27.1	582.2	3.553	0.450	0.173	0.113	0.0444	6.4	300	5.03
27.2	533.3	3.540	0.468	0.170	0.112	0.0444	6.4	297	1.62
27.3	483.6	3.526	0.464	0.170	0.112	0.0444	6.4	295	1.74
27.4	434.3	3.520	0.455	0.170	0.111	0.0439	6.4	294	1.78
27.5	383.1	3.508	0.459	0.169	0.111	0.0437	6.4	295	1.45
28.1	447.7	3.577	0.458	0.172	0.112	0.0447	6.5	301	3.98
28.2	433.5	3.538	0.456	0.171	0.111	0.0444	6.5	298	1.48
28.3	417.5	3.526	0.466	0.170	0.110	0.0437	6.5	295	0.86
28.4	403.3	3.517	0.445	0.170	0.110	0.0437	6.3	294	0.77
28.5	388.0	3.509	0.456	0.170	0.110	0.0437	6.4	293	0.39
29.1	324.2	3.514	0.449	0.170	0.109	0.0435	6.4	290	0.47
29.2	250.4	3.727	0.445	0.169	0.109	0.0432	6.4	290	0.72
29.3	175.1	3.725	0.445	0.168	0.109	0.0430	6.3	289	0.61
29.4	100.5	4.102	0.454	0.169	0.109	0.0429	6.3	288	0.19
29.5	24.9	8.429	0.457	0.169	0.110	0.0436	6.3	289	4.13

Table A.2. 1988 Spring Data

Spring	[Mg] (mM)	[K] (mM)	[Na] (mM)	[Ca] (mM)	[SiO2] (μM)	[Mn] (nM)
20	0.0658	0.0239	0.130	0.164	423	
16		0.0422			444	5.7
48	0.0209	0.0348	0.110	0.058	587	
2	0.0359	0.0237	0.067	0.063	625	2.0
38	0.1174	0.0288	0.169	0.226	552	
42	0.0531	0.0438	0.122	0.114	619	
19	0.1405	0.0156		0.293	133	2.0
11	0.0416	0.0169	0.202	0.049	611	
39	0.0205	0.0192	0.087	0.062	431	5.7
24		0.0084		0.522	605	
35	0.0101	0.0318	0.121	0.205	518	76.0

Table A.3. 1988 Hydrocast Data

Sample	Depth	T (°C)	[Mg] (mM)	[K] (mM)	[Na] (mM)	[SiO2] (µM)	[Ca] (mM)	[Cl] (mM)	[SO4] (mM)	pH	Alk (meq/l)	[Mn] (nM)
2.2-5	441.3	3.619	0.112	0.0446	0.463	304	0.172					8.2
2.2-6	434.4	3.597	0.112	0.0448	0.463	303	0.172					4.9
2.2-7	428.8	3.580	0.114	0.0448	0.475	302	0.172					4.1
2.3-1	448.2	3.610	0.111	0.0446	0.460	305	0.172					4.3
2.3-2	408.1	3.564	0.110	0.0436	0.455	302	0.169					0.3
2.3-3	398.1	3.561	0.110	0.044	0.455	301	0.170					0.5
2.3-4	387.4	3.559	0.110	0.0439	0.457	299	0.169					0.6
81801	439.0	3.599	0.112	0.0445	0.467	303		9.74	10.04	7.10	0.583	1.8
81802	429.5	3.586	0.110	0.0444	0.461	301		9.75	10.03	7.20	0.626	1.2
81803	419.1	3.578	0.111	0.0438	0.460			9.76	10.01	7.11	0.627	
81804	408.8	3.568	0.110	0.0442	0.457	297		9.61	9.99	7.10	0.629	
81807	378.6	3.563	0.110	0.0439	0.455	296		9.59	9.89	7.14	0.622	
81809	347.6	3.570	0.110	0.0435	0.453	296		9.51	9.96	7.23	0.605	
81811	318.0	3.572	0.108	0.0435	4.524	294		9.55	9.94	7.31	0.624	
82501	445.1	3.609	0.111	0.0442	0.467	303	0.172	9.67	10.06	7.17	0.634	4.4
82502	434.8	3.607	0.111	0.0445	0.455	302	0.172	9.65	10.06	7.18	0.636	4.8
82503	424.1	3.598	0.111	0.0444	0.456	299	0.171	9.74	10.02	7.26	0.634	3.2
82504	415.3	3.581	0.110	0.0442	0.453	300	0.170	9.61	10.04	7.15	0.613	1.3
82505	302.2	3.595	0.109	0.0431	0.447	295	0.169	9.66	9.81			1.5
82506	262.4	3.659	0.108		0.445	294	0.169	9.60	9.93			0.4
82507	221.5	3.731	0.109	0.0439	0.448	293	0.168	9.58	9.79			1.7